

1987

Textural and mineralogical characteristics of altered Grande Ronde basalt, northeastern Oregon : a natural analog for a nuclear waste repository in basalt

Paul M. Trone
Portland State University

Follow this and additional works at: https://pdxscholar.library.pdx.edu/open_access_etds



Part of the [Geology Commons](#), and the [Mineral Physics Commons](#)

Let us know how access to this document benefits you.

Recommended Citation

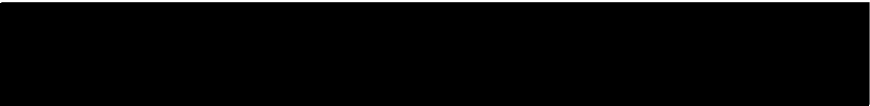
Trone, Paul M., "Textural and mineralogical characteristics of altered Grande Ronde basalt, northeastern Oregon : a natural analog for a nuclear waste repository in basalt" (1987). *Dissertations and Theses*. Paper 3824.
<https://doi.org/10.15760/etd.5706>

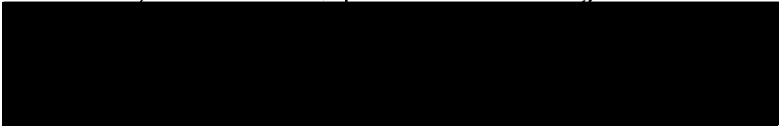
This Thesis is brought to you for free and open access. It has been accepted for inclusion in Dissertations and Theses by an authorized administrator of PDXScholar. Please contact us if we can make this document more accessible: pdxscholar@pdx.edu.

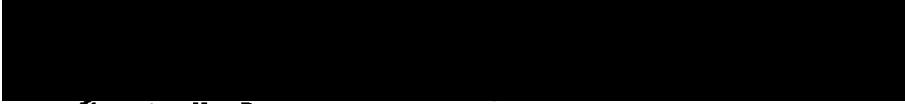
AN ABSTRACT OF THE THESIS OF Paul Max Trone for the Master of Science in Geology presented December 19, 1986.

Title: Textural and mineralogical characteristics of altered Grande Ronde Basalt, northeastern Oregon: A natural analog for a nuclear waste repository in basalt.

APPROVED BY MEMBERS OF THE THESIS COMMITTEE:


Michael L. Cummings, Chairman


Ansel G. Johnson


Marvin H. Beeson

Altered flows that are low-MgO chemical types of the Grande Ronde Basalt crop out in the steep walls of the Grande Ronde River canyon near Troy, Wallowa County, Oregon. The alteration effects in these flows are being investigated as a natural analog system to a high level nuclear waste repository in basalt. The flows within the study are referred to as the analog flow, in which the alteration effects are the strongest, and the superjacent flow. The analog flow crops out at Grande Ronde River level and a roadcut-outcrop is developed in the flow-top breccia of this flow. The two flows have been divided into flow zones based on intraflow structures observed in the field and primary igneous textures

observed in thin section. These zones include, from the base upward, the flow interior, transition, and flow-top breccia zones of the analog flow, the interflow contact zone, and the flow interior and flow-top breccia zone of the superjacent flow. The intraflow structures and textures of the transition and interflow contact zones are atypical of Grande Ronde Basalt flows. The transition zone is transitional in textures between the flow interior zone and flow-top breccia zone, and includes holocrystalline spines mantled with fused in situ breccias. The interflow contact zone reflects the dynamic interaction during the emplacement of the superjacent flow manifested as invasive basalt tongues, clasts shed from tongues, pipe vesicles and tree molds, and pockets of breccia caught up in the base of the superjacent flow.

The characteristics of the porosity are distinct among flow zones. In the flow interior zones the porosity is dominated by horizontal platy and vertical joint-related fractures. Vesicles and diktytaxitic cavities are a very minor contribution to the overall porosity, and are somewhat isolated in contrast to the fractures, which are highly interconnected.

Low within the transition zone the porosity is similar to the flow interior zone. High in the zone the porosity includes vesicles in resorbed clasts and surrounding incipient breccia clasts. The porosity and extent of interconnection increases laterally outward from the spines in the fused in situ breccia as interclast voids increase in size and abundance.

The flow-top breccia zone and brecciated portion of the interflow contact zone are the most porous zones due to large interclast voids. Vesicles and diktytaxitic cavities are the porosity within clasts, and are a minor component of the total porosity in these flow zones.

In the solid portion of the interflow contact zone the porosity is provided by platy fractures, large flattened vesicles, tree molds, and pipe vesicles.

Secondary minerals occur as replacements of primary phases and as precipitated phases in primary porosity. The variety of secondary minerals precipitated in vesicles and diktytaxitic cavities from aqueous solutions is greatest in the flow-top breccia and interflow contact zones and includes clay minerals, zeolites, silica minerals, and carbonate. The clay minerals include smectite and celadonite; zeolites include clinoptilolite, phillipsite, and chabazite; silica minerals include quartz, chalcedony, opal-CT lepispheres, and opal-CT; and the carbonate is calcite. The paragenetic sequence is clay minerals --> silica minerals --> zeolites --> carbonate --> silica minerals --> clay minerals. The individual mineral species differ among the two flow zones. Celadonite, chalcedony and quartz are the major secondary minerals in the interflow contact zone, whereas smectite, clinoptilolite, and opal-CT are the major minerals occurring in the flow-top breccia zone.

The differences in the secondary mineral suite, assemblages, and parageneses among the flow-top breccia and interflow contact

zones are attributed to solution composition differences. Assuming the basalt is inert to altering solutions, and the solution composition is not influenced by the relative proportions of glass and crystalline phases in the basalt or water/rock ratios, the differences in solution composition are reasonably explained if a thermal gradient is present during alteration. A geothermal gradient, even if elevated above the assumed present day gradient, is not sufficient to produce the alteration effects. An elevated gradient related to the cooling of the superjacent flow is necessary.

TEXTURAL AND MINERALOGICAL CHARACTERISTICS
OF ALTERED GRANDE RONDE BASALT, NORTHEASTERN OREGON:
A NATURAL ANALOG FOR
A NUCLEAR WASTE REPOSITORY IN BASALT

by

Paul M. Trone

A thesis submitted in partial fulfillment of the
requirements for the degree of


MASTER OF SCIENCE
in
GEOLOGY

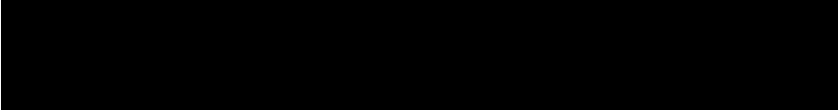
Portland State University


1987

TO THE OFFICE OF GRADUATE STUDIES AND RESEARCH:

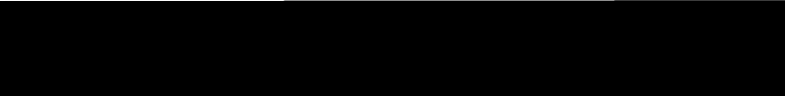
The members of the Committee approve the thesis of Paul Max Trone presented December 19, 1986.

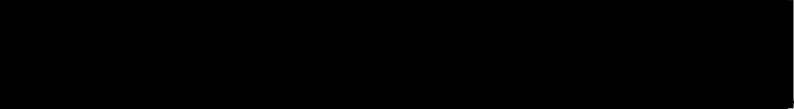

Michael L. Cummings, Chairman


Ansel G. Johnson


Marvin H. Beeson

APPROVED:


Paul E. Hammond, Head, Department of Geology


Bernard Ross, Dean of Graduate Studies and Research

ACKNOWLEDGEMENTS

This study was made possible through the encouragement and support of all the people involved. I would like to thank the Northwest College and University Association for Science (NORCUS) for offering me a research training appointment which supported the field research. Furthermore, I would like to extend a sincere thank you to Rockwell Hanford Operations for their generous funding, and technical assistance provided through Dr. Shirley Rawson and Dr. Jim Burnell.

I am indebted to my advisor, Dr. Michael Cummings, for introducing me to this study, the countless hours he spent procuring my financial support, and for his technical advice, general encouragement, and time invested in editing the thesis. I am grateful to the other members of the thesis committee, Dr. Ansel G. Johnson and Dr. Marvin H. Beeson, for the time spent in editing the draft of the thesis, and for all of their helpful comments.

TABLE OF CONTENTS

	PAGE
ACKNOWLEDGEMENTS	iii
LIST OF TABLES	vii
LIST OF FIGURES	ix
 CHAPTER	
I INTRODUCTION	1
Scope and Methods	7
II PETROGRAPHY	9
Analog Flow	11
Flow Interior Zone	
Transition Zone	
Flow-top Breccia Zone	
Interflow Contact Zone	
Superjacent flow	25
Flow Interior Zone	
Flow-top Breccia Zone	
III PRECIPITATED SECONDARY MINERALS	28
Clay Minerals	29
Brown Clays	
Yellow Clays	
Olive Green Clays	
White Clays	
Blue-green Clays	
Zeolites	44
Clinoptilolite	
Phillipsite	

CHAPTER	PAGE
Chabazite	
Unidentified Zeolite 1	
Unidentified Zeolite 2	
Silica Minerals	61
Opal-CT Lepspheres	
Opal-CT	
Chalcedony	
Quartz	
Carbonate	72
IV SECONDARY MINERAL PARAGENESIS	75
V DISCUSSION	80
Primary Porosity	84
Secondary Minerals in Relation to Temperature	
and Solution Composition	86
At the Scale of a Vesicle	
At the Scale of Neighboring Vesicles	
At the Scale of a Hand Sample	
At the Scale of the Flow Zone	
Summary	103
Temperature	105
Reevaluation of Assumptions	109
VI CONCLUSIONS	112
REFERENCES	115
APPENDIX A	120
APPENDIX B	130
PRIMARY TEXTURES	130
Analog Flow	131
Flow Interior Zone	
Transition Zone	

Flow-top Breccia Zone
Interflow Contact Zone

Superjacent Flow 150

Flow Interior Zone

LIST OF TABLES

TABLE	PAGE
I	Major Element Geochemistry of the Analog and Superjacent Flows 12
II	Flow Zone Characteristics 14
III	Petrographic Data Summarized for Flow Zones 16
IV	Summary of Clay Minerals 30
V	Zeolite Comparisons With Published Data 47
VI	Thermal Analysis of Clinoptilolite 48
VII	Summary of Zeolites 50
VIII	Summary of Silica Minerals 63
IX	Summary of the Carbonate 73
X	Secondary Mineral Parageneses of the Outcrop in Context of Flow Zones 76
XI	Assumptions 82
XII	At the Scale of a Vesicle 88
XIII	At the Scale of Neighboring Vesicles 93
XIV	At the Scale of a Hand Sample 97
XV	At the Scale of the Flow Zone 99
XVI	Petrographic Summary of Individual Samples Flow Interior Zone/ Analog Flow 120 Sample: 84a 120 Sample: 83a 121

TABLE	PAGE
Sample: 83b	121
XVII Petrographic Summary of Individual Samples	
Transition Zone/ Analog Flow	122
Sample: 8b	122
Sample: 28a	123
Sample: 28c(a)	123
Sample: 28c(b)	124
Sample: 69d	124
Sample: 83c	125
XVIII Petrographic Summary of Individual Samples	
Flow-top Breccia Zone/ Analog Flow	126
Sample: 271	126
XIX Petrographic Summary of Individual Samples	
Interflow Contact Zone/ Analog and superjacent Flows	127
Sample: 36e	127
XX Petrographic Summary of Individual Samples	
Flow Interior Zone/ Superjacent Flow	128
Sample: 51	128
Sample: 22h	129

LIST OF FIGURES

FIGURE	PAGE
1. General Location of the Grande Ronde River Canyon . . .	6
2. Distant View of the Road-cut Outcrop	10
3. Cross-section of the Study Outcrop	13
4. Graphs Showing the Modal Range and Mean	18
Graphs Showing the Size Range and Mean	19
5. Schematic Diagram Showing the Distribution of the Breccia Types	21
6. Interflow Contact Showing an Invasive Tongue Developed in the Trough of an Undulation	24
7. Flow Interior and Flow-top Breccia Zones of the Superjacent Flow	26
8. Indexed Diffractograms for the Randomly Oriented Clay Minerals	32
9. Close-up of Brown Clay Linings Showing the Perpendicular Orientation of the Foliae	34
10. The Interference Colors of Foliated Linings Highlight the Shapes of Vesicles	34
11. The Boundary Between the Thin, Birefringent Foliated Lining and the Thick Massive Linings is Sharp	35
12. Cross-sectional View of Botryoidal Vesicle Linings . .	36
13. S.E.M. Plane View of Brown Clay Botryoidal Linings . .	36

FIGURE	PAGE
14. The Brown Clay Linings Coarsen Toward the Center of the Vesicle	37
15. Geopetal Fabric in Two Interconnected Vesicles	37
16. Black Clay Filling on Parallel Linings of Clinoptilolite and Brown Clay	39
17. Brown Filiform Clay Embedded in Blue-green Clay	39
18. Olive Green Clay Linings Intervened by Black Dendritic Linings	41
19. S.E.M. Photograph of Arborescent Olive Green Clays	41
20. S.E.M. Photograph of Celadonite Showing the Tabular Habit	43
21. Non-parallel Tufted Linings of Celadonite	43
22. Convolute Filaments of Celadonite Embedded in Fillings of Chalcedony and Quartz	44
23. Indexed Diffractograms of the Zeolite Minerals	46
24. S.E.M. Photograph Showing Clinoptilolite Intergrown With Opal-CT	51
25. Parallel Linings of Clinoptilolite	51
26. Sheaved Aggregates of Clinoptilolite on Dark Brown Clay Vesicle Linings	52
27. S.E.M. Photograph of Clinoptilolite Aggregates Showing the Sheaved Arrangement of Crystals	52
28. Clinoptilolite Aggregates Encrusting Arborescent Olive Green Clays	53

FIGURE	PAGE
29. S.E.M. Photograph Showing How Clinoptilolite Encrusts the Arborescent Olive Green Clays	53
30. S.E.M. Photograph of Clinoptilolite Showing Rough- textured Faces and Raised Edges Between Faces . .	55
31. Prismatic Crystals of Phillipsite on Clinoptilolite Vesicle Linings	55
32. S.E.M. Photograph Showing Blocky (Lamellar) Phillipsite on a Clinoptilolite Substrate	56
33. Phillipsite on a Brown Clay Vesicle Lining	57
34. S.E.M. Photograph of Prismatic Phillipsite	58
35. Pseudo-cubic Chabazite Crystals on Brown Clay Vesicle Linings	59
36. S.E.M. Photograph of Chabazite Showing the Pseudo- cubic (Rhombohedral) Crystal Habit	60
37. Unidentified Zeolite 1 Attached to a Vesicle Wall . .	60
38. Thin Linings of Unidentified Zeolite 2 Parallel the Filiform Celadonite	62
39. Same View as in Figure 38, Though Shown in Cross- polarized Light	62
40. Indexed Diffractogram of Cryptocrystalline Opaline Silica	65
41. This S.E.M. Photograph Shows Opal-CT Lepspheres . . .	66
42. Aggregates of Opal-CT Lepspheres Completely Cover the Celadonite Substrate	67

FIGURE

PAGE

43. Chalcedony Linings Parallel and Fill in Around
the Filiform Celadonite 69

44. Sharply Bounded Chalcedony Fillings. 69

45. Geopetal Fabric Developed in Chalcedony 70

46. Drusy Quartz 71

47. Quartz Fillings Developed in Chalcedony 71

48. Calcite Scalenohedrons Developed on Clinoptilolite
Vesicle Linings 74

49. Plagioclase Lath Intergrown With Augite in the Form of
Opposing, Optically Discontinuous Bud-shaped
Crystals 133

50. Optically Continuous Pyroxene Microphenocryst Intergrown
With Plagioclase 134

51. Orthopyroxene at Partial Extinction is Rimmed
by Augite 135

52. Cumuloporphyritic Mass of Pyroxene and Plagioclase
Microphenocrysts 135

53. Intergranular Holocrystalline Texture 137

54. Sharp Boundary Between Light-colored Groundmass Having
Opaque Polyhedra, and a Dark-colored Disseminated
Opaque Domain 141

55. Mixed Disseminated and Polyhedral Opaque Domains . . . 141

56. Incipient Dark-colored Clast Showing Sharp to
Gradational Boundaries 143

FIGURE

PAGE

57.	The Photomicrograph Shown Above is a Close-up of a Portion of a Boundary of a Dark-colored Clast Shown in the Photomicrograph Below	144
58.	Glass and Crystallites	147
59.	Dendritic Opaques	148
60.	Hypocrystalline Groundmass Showing Intersertal Glass Textures	152

CHAPTER I

INTRODUCTION

Subsurface geologic characterization of the Hanford Site in central Washington began in 1976 subsequent to the establishment of the Basalt Waste Isolation Project (BWIP) to investigate the feasibility of locating a high-level nuclear waste repository in a basalt medium. A reference repository location was identified within the Hanford Site. Originally, four basalt flows were identified as candidate repository horizons, as discussed in Gephart and others (1984). The four basalt flows are the Rocky Coulee, Cohasset, McCoy Canyon, and Umtanum flows of the Miocene Grande Ronde Basalt, Columbia River Basalt Group. The Cohasset flow is the preferred flow (Long, 1984), and is presently being evaluated as a repository horizon.

If the Hanford Site is selected, and licensed by the Nuclear Regulatory Commission (NRC) as a nuclear waste repository, and if the Cohasset flow serves as the repository horizon, the repository would be excavated in the Cohasset flow colonnade/entablature, centered approximately 970 meters below the surface of the site. To comply with NRC regulations, the waste form must be isolated from the groundwater environment for a minimum of 300 to 1,000 years by a series of geologic and natural barriers. The barriers would be designed around the waste

CHAPTER I

INTRODUCTION

Subsurface geologic characterization of the Hanford Site in central Washington began in 1976 subsequent to the establishment of the Basalt Waste Isolation Project (BWIP) to investigate the feasibility of locating a high-level nuclear waste repository in a basalt medium. A reference repository location was identified within the Hanford Site. Originally, four basalt flows were identified as candidate repository horizons, as discussed in Gephart and others (1984). The four basalt flows are the Rocky Coulee, Cohasset, McCoy Canyon, and Umtanum flows of the Miocene Grande Ronde Basalt, Columbia River Basalt Group. The Cohasset flow is the preferred flow (Long, 1984), and is presently being evaluated as a repository horizon.

If the Hanford Site is selected, and licensed by the Nuclear Regulatory Commission (NRC) as a nuclear waste repository, and if the Cohasset flow serves as the repository horizon, the repository would be excavated in the Cohasset flow colonnade/entablature, centered approximately 970 meters below the surface of the site. To comply with NRC regulations, the waste form must be isolated from the groundwater environment for a minimum of 300 to 1,000 years by a series of geologic and natural barriers. The barriers would be designed around the waste

packages according to the short horizontal borehole repository emplacement concept described in McCall and Krogness (1986). The conceptual design of the waste package as described by McCall and Krogness (1986) would consist of the waste form, thick-walled carbon steel container, crushed basalt and sodium bentonite clay packing material, and thin-walled carbon steel emplacement shell. The carbon steel container that will enclose the spent fuel waste form is 50 centimeters (20 in.) in diameter, and 403 centimeters (159 in.) long (McCall and Krogness, 1986).

The geologic repository is planned in terms of three periods, 1) operation/retrieval, 2) containment, and 3) limited release (McCall and Krogness, 1986). The first period will encompass repository construction, waste package emplacement, and if necessary, waste package retrieval. The first period will end 84 years later after the repository is permanently closed. The second period will begin after the repository is permanently closed, and will end after the containers are breached, a minimum of 300 to 1,000 years later. The third period will begin as radionuclides from the breached containers are slowly released into the groundwater environment, and continues over the life of the repository. According to NRC regulations, waste packaging must control the release of the radionuclides for a period lasting 10,000 years, defined as the design life of the repository.

During the containment period of the repository, hydrothermal processes will probably affect the host rock proximal to the waste packages. Thermal modelling indicates that

temperatures around the waste packages may reach 200°C shortly after the repository is closed (Yung and others, 1986).

An important aspect of the Basalt Waste Isolation Project (BWIP) is to simulate, through equilibrium step codes (Carnahan, 1978) and laboratory experimentation (Scheetz and others, 1978; White and others, 1985; Lane and others, 1985; Moore and others, 1985), the geochemical reactions and resulting physical and chemical conditions within the waste packages and enclosing geologic medium during the containment period of the repository. These experiments were undertaken to evaluate the stability of components of the waste packages, and provide details on the environment that will develop around the waste packages.

A second aspect of the Basalt Waste Isolation Project as summarized by Horton (1985) is to characterize the distribution and petrology of primary and secondary minerals (and textures) in the repository horizon basalt flow (Cohasset), particularly within major fluid flow paths (flow-tops and fractures). Much work has been done regarding primary minerals and textures (Noonan and others, 1981; Schiffman and Lofgren, 1982; Allen and Strope, 1983; Long and Strope, 1983; Reidel, 1983) and intraflow structures (Long and Wood, 1986) in Grande Ronde Basalt, though less work has been done regarding secondary minerals (Ames, 1980; Benson, 1978; Benson and others, 1979a,b; Teague, 1980; Benson and Teague, 1982; Horton, 1985; Rawson, 1986).

In the status report on secondary mineralogic and petrographic studies in Rocky Coulee and Cohasset flow-tops,

Horton (1985) comments: "In order to predict the geochemical environment over the life of the repository, the present and past environments must be studied, understood, and extrapolated into the future". The data obtained from natural analog systems may be usefully extrapolated to predict the environment within a nuclear waste repository.

Geologic investigations of natural analogs to a high-level nuclear waste repository in basalt allow additional insight into the interactions between a repository and the enclosing geologic medium. Ideally, a natural analog system should approximate the geological, chemical, and physical conditions in the host rock proximal to the waste packages at the end of the containment period and the beginning of the limited release period. At that point in time it is expected that the host rock and packing material in the waste packages will be hydrothermally altered, primary and secondary porosity will be reduced by precipitated secondary mineral phases, and temperatures will be reduced proximal to the waste packages.

The mineralogical and geochemical data obtained through investigations of these natural analog systems provides information on the

- 1) dissolution of primary minerals and precipitation of secondary minerals,
- 2) paragenesis of secondary minerals,
- 3) distribution of alteration zonation in response to the geometry of the heat source, thermal gradients, and rock

permeability,

- 4) long-term stability of secondary minerals developed in a basalt system,
- 5) effect of primary mineral dissolutions and secondary mineral precipitation upon rock permeability, and
- 6) trace element mobility, particularly those elements that are geochemically similar to radionuclides in spent fuels.

Altered flows of Grande Ronde Basalt exposed in a roadcut-outcrop approximately 3.2 kilometers northeast of Troy, Oregon (Figure 1) are being investigated at Portland State University, Portland, Oregon, as a natural analog system. The natural analog study will investigate the

- 1) primary textures in basalt flows,
- 2) secondary mineralogy and its distribution within the flows,
- 3) chemical composition of secondary phases,
- 4) changes in the bulk composition of the basalt produced by alteration, and
- 5) conditions under which the alteration occurred.

The current study investigates the

- 1) porosity type and distribution within the basalt flows of the natural analog system,
- 2) precipitated secondary mineralogy and paragenesis within vesicles and diktytaxitic cavities,
- 3) uniformity of solution composition during alteration and what it implies about the conditions of alteration.

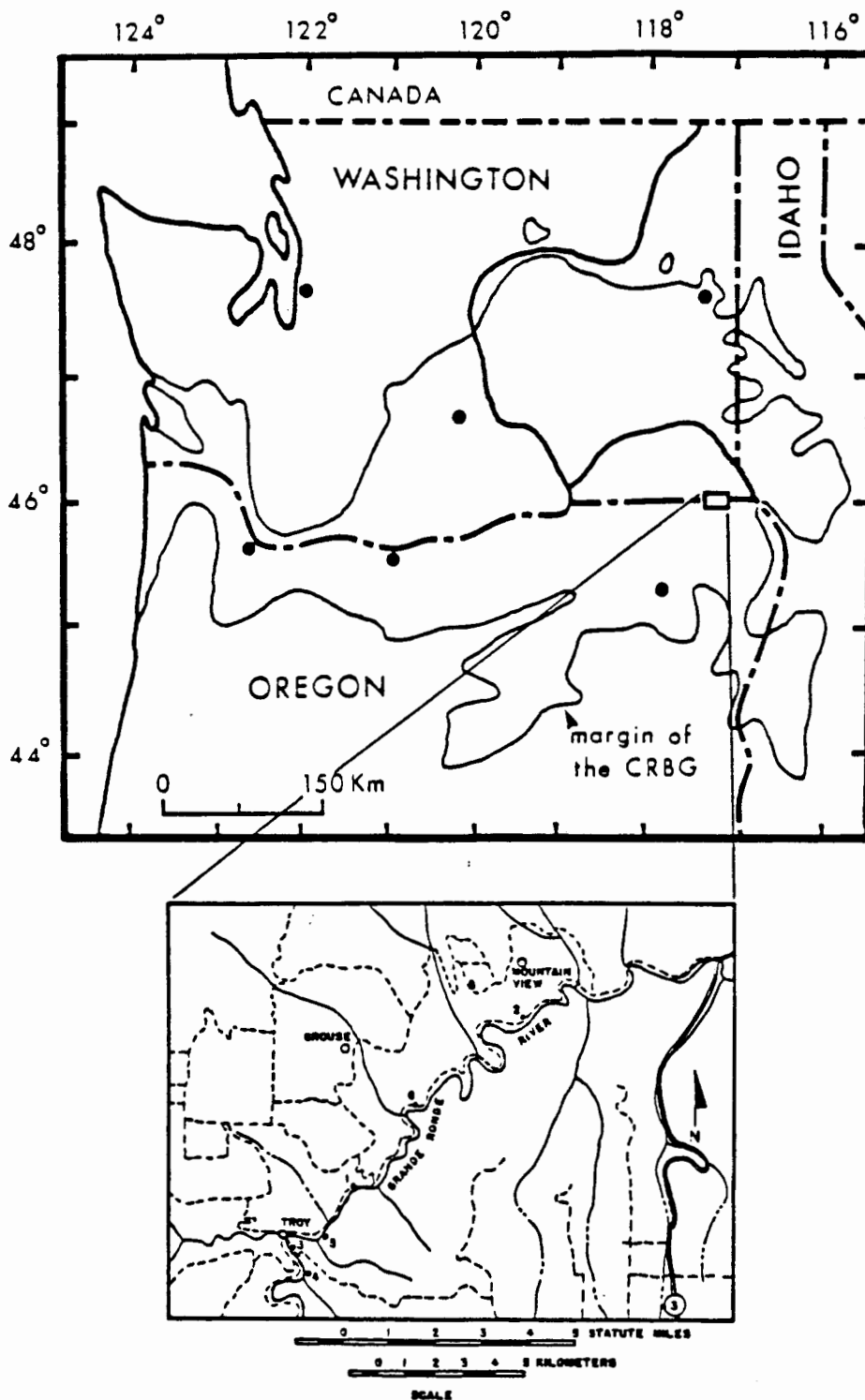


Figure 1. General location of the Grande Ronde River Canyon. The location of the analog study outcrop is number 1 on the bottom inset.

SCOPE AND METHODS

The scope of this study includes:

- 1) Description of field relations including the physiography of the basalt flows included in the natural analog system, and macroscopic characteristics of the flows.
- 2) Division of the flows into flow zones.
- 3) Petrography of the flow zones particularly as it relates to primary porosity.
- 4) Characterization of the precipitated secondary mineral suites in vesicles and diktytaxitic cavities as obtained from hand sample descriptions, binocular microscope examinations, optical mineralogy and petrography, x-ray diffraction (XRD), and scanning electron microscopy (S.E.M.).
- 5) The paragenesis of precipitated secondary minerals in context of flow zones.

Field mapping and sampling of the natural analog study outcrop began during the summer of 1985, and was completed in approximately 4-5 weeks. Additional sampling was done during September, 1986. The field methods were performed according to the guidelines established in Portland State University Operating Procedure 1.1 entitled "Mineralogic and Lithologic Sampling". This operating procedure was developed within the Quality Assurance Plan for Contract SA-984 between Portland State University and Rockwell Hanford Operations. This procedure and those listed below are available through the Geology Department at

Portland State University, Portland, Oregon.

The following analytical methods have been utilized in this study:

- 1) X-ray diffraction (XRD)
- 2) Standard petrographic analysis
- 3) Scanning electron microscopy (S.E.M.)
- 4) X-ray fluorescence (XRF)

These methods were performed according to the guidelines established in Portland State University Operating Procedures 3.1 (X-Ray Diffraction), 6.1 (Standard Petrographic Analysis and Reflected Light Microscopy), 7.1 (Scanning Electron Microscopy), and 9.1 (X-Ray Fluorescence) by personnel certified according to the requirements in 10.1 (Certification of Research personnel). Prior to these analyses, the samples were prepared according to operating procedure 2.1 (Sample Separations and Preliminary Preparation of Samples for Analysis).

CHAPTER II

PETROGRAPHY

The hamlet of Troy, Oregon is located in the rugged canyon country in the eastern part of the Columbia Plateau (See Figure 1). In this area, the Grande Ronde River and its tributaries have incised steep-walled canyons into flows of the Columbia River Basalt Group. These flows comprise the Grande Ronde, Wanapum, and Saddle Mountains Formations and are interbedded with sediments of the Ellensburg Formation (Ross, 1978, 1980; Stoffel, 1984). The basalt flows were erupted from vents near the Troy area, in the 3-corners region of Oregon, Washington and Idaho (Taubeneck, 1970; Price, 1977; Ross, 1978, 1983; Stoffel, 1984).

The natural analog system consists of two flows that were mapped by Ross (1978) as part of the Grande Ronde Basalt. One is the flow exposed at river level, and the other is the immediately overlying flow. The alteration effects are strongest in the flow-top breccia near the contact between flows, subside abruptly in the overlying flow, and gradually diminish downward in the interior of the lower flow. Since the alteration effects are focused mainly in the flow-top breccia of the lower flow, it is referred to as the analog flow. The flow overlying the analog flow is referred to as the superjacent flow. The roadcut is developed in the flow-top breccia of the analog flow over a length

of 252 meters, of which 26 meters is covered by talus from overlying flows. In the vicinity of the outcrop the terrain is steepened. Above the flow-top breccia, the overlying flows occur as near-vertical cliffs intervened by narrow retreating slopes developed in scoriaceous flow-tops of individual flows (Figure 2).

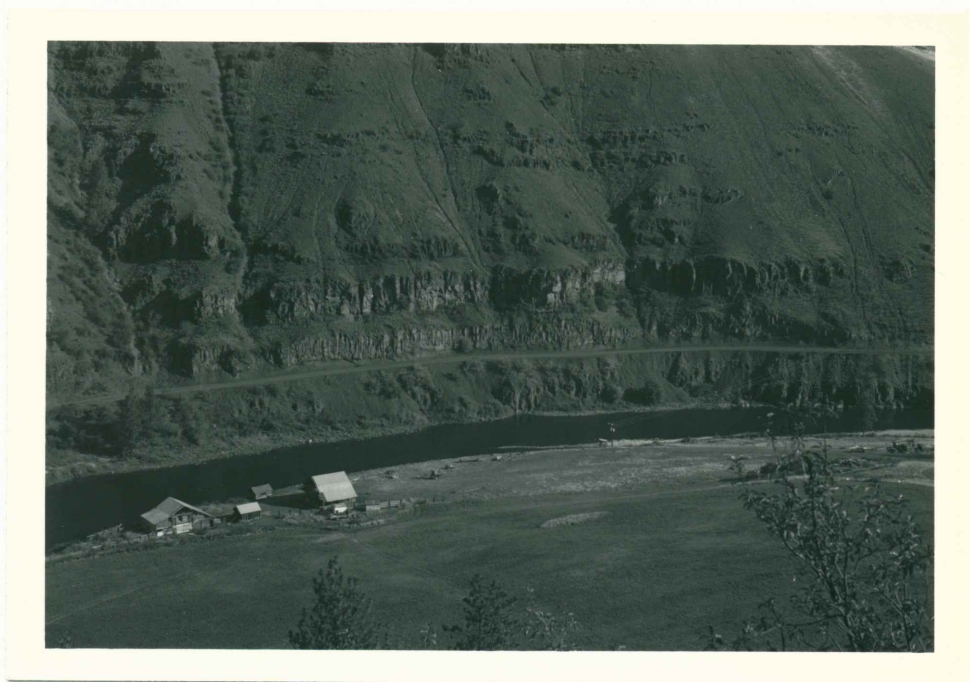


Figure 2. Distant view of the road-cut outcrop showing the altered flow-top breccia (thin band at road level) and superjacent basalt flows.

The major element geochemistry of the analog and superjacent flows presented in Table I is consistent with the composition of Grande Ronde Basalt as defined by Wright and others (1973). The chemical composition of the flows is similar to the low-MgO chemical type of the Grande Ronde Formation and may be further constrained on the basis of their chemical composition to the Wapshilla Ridge Member of the Grande Ronde Formation (M. Beeson,

personal communication, October, 1986). The flows were determined to be reversely polarized by use of a fluxgate magnetometer. On the basis of their stratigraphic position the flows are of the R₂ magnetostratigraphic unit as defined by Swanson and Wright (1976).

The variation in gross characteristics within the analog and superjacent flows has allowed division into flow zones that are defined by textural features observed in the field. The zones are not wholly defined on the basis of fracturing and/or jointing although these features are part of the characteristics used to recognize the zone in the field. Figure 3 contains a scaled cross-section of the outcrop, illustrates the geomorphic patterns noted in the flows, and indicates the distribution of the flow zones. Characteristics of the zones are summarized in Table II. Petrographic data is summarized according to flow zones in Table III, and for individual samples in Appendix A. A comprehensive description of the primary textural features in the flow interior zone is included in Appendix B.

ANALOG FLOW

The analog flow is composed of the flow interior, transition, and flow-top breccia zones. The base of the analog flow is not exposed in the area.

Flow Interior Zone

The flow interior zone forms a near vertical cliff above the Grande Ronde River. From the Grande Ronde River level upward, the

TABLE I

MAJOR ELEMENT GEOCHEMISTRY OF THE ANALOG AND SUPERJACENT FLOWS

Weight percent oxide	51	Sample number		
		22h	84a(1)	84a(2)
SiO ₂	54.04	54.06	55.01	55.24
Al ₂ O ₃	14.82	14.91	15.01	15.11
TiO ₂	2.41	2.42	2.29	2.28
Fe ₂ O ₃	2.00	2.00	2.00	2.00
FeO	11.45	11.40	10.63	10.50
MnO	.22	.28	.20	.20
CaO	7.22	7.05	6.67	6.70
MgO	3.73	3.50	3.54	3.49
K ₂ O	1.29	1.45	1.63	1.62
Na ₂ O	2.46	2.56	2.69	2.53
P ₂ O ₅	.36	.37	.32	.32

Analysis by x-ray fluorescence at Washington State University run # 8623, June 30, 1986.

51 and 22h are samples from the superjacent flow; samples 84a(1) and 84a(2) are from the analog flow.

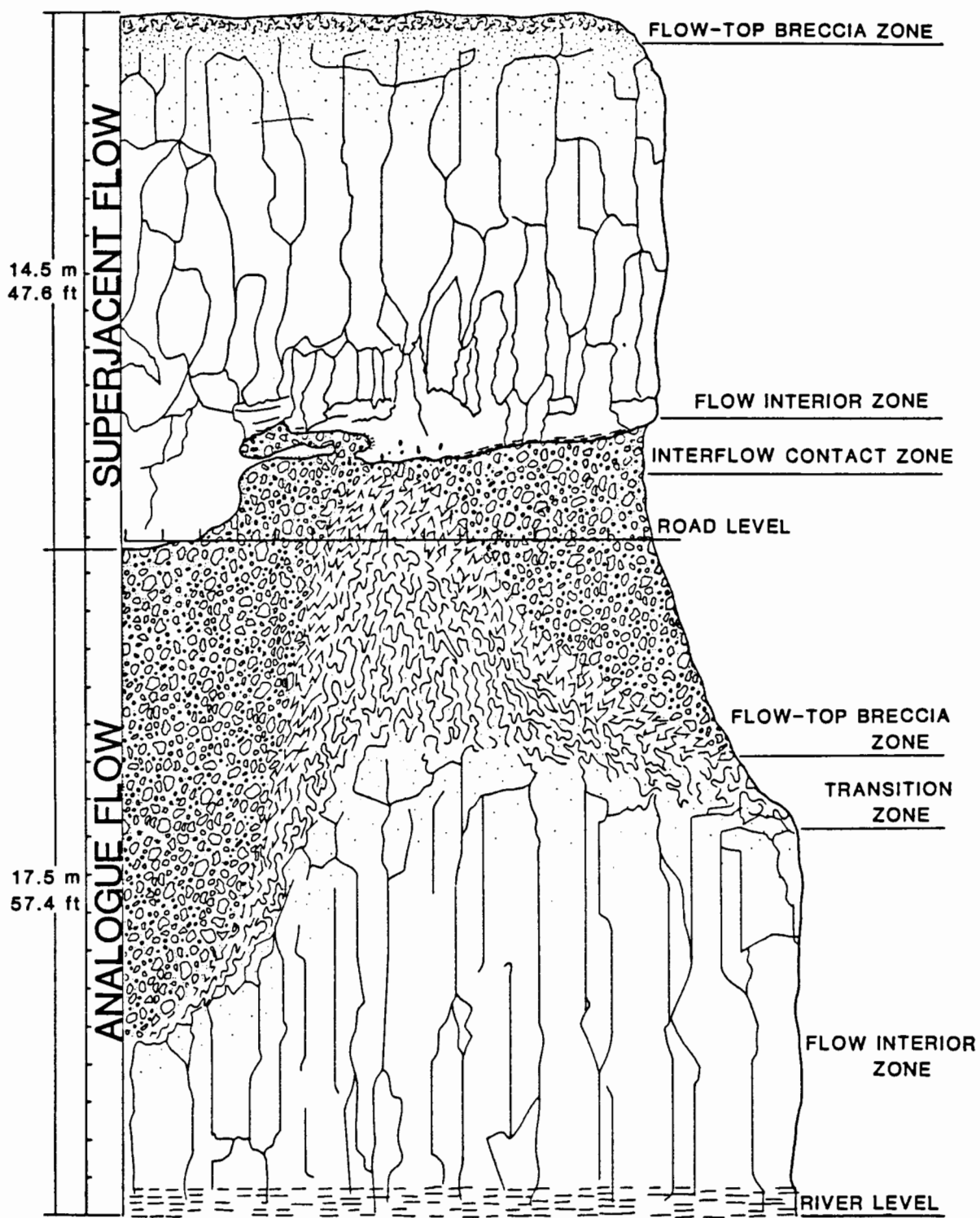


Figure 3. Cross-section of the study outcrop. The base of the flow is not exposed in the area. See Figure 5 for a detailed sketch of the transition zone.

TABLE II

FLOW ZONE CHARACTERISTICS

<u>Flow zone:</u>	<u>Distinguishing features</u>
Flow interior:	<p>Cliff-former; thickness varies by up to 7 m in the analog flow, though of more constant thickness (10 m) in the superjacent flow; platy, columnar, and/or irregular joint fracture patterns; sparsely vesicular near base, increasing vesicularity upwards; gradational with the transition or flow-top breccia zones.</p> <p>Hypocrystalline with intersertal glass near flow base; holocrystalline intergranular upwards with little size contrast between microphenocrysts and microlites; polyhedral opaques low in the zone, and finely disseminated opaques in darkened streaked domains high in the flow zone.</p>
Transition:	<p>Forms retreating slope below road level in the analog flow: not present in the superjacent flow; variable thickness (7-13 m); non-brecciated to brecciated; composed of dense dark gray basalt spines mantled by fused <u>in situ</u> breccia that is matrix-supported inward to clast-supported outward from the spine center; gradational undulatory intraflow contact with the flow-top breccia zone (undulations range through zone thickness); no periodicity recognized in the undulations.</p> <p>Spine centers are holocrystalline and contain resorbed clasts; spine margins are non-brecciated and hypocrystalline with streaked disseminated opaque domains that may be delineated by diktytaxitic cavities elongate vesicles, and plagioclase microlites; noticeable size contrast throughout between microphenocrysts and microlites; cavities and plagioclase microlites show preferred orientations; fracture displacement is observed through microphenocrysts, groundmass, and cavities; microphenocrysts may be bent.</p>

Flow-top breccia: Forms a near vertical exposure in the road-cut; up to 13 m total thickness; composed of vesicular to scoriaceous clasts and clast fragments that commonly have pahoehoe surfaces and red oxidized rinds; most clasts are lapilli-size, though clasts up to 1 m in greatest dimension are present; flow-top breccia is clast-supported with loosely to tightly packed clasts; clasts are not fused.

Hypocrystalline with intersertal glass between crystalline phases; vesicles are commonly elongate and show preferred orientation; noticeable size contrast between microphenocrysts and microlites; pyroxene buds on opposing sides of plagioclase microphenocrysts and interpenetrating plagioclase/ pyroxene microphenocrysts are common; opaques are commonly polyhedral and less commonly dendritic; disseminated opaques are absent; weakly birefringent crystallites may be present in the groundmass.

Interflow contact: Encompasses the interflow contact itself, and those portions of the outcrop where the textures and fabrics reflect the dynamic interaction between the contemporary surface of the analog flow, and the advancing superjacent flow; includes superjacent flow invasive tongues, lenses, and blocks in the flow-top breccia, and pipe vesicles and tree molds in the base of the superjacent flow; superjacent flow lenses and blocks are dark gray, have sparse broad flattened vesicles, and lack pahoehoe surfaces and red rinds.

Hypocrystalline with intersertal glass and crystallites between crystalline phases; large size contrast between microphenocrysts and microlites; pyroxene buds on opposing sides of plagioclase microphenocrysts are common; plagioclase microlites and cavities commonly show preferred orientation; polyhedral opaques are common, disseminated opaques are rare, and dendritic opaques are absent; fracture displacement is observed through microphenocrysts, groundmass, and cavities; microphenocrysts may be bent.

TABLE III
 PETROGRAPHIC DATA SUMMARIZED FOR FLOW ZONES

Model Range (3) Percent	(1): ANALOG FLOW		(2): FLOW INTERIOR ZONE		(3): FLOW-TOP BRECCIA ZONE		(4): INTERFLOW CONTACT ZONE		(5): SUPERJACENT FLOW	
	3.4 - 5.9	2.0 - 6.4	0.5 - 4.1	1.1 - 4.0	0.5 - 4.1	1.1 - 4.0	0.5 - 2.9	0.3 - 2.5	0.5 - 2.7	2.0 - 3.5
Microphenocrysts	1.7 - 4.0	1.4 - 3.5	0.5 - 2.9	0.3 - 2.5	0.5 - 2.9	0.3 - 2.5	0.5 - 2.2	0.5 - 2.7	0.5 - 0.8	1.5 - 2.7
Plagioclase	1.5 - 1.9	0.5 - 2.9	0.3 - 1.8	0.3 - 1.8	0.3 - 1.8	0.3 - 1.8	0.3 - 1.8	0.3 - 1.8	0.3 - 1.8	0.5 - 0.8
Pyroxene										
Groundmass	89.6 - 94.0	56.8 - 92.2	36.4 - 85.3	67.3 - 92.0	36.4 - 85.3	67.3 - 92.0	36.4 - 85.3	67.3 - 92.0	36.4 - 85.3	88.3 - 93.0
Plagioclase (4)	39.0 - 43.9	16.0 - 47.0	11.8 - 31.2	26.0 - 46.0	11.8 - 31.2	26.0 - 46.0	11.8 - 31.2	26.0 - 46.0	11.8 - 31.2	32.9 - 53.0
Pyroxene (4)	30.0 - 39.0	5.0 - 30.2	0.7 - 24.0	5.0 - 31.0	0.7 - 24.0	5.0 - 31.0	0.7 - 24.0	5.0 - 31.0	0.7 - 24.0	5.5 - 25.2
Opaque	7.0 - 11.9	0.5 - 10.3	0.2 - 11.8	1.5 - 8.3	0.2 - 11.8	1.5 - 8.3	0.2 - 11.8	1.5 - 8.3	0.2 - 11.8	4.5 - 14.1
Glass (5)	0.0	0.0 - 55.5	16.7 - 41.2	15.5 - 41.0	0.0 - 55.5	16.7 - 41.2	15.5 - 41.0	0.0 - 55.5	16.7 - 41.2	16.1 - 29.5
Cavities (6)	2.5 - 6.0	3.3 - 41.1	11.0 - 61.8	6.0 - 28.6	3.3 - 41.1	11.0 - 61.8	6.0 - 28.6	3.3 - 41.1	6.0 - 28.6	5.0 - 8.3
Interstices		13.5								
Upper Size Range (mm)										
Microphenocrysts	1.3 - 1.5	0.7 - 3.0	0.7 - 2.6	0.8 - 3.5	0.7 - 2.6	0.8 - 3.5	0.7 - 2.6	0.8 - 3.5	0.7 - 2.6	0.9
Plagioclase	0.6 - 1.1	0.5 - 1.2	0.5 - 1.5	0.6 - 1.8	0.5 - 1.5	0.6 - 1.8	0.5 - 1.5	0.6 - 1.8	0.5 - 1.5	0.9
Pyroxene										
Groundmass	0.10 - 0.30	0.08 - 0.16	0.08 - 0.22	0.15 - 0.30	0.08 - 0.22	0.15 - 0.30	0.08 - 0.22	0.15 - 0.30	0.08 - 0.22	0.15 - 0.30
Plagioclase	0.07 - 0.30	0.02 - 0.09	0.02 - 0.22	0.07 - 0.30	0.02 - 0.09	0.07 - 0.30	0.02 - 0.22	0.07 - 0.30	0.02 - 0.09	0.12 - 0.30
Pyroxene	0.03 - 0.15	0.01 - 0.33	0.01 - 0.34	0.06 - 0.08	0.01 - 0.34	0.06 - 0.08	0.01 - 0.34	0.06 - 0.08	0.01 - 0.34	0.03 - 0.13
Opaque										
Glass										
Cavities	0.4 - 1.3	2.1 - 12.0	1.8 - 13.0	0.6 - 23.0	1.8 - 13.0	0.6 - 23.0	1.8 - 13.0	0.6 - 23.0	1.8 - 13.0	2.0 - 4.5
Vertical Range (7)	-10.0 to -21.0	-1.5 to -10.0	0.0 to -7.5	0.0 to +0.5	-1.5 to -10.0	0.0 to -7.5	0.0 to +0.5	0.0 to +0.5	0.0 to -7.5	0.0 to +0.5
Pyroxene Buds (8)	1/3 (11)	2/10	9/23	4/6	2/10	9/23	4/6	2/10	9/23	None
Inter-Pyroxene (9)	1/3	2/10	11/23	2/6	2/10	11/23	2/6	2/10	11/23	1/3
Preferred Orientations										
Microclites (10)	2/3	9/10	6/23	5/6	2/3	9/10	6/23	5/6	2/3	1/3
Cavities (6)	None	2/10	14/23	6/6	None	2/10	14/23	6/6	None	None
Crystallites	None	None	7/23	4/6	None	None	7/23	4/6	None	1/3
Opaque										
Polyhedral	3/3	Trace	17/23	5/6	3/3	Trace	17/23	5/6	3/3	3/3
Disseminated	Trace (12)	10/10	None	1/6	Trace (12)	10/10	None	1/6	Trace (12)	None
Dendritic	None	None	6/23	None	None	None	6/23	None	None	None

Notes: (1) See field relations section in text for definition and location of the analogue and superjacent flows. (2) The sample suites from which the data was obtained for each of the flow zones are as follows: Analogue flow interior- 83a, 83b, 84a, Transition- 8b, 27g, 27h, 27i, 28a, 28b, 28c(a), 28c(b), 694, 83c. Flow-top breccia- 38, 8d, 22g, 23j, 24h, 27i, 27j, 27n, 29i, 30a, 31d, 32d, 35a, 40c, 41i, 42d, 42e, 42f, 45c, 49b, 50g, 50i, 69h. Interflow contact- 6a, 20b, 30b, 32e, 36e, 38d. Superjacent flow interior- 51, 22h, 63d. (3) The two values represent the upper and lower modal extremes for each of the flow zones. (4) Microclites. (5) Original and/or altered glass. (6) Vesicles + diktytaxitic cavities. (7) Vertical distance above (+) or below (-) the interflow contact. (8) Pyroxene buds on opposing sides of plagioclase microphenocrysts as explained in text. (9) Interpenetrating microphenocrysts of plagioclase and pyroxene as explained in the text. (10) Plagioclase microclites. (11) Number of samples with (feature) out of the total number of samples in the flow zone suite. (12) Trace indicates trace amounts in all samples of the flow zone suite.

flow interior is composed of one meter of horizontal platy jointing, and four to nine meters of colonnade (Figure 3). The platy joints are spaced five to ten centimeters apart. The columns are broad, ranging from two to three meters in width, and are oriented normal to the horizontal platy joints. The flow interior is sparsely vesiculated, though vesiculation does increase upward in the colonnade near the boundary with the transition zone. The boundary between the flow interior and transition zone is gradational over two to three meters.

The porosity of the flow interior zone consists of joint-related fractures, vesicles, and diktytaxitic cavities. The modal range and size of vesicles and diktytaxitic cavities is indicated for the flow interior zone in Table III, and is graphically represented in Figure 4. Vesicles are characterized by having rounded walls reflecting development while the flow was still molten. The diktytaxitic cavities are developed interstitially to microlites and have their shapes controlled by the shape of crystals in the groundmass. A continuum exists between the two cavity types.

Transition Zone

This zone is the portion of the analog flow that has characteristics transitional between the flow interior and the flow-top breccia zones. The characteristics of the transition zone do not correspond to the typical intraflow structures in Grande Ronde Basalt flows as described by Long and Wood (1986).

ANALOG FLOW ————— SUPERJACENT FLOW

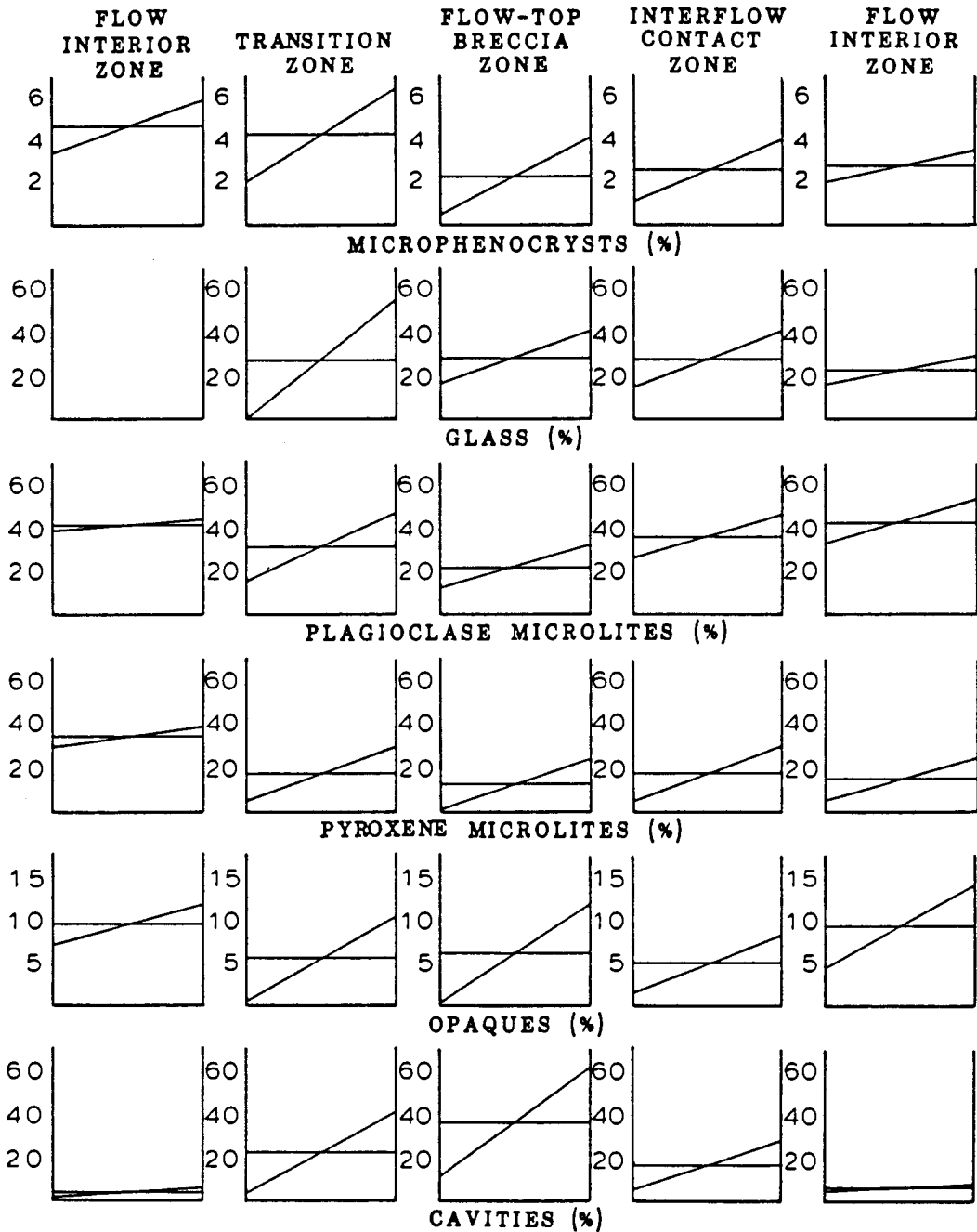


Figure 4. Graphs showing the modal range and mean (%) summarized according to flow zone. The data used to plot these graphs is given in Table III.

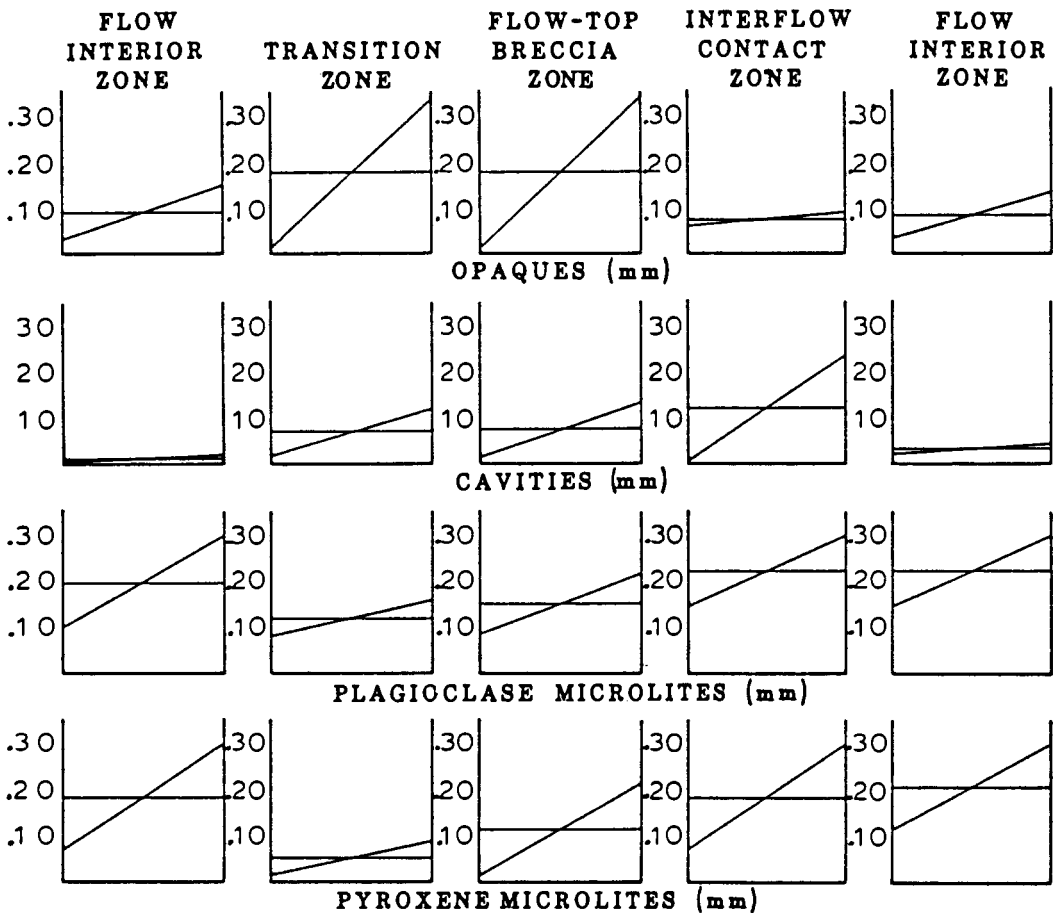


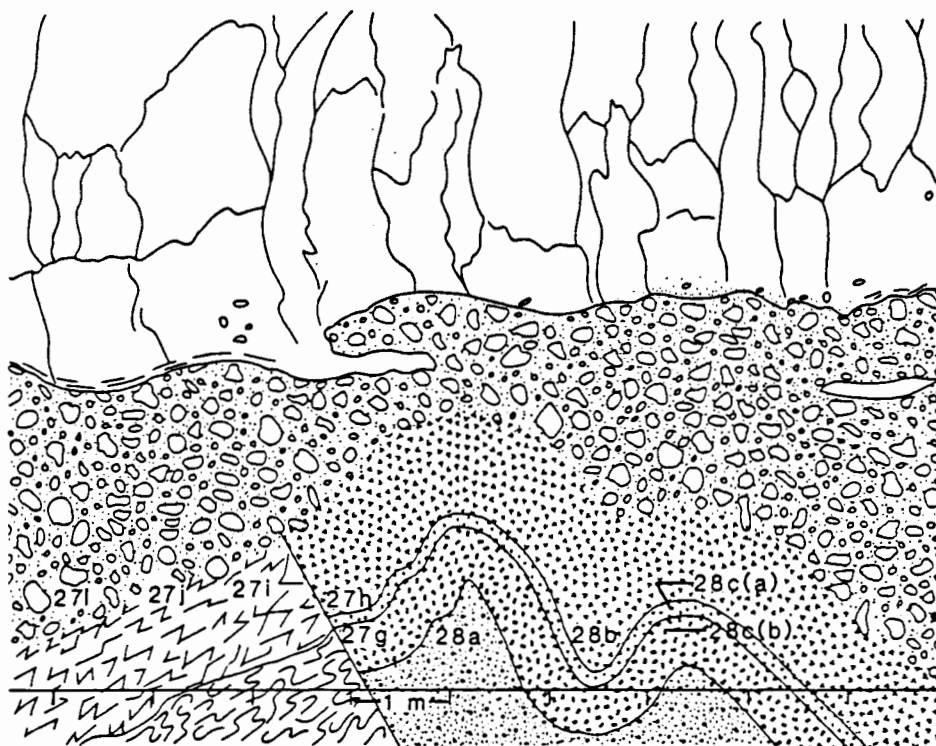
Figure 4 continued. Graphs showing the size range and mean (mm) for selected phases. The data used to plot these graphs is given in Table III.

The transition zone is composed of basalt spines (similar to those described by Orzol and Cummings (1986)) that are mantled with breccias whose clasts formed in situ. Figure 5 is a schematic diagram showing the distribution of the breccia types that mantle the basalt spines. The porosity of the spines consists of vesicles that occur within resorbed clasts and surround disseminated opaque domains. Outward from the spine, within the fused in situ breccias, the porosity consists of vesicles that surround incipient clasts and clast fragments, and vesicles within clasts. Outward toward the boundary with the flow-top breccia zone, within the loosely fused breccia, the porosity is dominated by interclast voids, and vesicles; diktytaxitic cavities in clasts are sparse. The modal range and size of cavities in the transition zone is included in Table III, and shown graphically in Figure 4.

The transition zone forms a retreating slope five to ten meters above the Grande Ronde River level (See Figure 3). The gradational boundary between the flow interior zone and transition zone is undulatory, up to seven meters in height from peak to trough in this outcrop. At its highest point, the boundary between the transition and the flow-top breccia zones occurs approximately at road level, 18 meters above the Grande Ronde River.

Flow-top Breccia Zone


The flow-top breccia zone ranges from two to 13 meters in




 FLOW-TOP BRECCIA ZONE

SEE FIGURE 3

 FUSED IN SITU BRECCIA/ TRANSITION ZONE

 STRONGLY TO LOOSELY FUSED BRECCIA

 INCIPIENT BRECCIA: CAVITIES AROUND CLASTS

 SPINE/ TRANSITION ZONE

 NON-BRECCIATED: VARIABLE OPAQUE TEXTURES

 AREA OF RESORBED CLASTS

Figure 5. Schematic diagram showing the distribution of the breccia types. Note: The breccia types are gradational and their distribution is inferred. Samples 27g, 27h, 27i, 27j, and 28b are found in the sample collection of the outcrop.

thickness and extends from the transition zone upward to the interflow contact zone (See Figure 3). The boundaries of this zone are loosely defined based on the presence and/or absence of certain clast types or textures. Breccia at the boundary between the flow-top breccia and transition zones may be clast-supported. Below the boundary in the transition zone, the clasts are fused together and mantle the basalt spines. Above the boundary in the flow-top breccia zone, the clasts are never fused. Therefore, the boundary of the flow-top breccia zone with the transition zone is where the clast-supported breccia changes from being dominantly fused to non-fused.

The boundary between the flow-top breccia zone and the interflow contact zone is defined on the presence of clast fragments which were generated during the emplacement of the superjacent flow. This boundary occurs up to four meters above road level at the northeast end of the outcrop and is locally below road level at the southwest end of the outcrop.

The porosity in the flow-top breccia zone is of three types including interclast voids, vesicles, and diktytaxitic cavities. The predominant type is interclast voids. Vesicles and diktytaxitic cavities are the porosity within clasts. The modal and size range of cavities is included in Table III and is shown graphically in Figure 4.

Interflow Contact Zone

The interflow contact zone encompasses the interflow contact

itself, and those portions of the outcrop where the textures and fabrics reflect the dynamic interaction between the contemporary surface of the analog flow, and the advancing superjacent flow. The interaction is manifested as tongues and lenses of basalt from the superjacent flow that have invaded the flow-top breccia, clasts shed from tongues and lenses mixed with flow-top breccia, and tree molds and pipe vesicles in the base of the superjacent flow (Figure 3). The boundaries against adjacent zones are gradational.

The interflow contact itself is undulatory, and the contact undulations have a maximum relief of three meters. The undulations do not appear to have a regular periodicity, but are related to the positioning of the invasive tongues. The invasive tongues occur in the troughs of the undulations (Figure 6). The interflow contact occurs up to six meters above road level at the northeast end of the outcrop, and occurs below road level at the southwest end of the outcrop (See Figure 3).

The interflow contact zone is composed of non-brecciated and brecciated parts. The porosity in the brecciated part is similar to that in the flow-top breccia zone. The porosity in the non-brecciated part consists of vesicles, pipe vesicles, platy joint-related fractures, and tree molds. The vesicles may be rounded or are broad and flattened parallel to the plane of platy jointing. The modal and size range of cavities is included in Table III, and is shown graphically in Figure 4. The pipe vesicles are up to six centimeters in diameter, occur up to 0.9 meters from the base of



Figure 6. Interflow contact showing an invasive tongue (center of photograph) developed in the trough of an undulation. For scale, the distance from road level to peak of the undulation is 4.5 meters.

the superjacent flow, may exceed 30 centimeters in length, and are steeply plunging to vertical. The joint-related fractures are most commonly oriented in planes parallel to the interflow contact. Tree molds with or without fillings are common at the interflow contact and within the superjacent flow up to 30 centimeters from the base. The largest molds average 14

centimeters in diameter. Attenuated vesicles may occur in groupings concentric to tree molds.

SUPERJACENT FLOW

The superjacent flow is up to 14 to 15 meters thick, and is composed of a flow interior and flow-top breccia zone.

Flow Interior Zone

The flow interior zone of the superjacent flow forms a vertical cliff above the flow-top breccia and interflow contact zones. The flow interior is composed of a 0.1 to one meter platy jointed base, followed by two to three meters that are massive to irregularly jointed, and 10 to 11 meters of colonnade (Figures 3 and 7). A distinct entablature is lacking. The platy jointed base is sparsely vesicular to vesicular. Broad flattened vesicles are oriented parallel to the jointing plane. The colonnade consists of broad tapering columns that are two to three meters wide. The basalt is non-vesiculated to vesiculated. Vesicles in the lower portion of the colonnade are flattened and are oriented in horizontal planes parallel to the flow base. The upper portion of the colonnade contains rounded vesicles, that increase in size and abundance upward towards the scoriaceous flow-top and flow-top breccia. The flow interior zone is gradational with the flow-top breccia zone over two to three meters.

The porosity consists predominantly of joint-related fractures; vesicles are a very minor contribution to the total

porosity. The modal and size range of cavities is given in Table III, and is shown graphically in Figure 4.

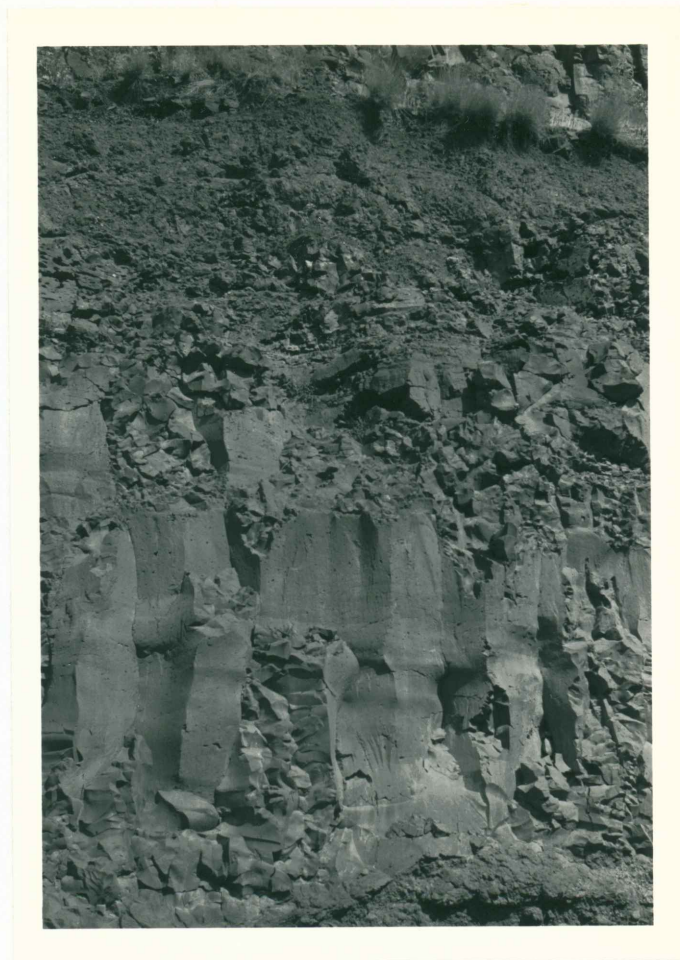


Figure 7. Flow interior and flow-top breccia zones of the superjacent flow. Nearly the entire flow thickness (12 to 13 meters) is shown in this photograph.

Flow-top breccia zone

The flow-top breccia zone forms a retreating slope above the vertical cliffs of the flow interior zone. The flow-top breccia zone is approximately one meter thick, and is composed

of a scoriaceous flow-top that grades into a flow-top breccia (Figure 3). A red-orange saprolite is locally present in the upper one third of the flow-top breccia zone. The breccia is composed of scoriaceous lapilli-size clasts that are orange-red in color. The flow-top breccia zone of the superjacent flow is rather thin and inconspicuous, and composed of scoria or scoriaceous clasts, in contrast to the flow-top breccia zone of the analog flow. The porosity consists predominantly of interclast voids and scoriaceous cavities. The superjacent flow thickness and internal structures and textures described are consistent with Type I Grande Ronde Basalt flows defined by Long and Wood (1986).

CHAPTER III

PRECIPITATED SECONDARY MINERALS

Secondary minerals occur as replacement and precipitated phases in all flow zones excepting the flow interior zone of the superjacent flow. Secondary minerals may occur as replacements of the primary mineral assemblage and as precipitated secondary minerals that occur in 1) vesicles and diktytaxitic cavities, 2) interclast voids, and 3) cooling fractures and joints in the base of the superjacent flow. The precipitated phases and their patterns in vesicles and diktytaxitic cavities show greater diversity than the latter two occurrences of precipitated phases or replacement phases, and are thus more suitable to this study which relates secondary minerals to changing solution composition.

Clay minerals, zeolites, silica minerals, and a carbonate, compose the precipitated secondary mineral suite in vesicles and diktytaxitic cavities. Clay minerals include smectite and celadonite; zeolites include clinoptilolite, phillipsite, chabazite, and two unidentified zeolites; silica minerals include quartz, chalcedony, and opal-CT, and the carbonate is calcite. Firstly, the individual secondary minerals in the suite will be described, and secondly, the mineral parageneses will be presented within the framework of flow zones.

CLAY MINERALS

Various colors of clay minerals occur as

- 1) linings parallel to the surfaces of vesicles or diktytaxitic cavities,
- 2) geopetal fabrics (horizontal layers and/or surfaces), and
- 3) vesicle and diktytaxitic cavity fillings.

Color is the main characteristic used for differentiating clay minerals in hand samples. Brown, yellow, olive green, white, and blue-green are the observed colors and Table IV summarizes the clay minerals according to these colors. The color of geopetal fabrics and fillings in thin section is fairly uniform and coincides with the color in hand sample. For parallel linings only the outer surface color can be discriminated in hand sample. Microscopic examination of these parallel clay linings commonly shows layers of clay minerals of different colors. Microscopic examination of fillings and geopetal fabrics shows that they commonly develop on parallel linings. Table IV includes the range of colors observed in thin section, other optical properties of the clay minerals, and the occurrences of the clay minerals of the five main color designations.

Clay mineral identification is in the preliminary stage of investigation. X-ray analysis of randomly oriented mounts prepared from separates of brown, olive green, and blue-green clay has been performed. In addition, sequential x-ray diffraction analysis of an untreated, ethylene glycolated, and heated (550° C for 1 hr) oriented mount of blue-green clay has been performed.

TABLE IV
SUMMARY OF CLAY MINERALS

COLOR	:	Brown	:	Yellow	:	Olive Green	:	White	:	Blue-green	:
CRYSTAL HABIT	:	Foliated, botryoidal, fibriiform and massive.	:	Foliated, massive and botryoidal.	:	Massive, foliated and arborescent (stellate cross-section).	:	Massive.	:	Tabular and fibriiform.	:
CRYSTAL FORM	:	Indeterminate for all clay minerals.									
OPTICAL PROPERTIES											
Color	:	Green-yellow, pale yellow, orange, red, brown and black layers. Commonly gradational.	:	Discrete green-yellow to yellow-green and pale olive green to green layers. Commonly gradational.	:	Green-yellow, yellow-green to pale green and olive green to green layers. Commonly gradational.	:	Colorless, muddy, pale green and pale brown layers.	:	Yellow-green to olive green, green and blue-green layers.	:
Transparency	:	All are translucent.									
Pleochroism	:	Slow direction brown. Fast direction yellow.	:	Non-pleochroic	:	Non-pleochroic	:	Non-pleochroic	:	Slow direction blue-green. Fast direction yellow-green.	:
Birefringence	:	Birefringence = .025 if interference colors are not masked.	:	Birefringence = .025	:	Birefringence = .025 if interference colors are not masked.	:	Interference colors are masked.	:	Birefringence = .013 if interference colors are not masked.	:
Indicatrix and optic sign	:	Indeterminate for all clay minerals.									
Sign of elongation of foliae	:	Foliae are commonly positive and less commonly negative.	:	Foliae are commonly positive and less commonly negative.	:	Foliae are commonly positive and less commonly negative.	:	Not foliated	:	Not foliated	:
OCCURRENCE	:	Parallel linings (.04-.70 mm), fillings, and geopetal fabric. Filaments (.03 mm dia).	:	Parallel linings (.01-.18 mm), fillings, and geopetal fabric.	:	Parallel linings (.07-.51 mm), fillings, and geopetal fabric. Arborescent tubes (.35-.40 mm dia).	:	Fillings.	:	Fillings, parallel linings (.7 mm), filaments (.3 mm dia), tabular crystals (.02-.03 mm long).	:

Indexed diffractograms for the randomly oriented clay minerals are given in Figure 8.

Analysis of the clay minerals is incomplete for all but the blue-green clays, but tentative identification of the clays is possible. The brown and olive green clays have a very strong, broad peak corresponding to a basal (001) d-spacing of 14.7 Å and are thus smectites. Furthermore, these clays also have in common a strong, broad asymmetrical peak with a d-spacing of 4.43 Å that corresponds to the (110) and (020) planes of montmorillonite (JCPDS 13-0135). The diffractogram of the brown clay was run beyond $60^\circ 2\theta$ to check the spacing of the smectite (060) plane. Two very weak, broad peaks at 1.52 Å and 1.49 Å may correspond respectively to nontronite (JCPDS 2-0008) and montmorillonite (JCPDS 13-135). Oriented clay mineral analysis of the brown and olive green clays should assist further identification of the smectites.

The blue-green clay is a 10 Å (9.81-9.94 Å) clay (Figure 8). The d-spacing and relative intensity of peaks from the diffractogram of the randomly oriented mount correspond well to celadonite (JCPDS 17-0521). The d-spacing of the basal (001) peak does not shift when glycolated or heated, nor does the peak intensity significantly change, thus suggesting an illite-type clay. The diffraction patterns of the randomly oriented blue-green clay, coupled with the results from the oriented clay mineral analysis confirms its identity as an illite-type clay, or more precisely, celadonite.

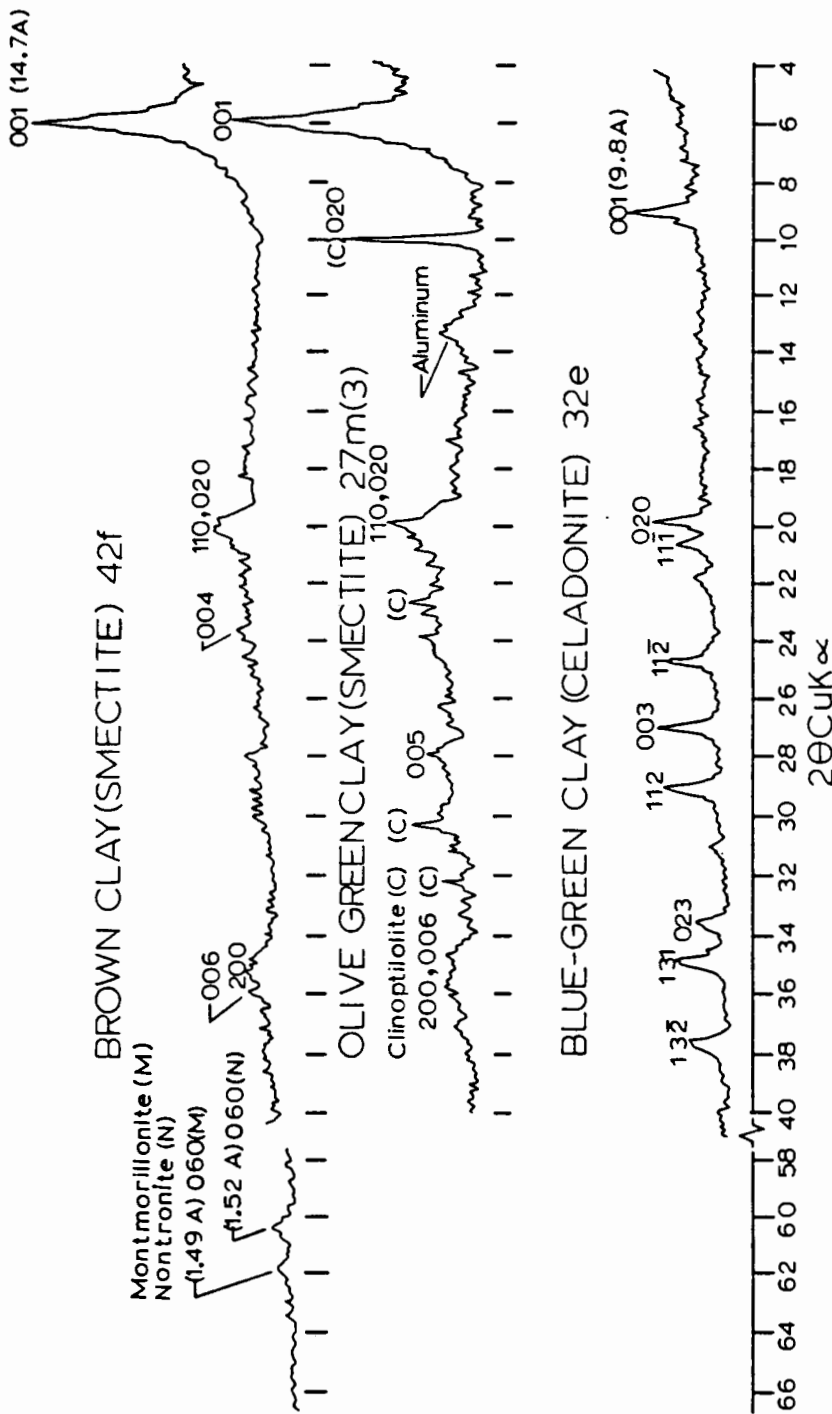


Figure 8. Indexed diffractograms for the randomly oriented clay minerals. The hkl values shown for nontronite, montmorillonite, clinoptilolite, and celadonite are respectively from JCPDS 2-0008, JCPDS 13-0135, JCPDS 22-1236, and JCPDS 17-0521.

Target- CuKα/ Filter- Ni/ Soller slit- MR
 Beam Tunnel- 1°/ Detector slit- .1°/ Rate
 meter- 500 cps/ Time constant- 2.0/ Scan
 speed- 2(2θ/min)/ Chart speed- 1 in/ min.

As indicated in Table IV, the crystal habit and optical properties of the brown, and olive green clays are consistent with smectite, whereas the crystal habit and optical properties of the blue-green clays are consistent with celadonite. The yellow and white clays are tentatively identified as smectite, based on their crystal habits, optical properties (primarily birefringence), and physical characteristics (expands if wetted with water).

Brown Clays

The brown clays include layers in the color range shown in Table IV. These clays commonly occur in parallel linings, and the usual sequence of linings from the vesicle wall inward (early to late) is green-yellow foliated, pale yellow massive (nonfoliated), orange massive to foliated, and brown massive to foliated. The total range in thickness of the sequence is indicated in Table IV.

Foliated linings are typically thin (.01-.18 millimeter) in comparison to massive linings (up to .40 millimeter). The foliae are oriented perpendicular to the vesicle wall (Figure 9), and commonly show a positive sign of elongation. The interference colors are marked where foliation is pronounced, and masked where foliation is absent. In cross-polarized light, the interference colors of foliated linings highlight the shapes of vesicles and outlines massive linings (Figure 10). The boundary between an adjacent foliated and massive lining is typically sharp, whereas the boundary between two adjacent massive linings is gradational (Figure 11).

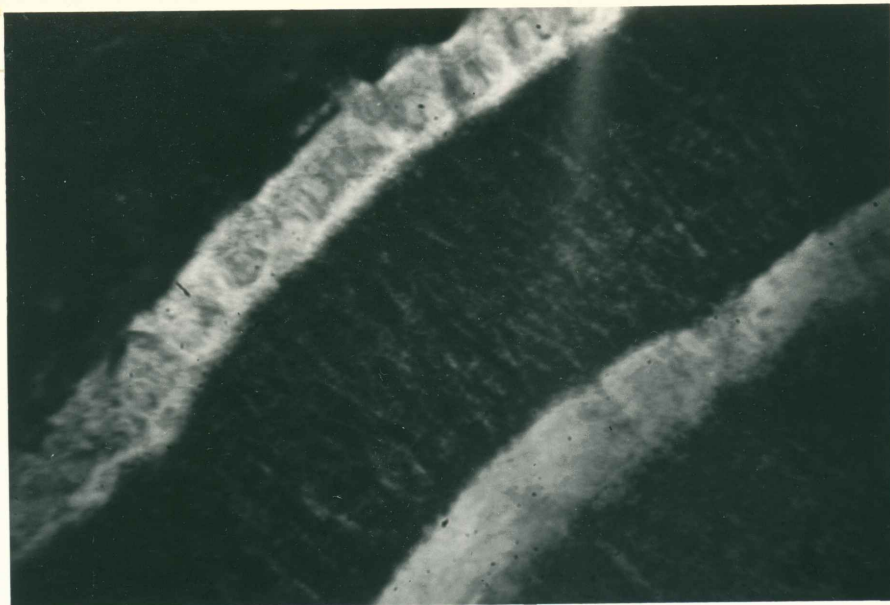


Figure 9. Close-up of brown clay linings showing the perpendicular orientation of the foliae relative to the vesicle wall located in the upper left-hand corner of the photomicrograph. Sample 22g, crossed-polars, field of view .32 millimeters.

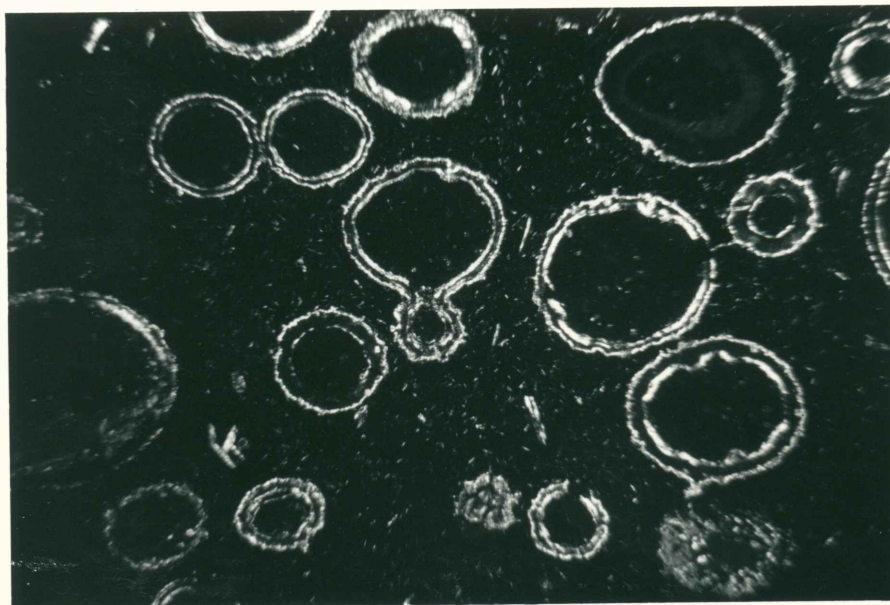


Figure 10. The interference colors of foliated linings highlight the shapes of vesicles. Sample 3g, crossed-polars, field of view 5.2 millimeters.

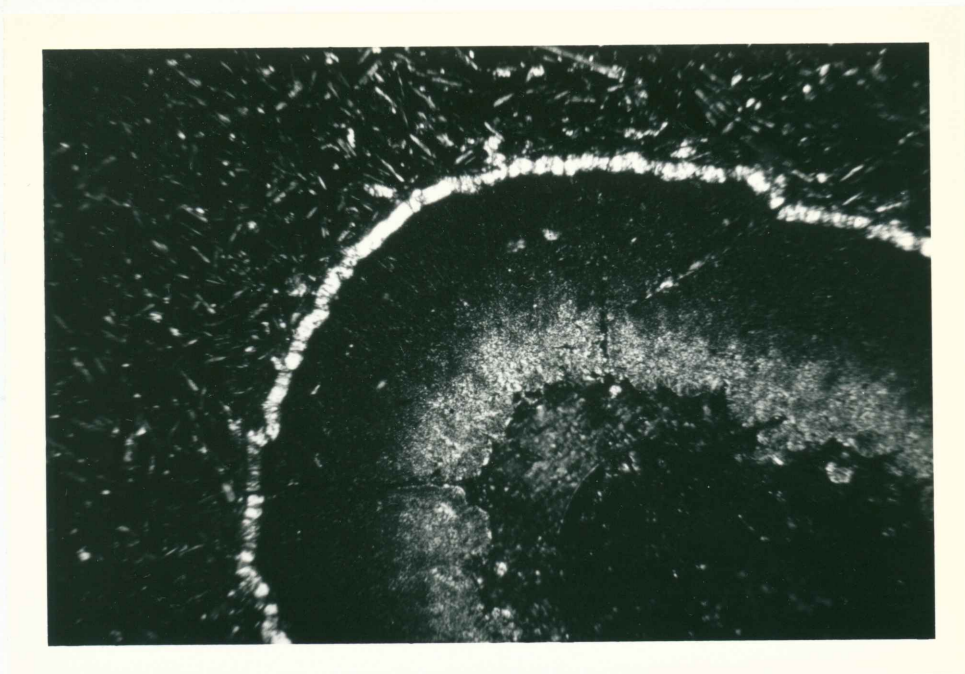


Figure 11. The boundary between the thin, birefringent foliated lining and the thick massive linings is sharp, whereas the boundary between the massive linings is gradational. Sample 24h, crossed-polars, field of view 1.3 millimeters.

Brown clay linings commonly develop a botryoidal crystal habit as shown in cross-sectional view in the photomicrograph in Figure 12, and plane view in the S.E.M. photograph in Figure 13. Also, clay linings may gradually become coarser grained (Figure 14) so that individual pleochroic grains are discernible under the petrographic microscope.

The geopetal fabric is commonly developed in brown clays as illustrated in the photomicrograph in Figure 15. In this example two neighboring connected vesicles are partly filled with smectite and the remaining portions of the vesicles are lined by clinoptilolite. In such vesicles the clinoptilolite linings



Figure 12. Cross-sectional view of botryoidal vesicle linings. The vesicle interior is unoccupied by secondary minerals. Sample 27n, plane-polarized light, field of view 1.3 millimeters.

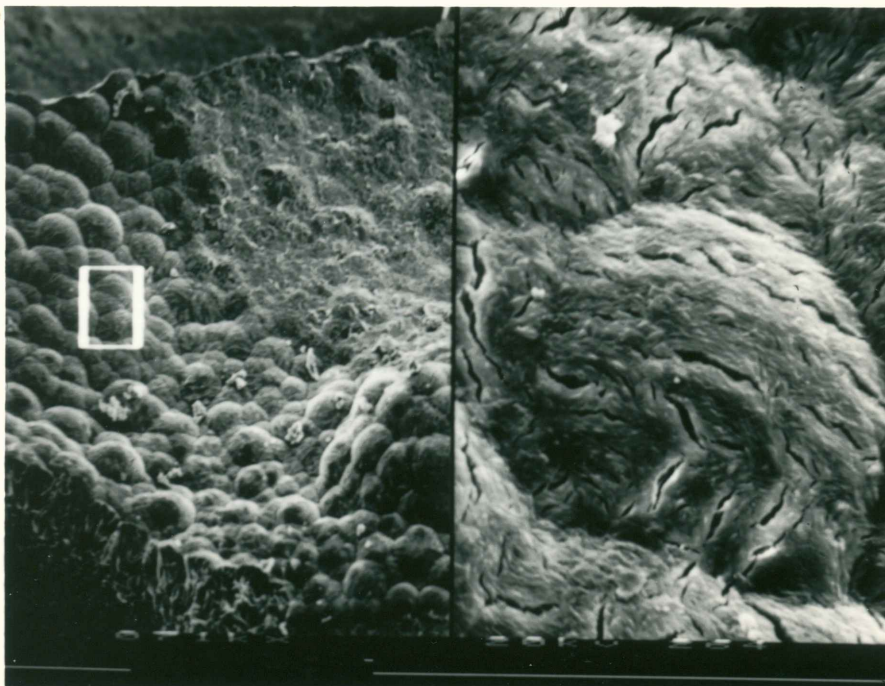


Figure 13. S.E.M. plane view of brown clay botryoidal linings. Individual botryoids are .080 millimeter in diameter. Sample 65a(1).



Figure 14. The brown clay linings coarsen toward the center of the vesicle. The vesicle interior is unoccupied by secondary minerals. Sample 22g, crossed-polars, field of view 1.3 millimeters.

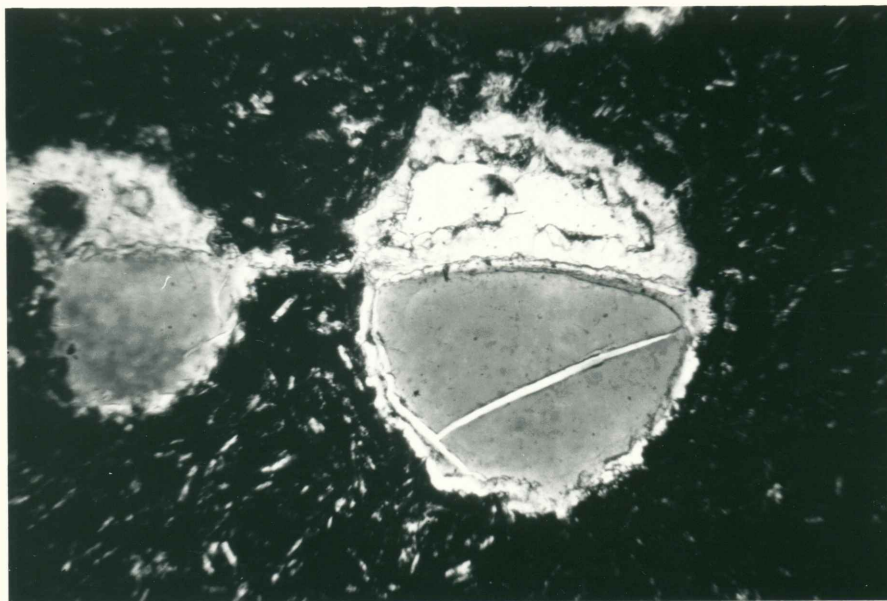


Figure 15. Geopetal fabric in two interconnected vesicles. The lower portion of the vesicle is filled with brown clay while the upper portion is lined by clinoptilolite. The boundary between the clay and clinoptilolite is convex-up. Sample 27h, plane-polarized light, field of view 1.3 millimeters.

superpose the smectite fillings and the surface between the linings and fillings are meniscus-shaped. In samples of clasts having vesicles that show these features the meniscus surfaces are all parallel to the same plane indicating a geopetal fabric pervades the sample. Figure 16 is a photomicrograph showing a filling developed upon parallel linings.

The brown clays may develop a filiform crystal habit, as shown in the photomicrograph in Figure 17, in which thread-like forms (.03 millimeter diameter) of orange-brown clay are embedded in blue-green clay.

Yellow Clays

The yellow clays include layers in the color range indicated in Table IV. Parallel linings are the most common occurrence. The sequence of linings from the vesicle wall inward (early to late) is green-yellow to yellow-green foliated, and pale yellow massive, similar to the early clay linings of the sequence in the brown and olive green clays. However, the yellow clays conspicuously lack the orange and brown clay linings present in the brown clay sequence, and the green to olive green linings present in the olive green clay sequence.

Olive Green Clays

Fillings and geopetal fabrics are most commonly formed of olive green clays. In thin section, the fillings and geopetal fabrics are colored various shades of green and yellow, and



Figure 16. Black clay filling on parallel linings of clinoptilolite and brown clay. Sample 42f, plane-polarized light, field of view 5.2 millimeters.

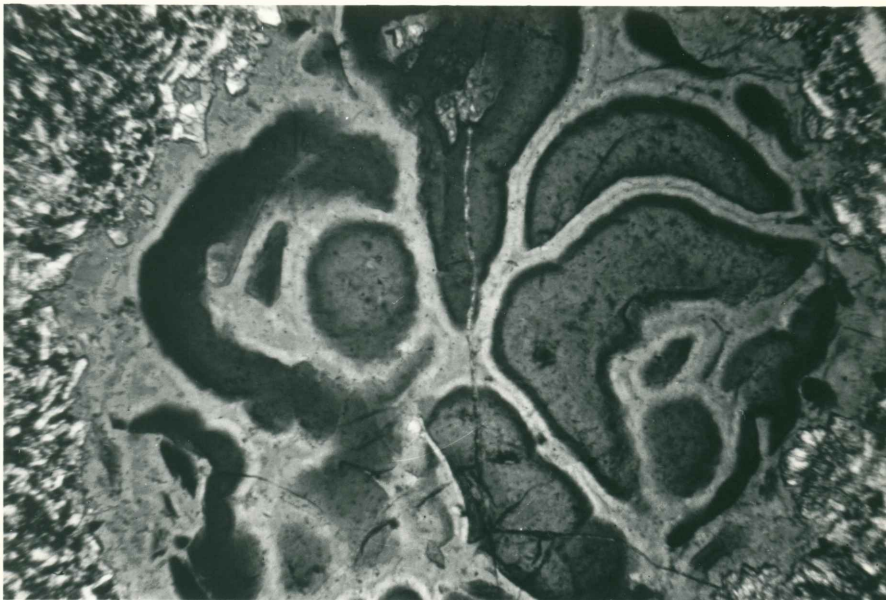


Figure 17. Brown filiform clay embedded in blue-green clay. Sample 83a, plane-polarized light, field of view 1.3 millimeters.

usually are developed on a substrate of parallel linings. The general color sequence of the parallel linings from the vesicle wall inward (early to late) is green-yellow foliated, yellow-green to pale green massive, and olive green to green massive. The range in total thickness of the linings is given in Table IV. The linings are commonly intervened by gray to black linings that may show dendritic textures (Figure 18). The early foliated linings are thin (.01-.09 millimeters) and discrete in comparison to the thick (.07-.51 millimeters), gradational massive linings that occur later in the sequence. The interference colors are marked in the foliated linings and masked in the massive linings. These linings are not commonly botryoidal, nor do they coarsen into discernible pleochroic grains.

Olive green clays may develop into an arborescent crystal habit as shown in the S.E.M. photomicrograph in Figure 19. Cores of olive green foliated clay (stellate in cross-section) are surrounded by massive pale green clay. In thin section, the cores are yellow-green, foliated, and the birefringence is consistent with smectite. The clays surrounding the cores are similar to the very fine-grained massive yellow clay linings. The arborescent clay features are .35-.40 millimeters in diameter (Table IV).

White Clays

The white clays are colorless, muddy, pale green or pale brown in thin section, and lack any distinctive crystal habits or optical properties. White clays commonly occur as fillings, and



Figure 18. Olive green clay linings intervened by black dendritic linings. The vesicle interior is occupied by extraneous clay linings. Sample 22g, plane-polarized light, field of view 1.3 millimeters.

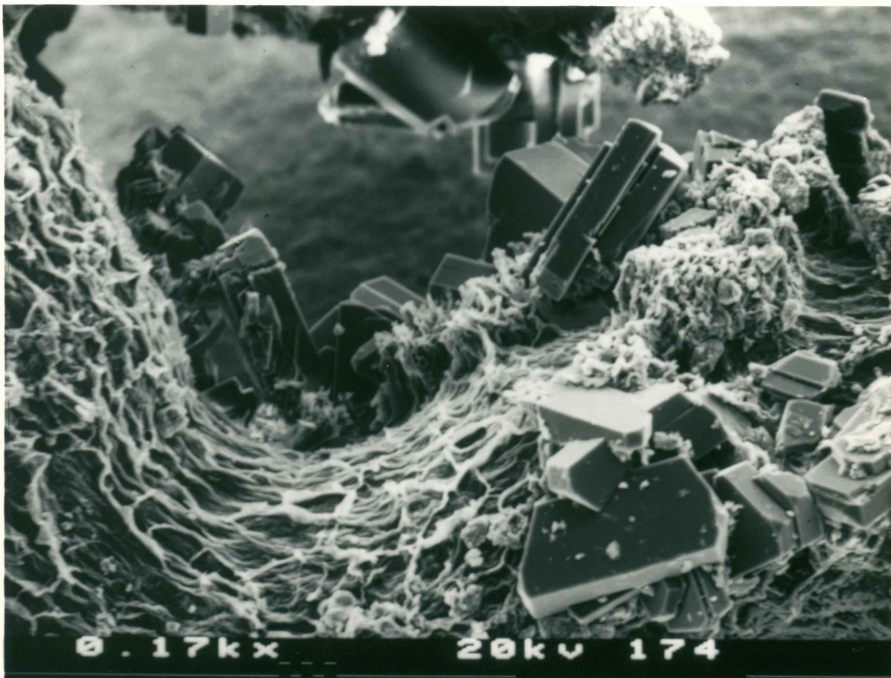


Figure 19. S.E.M. photograph of arborescent olive green clays with some clinoptilolite adhering to the surface. The clinoptilolite crystal in the foreground is about .100 millimeter long. Sample 3j(4).

rarely as parallel linings.

Blue-green Clays

Blue-green clays, celadonite, are composed of layers in the color range indicated in Table IV. The sequence of parallel linings from the vesicle wall inward (early to late) is yellow-green to olive green foliated, green massive, and blue-green massive to tabular. The range in total thickness of the sequence is given in Table IV. The early lining is thin, foliated and has discrete boundaries in comparison to the thick, very gradational, later massive linings. The interference colors of the clay linings are masked by their green body color, though it is possible to discern the interference colors in the coarser grained parts. The early foliated lining is more strongly birefringent (.025) than the later massive linings (.013). The extinction of the clays occurs in sweeping fibrous patterns. The blue-green lining may coarsen into distinct tabular pleochroic grains. The tabular habit of the individual crystals is shown in the S.E.M. photomicrograph in Figure 20. The size of these grains and their partial pleochroic scheme is indicated in Table IV. These clays are not generally botryoidal.

The above sequence is varied by deleting one or more of the linings, particularly the early discrete foliated lining. Also, the massive gradational lining(s) may develop thick (.7 millimeter) tufted linings in which the inner surface is no longer parallel to the shape of the vesicle (Figure 21). Fillings are



Figure 20. S.E.M. photograph of celadonite showing the tabular habit. The field of view in the enlarged inset is .02 millimeter. The spheroidal object in the left portion of the photograph is an opal-CT lepisphere. Sample 5b(2).



Figure 21. Non-parallel tufted linings of celadonite. The vesicle interior is occupied primarily by chalcedony. Sample 32e, plane-polarized light, field of view 1.3 millimeters.

presumably composed of a massive gradational lining (or linings) that developed inward until the vesicle was filled. No evidence of horizontal layering (geopetal fabrics) has been observed in the blue-green clays.

The filiform crystal habit is a variation to the above scheme. Rather than occurring in parallel linings, convoluted hair-like filaments of clay (.3 millimeter diameter) are embedded in fillings of chalcedony and quartz (Figure 22).

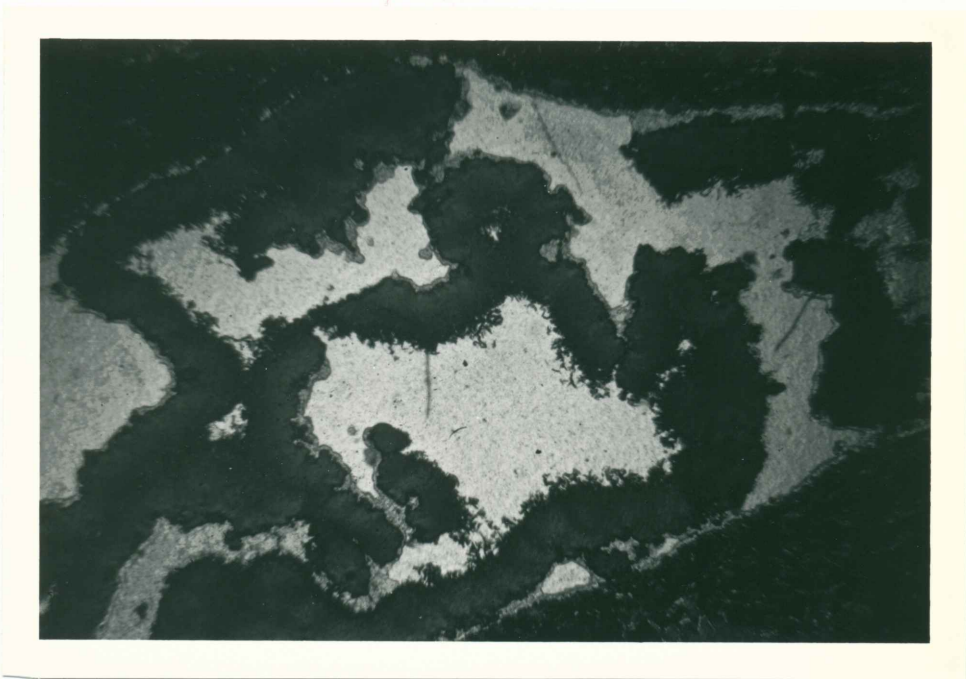


Figure 22. Convoluted filaments of celadonite embedded in fillings of chalcedony and quartz. Sample 38d, plane-polarized light, field of view 5.2 millimeters.

Zeolites

Zeolites occur as single crystals and crystal aggregates in vesicles, and rarely occur in diktytaxitic cavities. Zeolite

crystal aggregates develop linings that parallel the shape of the vesicle or secondary mineral substrate, radiating hemispherical forms, and encrustations on arborescent and filiform clay minerals.

X-ray diffraction analysis has been performed on randomly oriented mounts prepared from zeolite separates. The indexed diffractograms are included in Figure 23, and the corresponding d-spacings and intensities of peaks are compared with published x-ray powder diffraction data (Passaglia, 1970; JCPDS, 1974; Sheppard and Gude, 1973) in Table V. The zeolites are identified as heulandite group, phillipsite, and chabazite group zeolites based on the likeness of their diffraction patterns to published data for zeolites from these groups.

The heulandite group zeolite has been heat treated, and analyzed by XRD according to the procedure of Boles (1972) to test for the appearance of the contracted phases I and B, and specifically to determine the type of heulandite group zeolite. The x-ray powder diffraction data from the thermal analyses in Table VI show that during testing no contracted phases appeared, and the (020) peak remained stable with only a minor decline in the peak intensity even after heating at 450° C for 15 hours (under these conditions heulandite becomes amorphous to x-rays). The results of these analyses indicate the zeolite is clinoptilolite, a type 3 heulandite group zeolite (Boles, 1972).

X-ray diffraction analysis has not been performed on two species of suspected zeolites due to their small size, and the

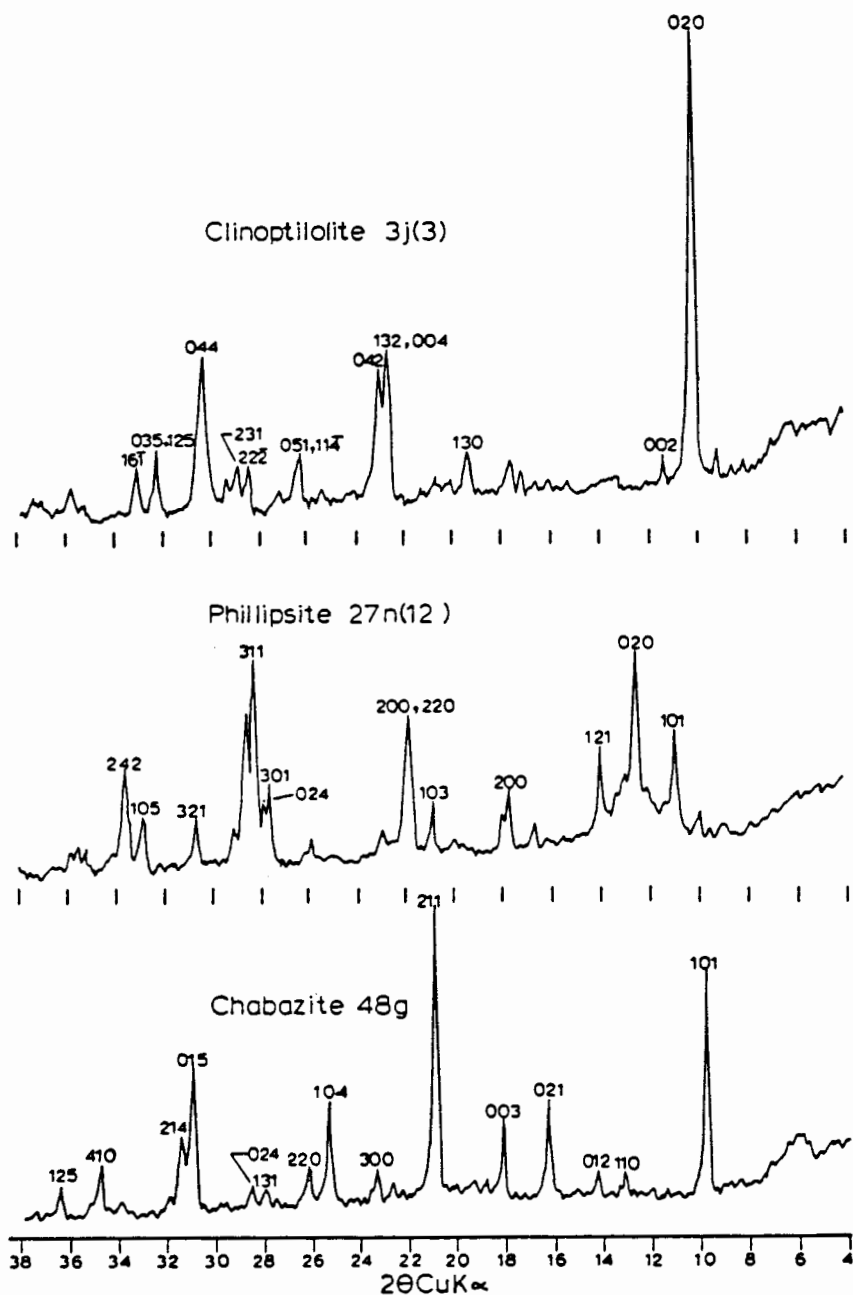


Figure 23. Indexed diffractograms of the zeolite minerals. The hkl values shown for clinoptilolite, phillipsite, and chabazite are respectively from JCPDS 22-1236, Sheppard and Gude (1973), and Passaglia (1970).

Target- $CuK\alpha$ / Filter- Ni/ Soller slit- MR
 Beam Tunnel- 1° / Detector slit- $.1^\circ$ / Rate
 meter- 500 cps/ Time constant- 2.0/ Scan
 speed- $2(2\theta/min)$ / Chart speed- 1 in/ min.

TABLE V
ZEOLITE COMPARISONS WITH PUBLISHED DATA

CHABAZITE	PHILLIPSITE	CLINOPTILOLITE
48g(1)/Passaglia (1970)	27n(12)/Sheppard and Gude (1973)	3j(3)/JCPDS 22-1236
d(A) (I/I ₀)/ d(A) (I/I ₀)	d(A) (I/I ₀)/ d(A) (I/I ₀)	d(A) (I/I ₀)/ d(A) (I/I ₀)
9.11 (080)/ 9.26 (070)	8.03 (053)/ 8.14 (025)	8.83 (100)/ 8.92 (100)
6.75 (009)/ 6.85 (022)	7.01 (086)/ 7.07 (071)	7.75 (007)/ 7.97 (004)
6.23 (010)/ 6.30 (008)	6.32 (044)/ 6.33 ()	4.69 (010)/ 4.65 (014)
5.43 (040)/ 5.51 (032)	5.30 (014)/ 5.34 (030)	3.93 (036)/ 3.96 (055)
4.89 (030)/ 4.96 (038)	4.97 (030)/ 4.97 (043)	3.86 (031)/ 3.90 (055)
4.26 (100)/ 4.29 (100)	4.24 (023)/ 4.26 (014)	3.38 (011)/ 3.48 (004)
3.91 (008)/ 3.957 (005)	4.05 (067)/ 4.07 (028)	3.13 (011)/ 3.17 (014)
3.51 (040)/ 3.549 (047)	3.22 (039)/ 3.22 (064)	3.09 (008)/ 3.07 (008)
3.39 (015)/ 3.427 (021)	3.19 (030)/ 3.16 ()	2.94 (037)/ 2.974 (080)
3.19 (009)/ 3.217 (010)	3.15 (100)/ 3.148 (100)	2.77 (016)/ 2.793 (015)
3.12 (010)/ 3.152 (011)	2.90 (023)/ 2.937 (035)	2.71 (011)/ 2.738 (035)
2.89 (050)/ 2.885 (022)	2.72 (028)/ 2.724 (025)	
2.84 (025)/ 2.864 (034)	2.66 (049)/ 2.669 (029)	
2.58 (020)/ 2.591 (011)		
2.46 (012)/ 2.481 (012)		

TABLE VI
THERMAL ANALYSIS OF CLINOPTILOLITE

SAMPLE: 50f

Conditions	d(020)	Relative Intensities
Before heating (1)	8.92 A	100
262° C for 0.5 hr (2)	8.83 A	65
262° C for 4.0 hr	8.83 A	95
450° C for 15.0 hr	8.83 A	55

Note: 1) Back-packed in a dimpled glass holder.
2) Stepwise heating with x-ray analysis between steps.

difficulty of physical separation from the adjacent secondary minerals. The crystal and optical characteristics of unidentified zeolite 1 suggests a heulandite group zeolite (Table VII); the characteristics of unidentified zeolite 2 are not distinct enough to allow identification.

Clinoptilolite

Clinoptilolite occurs as crystal aggregates and rarely as single crystals. Single crystals occur intergrown with opal-CT as shown in the S.E.M. photomicrograph in Figure 24. XRD analysis confirms that the zeolite is clinoptilolite.

The crystal aggregates occur as parallel linings, sheaves, and as encrustations on arborescent clays. Parallel linings, the most common occurrence of clinoptilolite, are shown in the photomicrograph in Figure 25. The range in thickness of these linings is indicated in Table VII.

The second most common occurrence of clinoptilolite is as sheaved aggregates shown on a brown clay mineral substrate in Figure 26. A S.E.M. photograph of these aggregates in Figure 27 shows the sheaved arrangement of crystals. The diameter of the aggregates is indicated in Table VII.

Clinoptilolite occurs least commonly as arborescent aggregates, shown in Figure 28. Examination of these aggregates with the S.E.M. shows clinoptilolite encrustations on arborescent clay cores (Figure 29). The characteristics of the clay cores have been given in Table IV, and are described in the clay mineral

TABLE VII
SUMMARY OF ZEOLITES

GROUP	:	Heulandite	:	Phillipsite	:	Chabazite	:	Heulandite ?	:	Indeterminate
TYPE	:	Clinoptilolite	:	Phillipsite	:	Chabazite	:	Unidentified 1	:	Unidentified 2
COLOR	:	Colorless	:	Colorless	:	Colorless, amber	:	Colorless	:	Yellowish
CRYSTAL HABIT	:	Platy, sheaved	:	Prismatic, blocky	:	Rhombohedral	:	Platy, radiating	:	Massive
CRYSTAL FORM (1) System	:	Monoclinic	:	Monoclinic	:	Trigonal	:	Monoclinic ?	:	Indeterminate
Space group	:	C2/m	:	P2 ₁ /m	:	R32/m	:	Indeterminate	:	Indeterminate
Point group	:	m	:	2/m	:	32/m	:	Indeterminate	:	Indeterminate
Cleavage	:	Perfect (010)	:	Good (010) and (100)	:	Poor {101} (1)	:	Indeterminate	:	Indeterminate
Twinning	:	None	:	Fourling twin and comp. planes (201) and (001). Eightling has 2 fourlings combined on {011}.	:	Twin planes {100}, {001} and comp. plane {101}.	:	Indeterminate	:	Indeterminate
Miller indices:		{100} {001} {101} {110} {101} {110} {101} {010} {110} {101} {012} {021} {101}								
OPTICAL PROPERTIES										
Color	:	All except unidentified zeolite 2 are colorless in thin section.								
Transparency	:	Transparent	:	Transparent	:	Transparent	:	Transparent	:	Transparent
Pleochroism	:	All are non-pleochroic.								
Birefringence	:	Birefringence = .006	:	Birefringence = .006	:	Birefringence = .007	:	Birefringence = .006	:	Birefringence = .008
Indicatrix and optic sign	:	Indeterminate	:	Biaxial (+)	:	Not in thin section	:	Indeterminate	:	Indeterminate
Orientation	:	As in Deer and others (1963).	:	$\gamma:Z = 38^\circ$ $\beta:X = 37^\circ$:	Not in thin section	:	Indeterminate	:	Indeterminate
Relief	:	All negative relative to adjacent secondary mineral phases excepting unidentified zeolite 2.								
OCCURRENCE	:	Parallel linings (.12-.37 mm), encrusts arborescent clays in shells .6-.8 mm dia, aggregates (1 mm dia). Single crystals (.2-.3 mm) long.	:	Single crystals (1-3 mm long).	:	Single crystals up to 1 mm greatest dimension. Crystals up to .5 mm long.	:	Radiating aggregates up to .5 mm radius. Crystals up to .5 mm long.	:	Irregular discontinuous linings or blebs up to .04 mm thick.
NOTES: (1) Crystal form data is from Frye (1974) and Zoltai and Stout (1984) except as noted. (2) Gottardi and Galli (1985).										

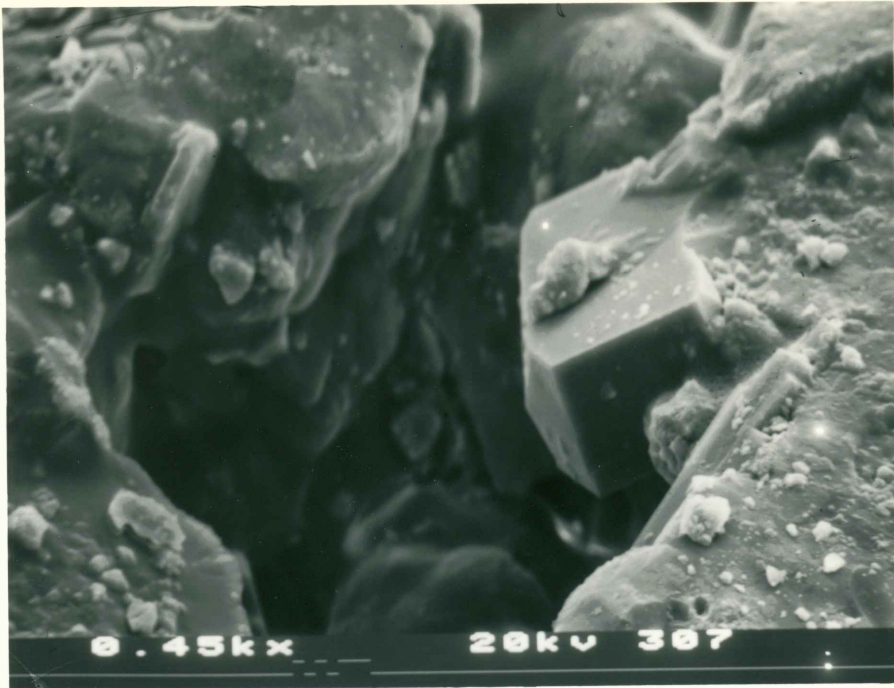


Figure 24. S.E.M. photograph showing clinoptilolite (right center) intergrown with opal-CT. The clinoptilolite crystal is approximately .09 millimeter in greatest dimension.



Figure 25. Parallel linings of clinoptilolite. The interior of the vesicle is unoccupied by secondary minerals. Sample 42e, plane-polarized light, field of view 1.3 millimeter.

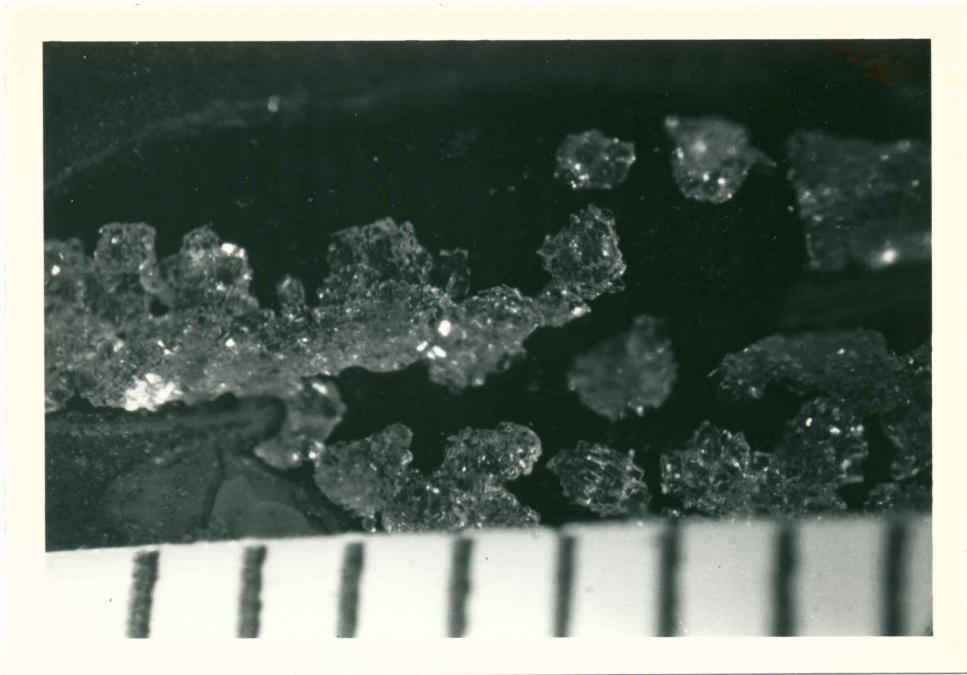


Figure 26. Sheaved aggregates of clinoptilolite on dark brown clay vesicle linings. Millimeter scale. Sample 65a.

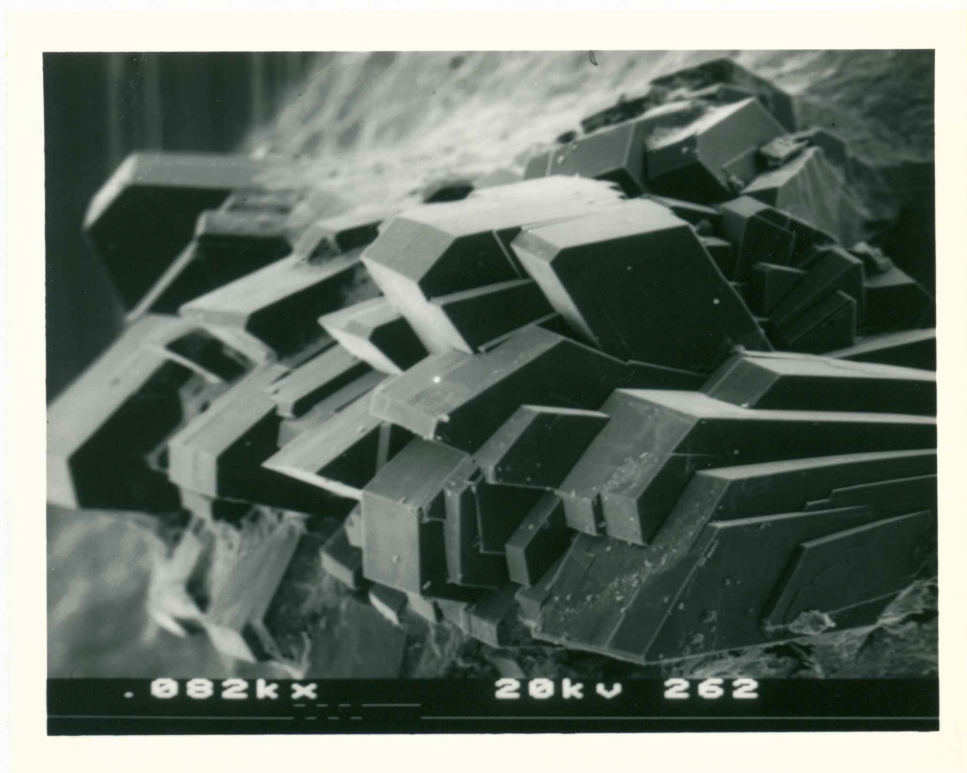


Figure 27. S.E.M. photograph of clinoptilolite aggregates showing the sheaved arrangement of crystals. Sample 65a(2), field of view 1.4 millimeters.

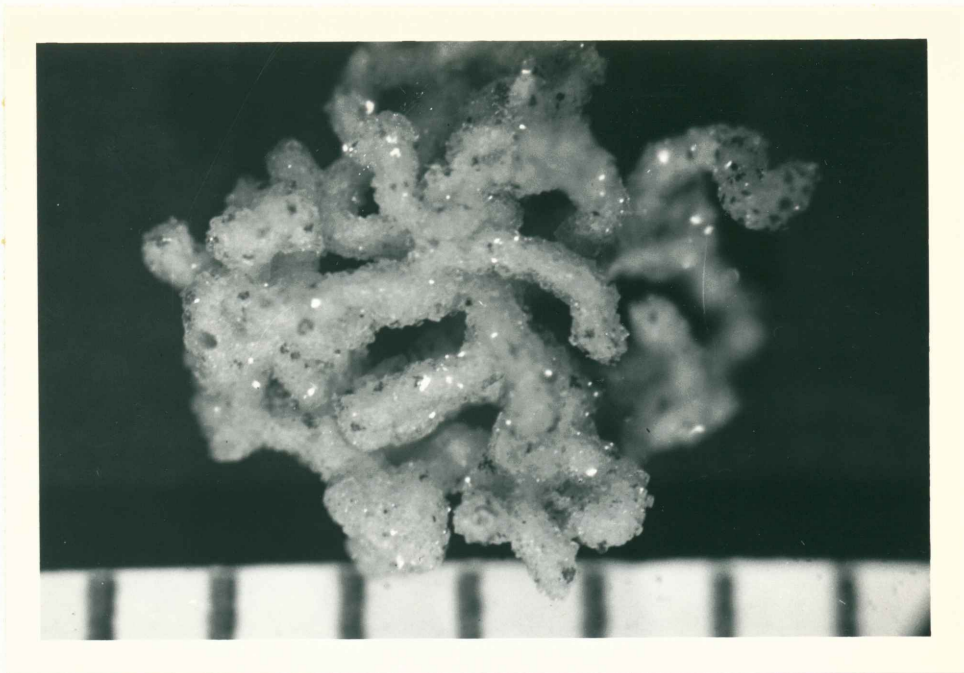


Figure 28. Clinoptilolite aggregates encrusting arborescent olive green clays. Millimeter scale. Sample 3j.

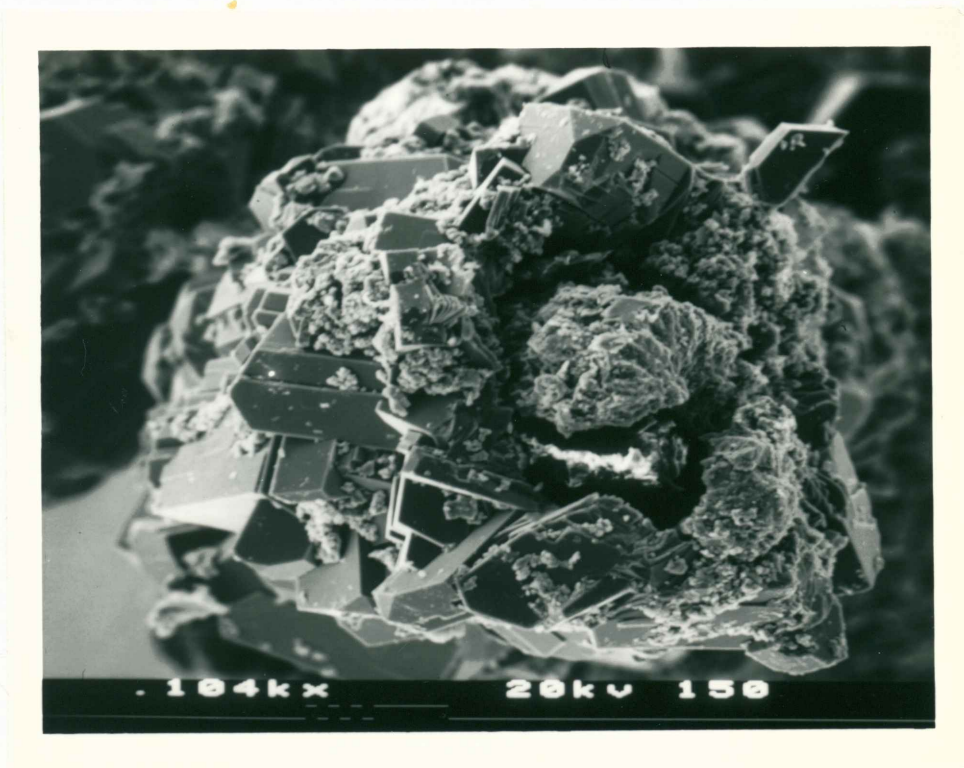


Figure 29. S.E.M. photograph showing how clinoptilolite encrusts the arborescent olive green clays (right center). Sample 3j, field of view 1.1 millimeters.

section. The total aggregate diameter is indicated in Table VII.

Clinoptilolite crystals are colorless, platy, and the largest crystals are .2-.3 millimeter long (Table VII). Diagnostic optical characteristics include low birefringence and negative relief relative to clay minerals (Table VII). The orientation of the principle indicies corresponds to heulandite/clinoptilolite as presented in Deer and others (1963).

The crystal form is also diagnostic. The monoclinic symmetry and perfect (010) cleavage are apparent in thin section and the S.E.M. photomicrograph shown in Figure 27. The individual crystal faces shown in the photomicrograph represent the form given by the Miller indicies indicated in Table VII. The crystal faces are smooth in most samples; however, a S.E.M. photomicrograph of one sample shows rough-textured faces and raised edges between faces (Figure 30).

Phillipsite

Phillipsite occurs as colorless single crystals and rarely in aggregates. At most, two to three crystals may be touching. Single crystals are either prismatic or blocky. Prismatic crystals are shown on a clinoptilolite substrate in the photomicrograph in Figure 31. Blocky crystals on a clinoptilolite substrate are shown in the S.E.M. photomicrograph in Figure 32. The range in crystal size is indicated in Table VII. Phillipsite is about an order of magnitude larger than clinoptilolite.

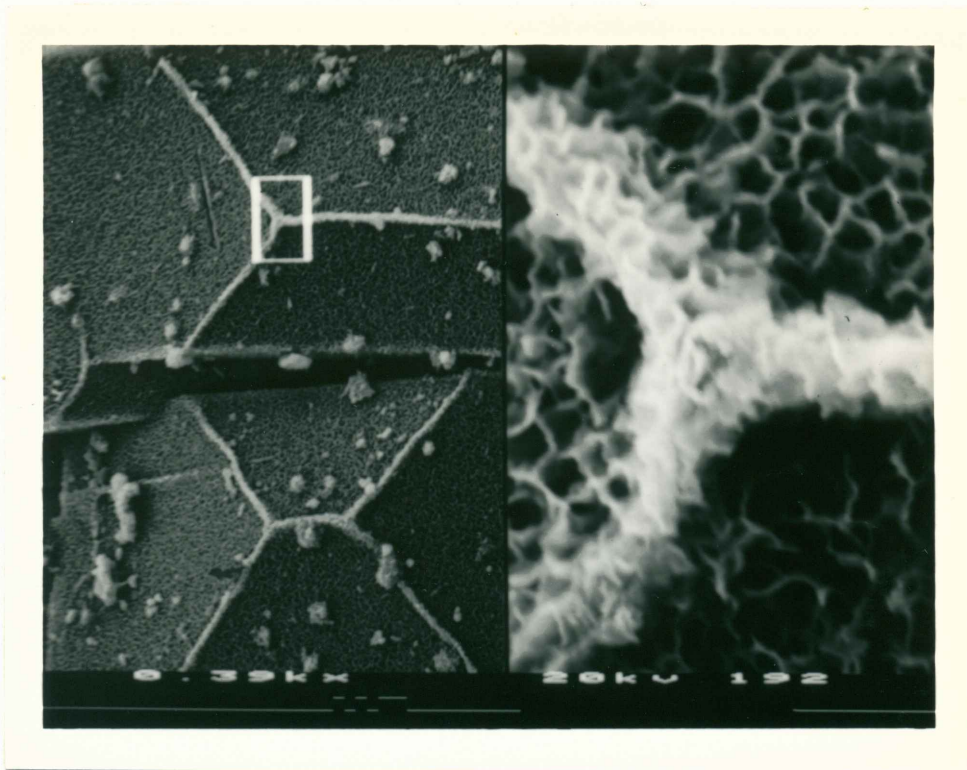


Figure 30. S.E.M. photograph of clinoptilolite showing rough-textured faces and raised edges between faces. The field of view in the enlarged inset is .013 millimeter. Sample 3g(11).



Figure 31. Prismatic crystals of phillipsite on clinoptilolite vesicle linings. Millimeter scale. Sample 26h.



Figure 32. S.E.M. photograph showing blocky (lamellar) phillipsite on a clinoptilolite substrate. Sample 3h(1), field of view 2.4 millimeters.

The occurrence of phillipsite is rare in comparison to clinoptilolite. Figure 33 is a photomicrograph of the one vesicle found in thin section that contains crystals of phillipsite. Phillipsite is distinguished from clinoptilolite by larger grain size (1 millimeter as opposed to .1-.3 millimeter), and optically by slightly higher birefringence (.007 as opposed to .006), and presence of twinning lamellae. Also, optic sign determination is possible for phillipsite (biaxial +) and not clinoptilolite due to the larger grain size. The principle indicies and optic plane have been oriented in one of the crystal grains shown in Figure 33. The angles between the principle indicies and vibration axes

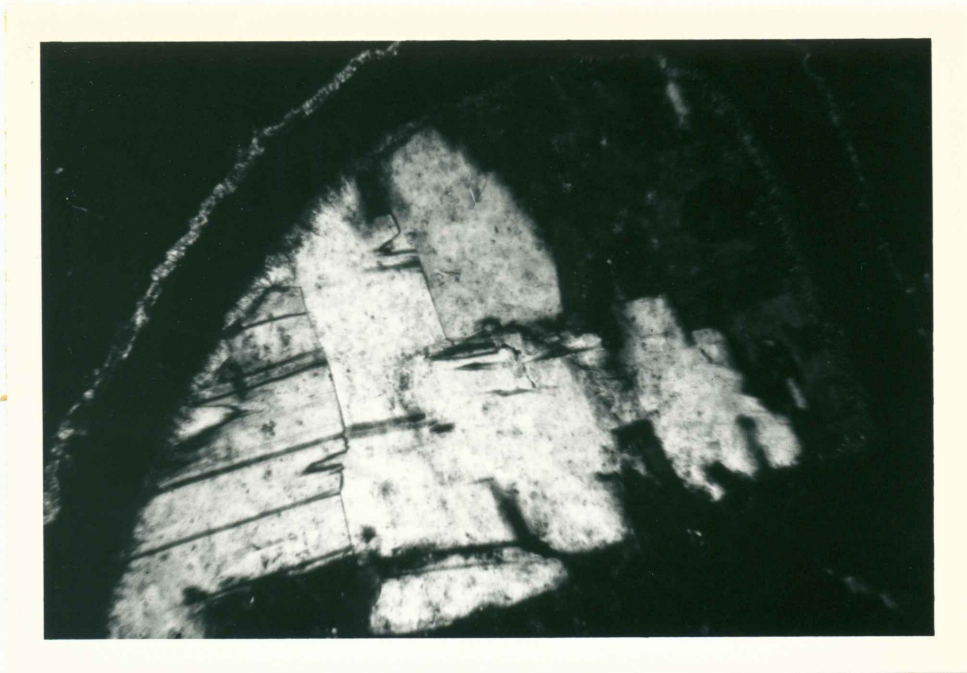


Figure 33. Phillipsite on a brown clay vesicle lining. Sample 49b, crossed-polars, field of view 1.3 millimeters.

are noted in Table VII for all but α and \underline{Y} . These angles do not conform too well to those given in Deer and others (1963); however, the basic orientation is similar.

The prismatic habit and form of phillipsite are apparent in the S.E.M. photomicrograph in Figure 34. The monoclinic symmetry and cleavage are apparent in the photomicrograph, and the crystal faces correspond to the Miller indices indicated in Table VII. The prismatic phillipsite is apparently a fourling twin (Gottardi and Galli, 1985); twin and composition planes are indicated in Table VII.

The blocky habit (Figure 32) is apparently twinned in eightlings (fourlings combined on the $\{001\}$) according to the manner described in Gottardi and Galli (1985). The crystals shown



Figure 34. S.E.M. photograph of prismatic phillipsite. Sample 26h, field of view 2.1 millimeters.

in the photomicrograph in Figure 32 appear to be composed of lamellae, but produce an x-ray diffraction pattern identical to the prismatic crystals.

Chabazite

Chabazite occurs as colorless to amber-colored single crystals and rarely as aggregates of crystals. Single rhombohedral (pseudo-cubic) crystals are shown on a clay mineral substrate in Figure 35. The size of the crystals is equivalent to the lower size range of phillipsite, and almost an order of magnitude larger than clinoptilolite. Chabazite has not been identified in thin section, so the optical properties are not



Figure 35. Pseudo-cubic chabazite crystals on brown clay vesicle linings. Millimeter scale. Sample 48g.

indicated in Table VII. However, the crystal habit and form of chabazite is distinctive.

A close-up of chabazite is shown in the S.E.M. photomicrograph in Figure 36. The trigonal symmetry and cleavage is readily visible in this photomicrograph, and the faces represent the form given by the Miller indices in Table VII.

Unidentified zeolite 1

Unidentified zeolite 1 occurs as radiating aggregates of colorless crystals (Table VII). These aggregates are attached directly to the vesicle wall as shown in the photomicrograph in Figure 37. The crystals occur side to side, are slightly more slender at the point of attachment, and fan outward toward the

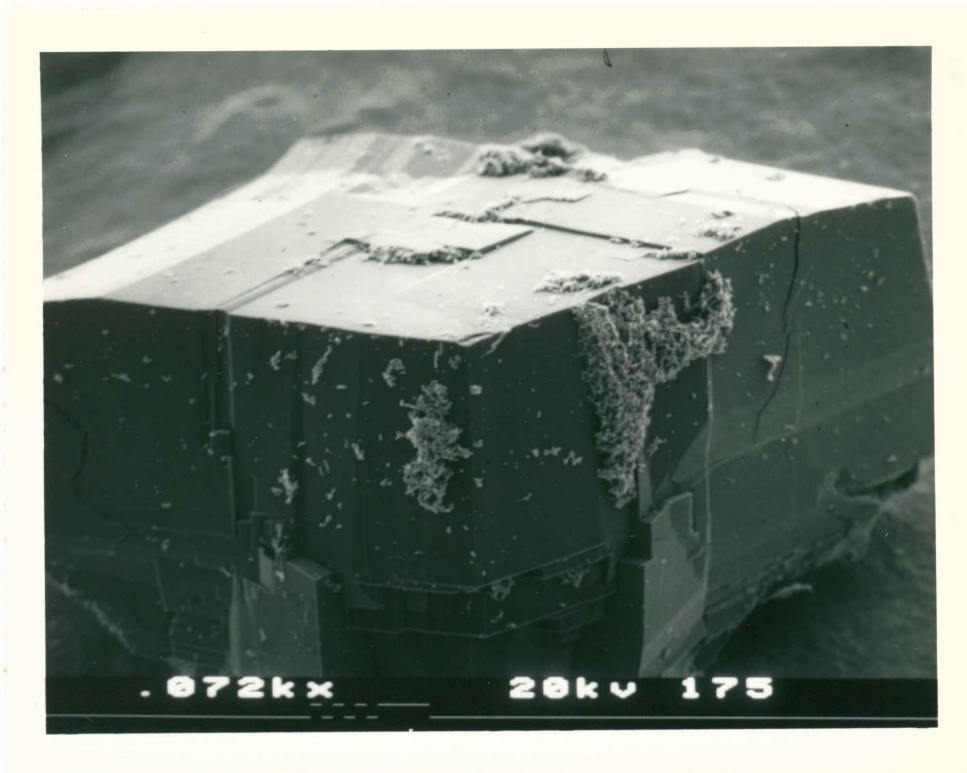


Figure 36. S.E.M. photograph of chabazite showing the pseudo-cubic (rhombohedral) crystal habit. Sample 48g, field of view 1.6 millimeters.

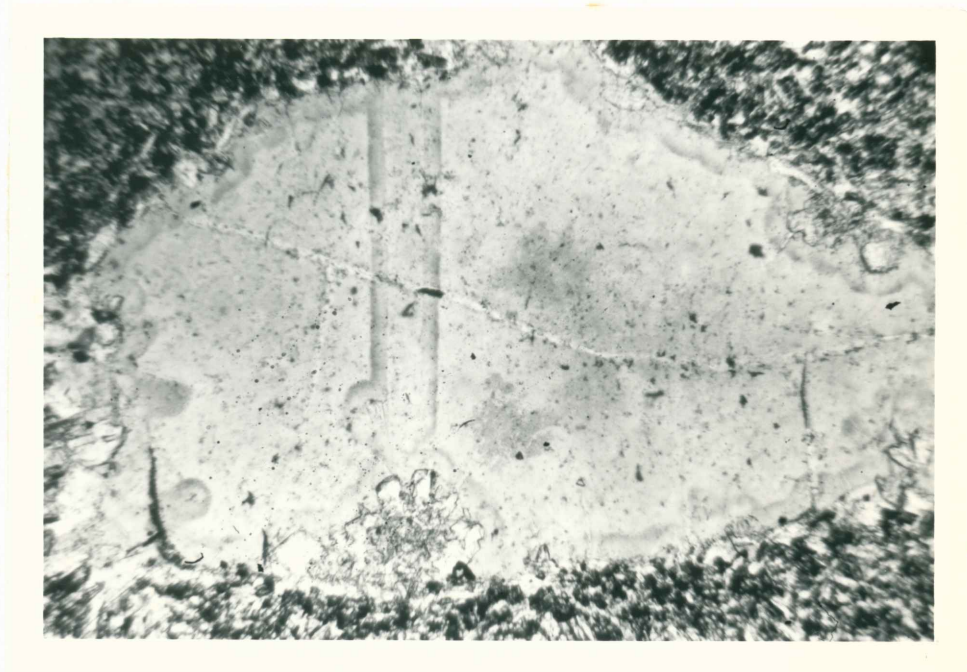


Figure 37. Unidentified zeolite 1 attached to a vesicle wall (lower center) showing the radiating habit. A geopetal fabric is developed in the olive green clays. Sample 83a, plane-polarized light, field of view 1.3 millimeters.

center of the vesicle. The length of the crystals coincide with the radius of the aggregate, and the crystal habit is bladed. The crystal form and optical properties of this zeolite are similar to clinoptilolite (Table VII). The crystal form is not as well developed in the former as the latter, making optical determinations even more difficult for this unidentified zeolite.

Unidentified Zeolite 2

Unidentified zeolite 2 occurs as yellowish crystal aggregates. The aggregates are either discontinuous parallel linings as shown in Figure 38, or blebs on filiform (blue-green) clay. The thickness of the linings is indicated in Table VII. The individual crystals cannot be clearly defined in the linings.

The massive crystal habit of this apparent zeolite is distinctive from the other zeolites. Furthermore, the birefringence and relief are higher than found in the other zeolites (positive relative to chalcedony). The color and transparency are also distinctive. In cross polarized light the fibrous extinction pattern is similar to that found in the adjacent chalcedony (Figure 39).

SILICA MINERALS

Silica minerals (Table VIII) occur in vesicles as single crystals and crystal aggregates. Silica minerals have not been

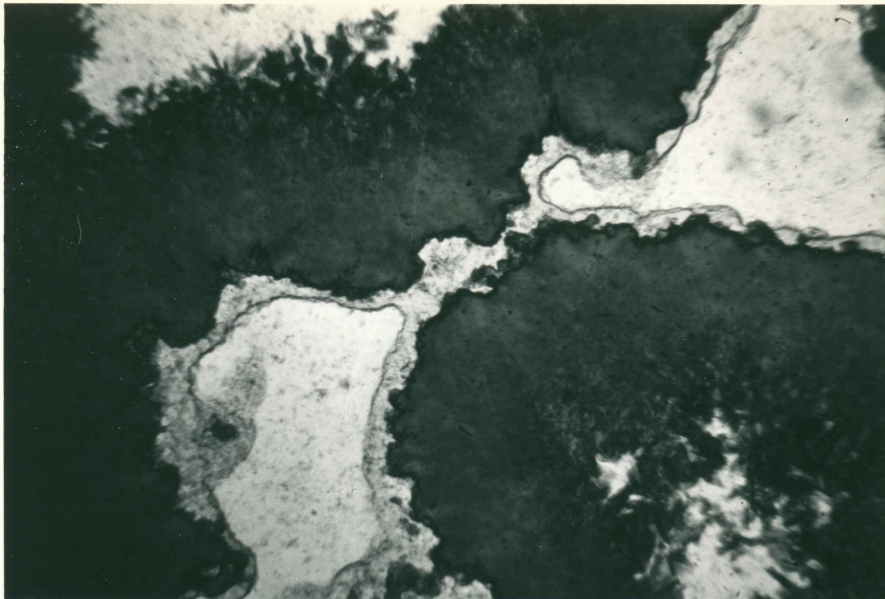


Figure 38. Thin linings of unidentified zeolite 2 (linings showing moderate relief against dark gray filaments) parallel the filiform celadonite, which is embedded in chalcedony and quartz fillings (white in the photograph). Sample 38d, plane-polarized light, field of view 1.3 millimeters.



Figure 39. Same view as in Figure 38, though shown in cross-polarized light. Unidentified zeolite 2 shows a fibrous extinction pattern. Sample 38d, field of view 1.3 millimeters.

TABLE VIII

SUMMARY OF SILICA MINERALS

TYPE	:	Opal-CT	:	Chalcedony	:	Quartz	:	Opal-CT lepispheres	:
COLOR	:	Colorless, milky, white to olive green.	:	Colorless	:	Colorless	:	Milky white	:
CRYSTAL HABIT	:	Massive, granular	:	Fibrous massive	:	Prismatic, massive Druze	:	Spherical	:
CRYSTAL FORM (1) System	:	As for α -cristobalite (tetragonal) and α -tridymite (orthorhombic).	:	Trigonal	:	Trigonal	:	Indeterminate	:
Space group	:	P4 2 2, P222 _{3 1}	:	As for quartz	:	R3 21 (right) R3 21 (left) 2	:	Indeterminate	:
Point group	:	422, 222	:	As for quartz	:	32	:	Indeterminate	:
Cleavage	:	None for all silica minerals.	:		:		:		:
Twinning	:	None visible in thin section.	:		:		:	(30 $\bar{3}$ 4) (10 $\bar{1}$ 6) (3)	:
Miller indices:	:	Indeterminate	:	Indeterminate	:	{101} {111} {010} {100} {111} (2)	:	Indeterminate	:
OPTICAL PROPERTIES									
Color	:	Pale brown translucent	:	Colorless	:	Colorless	:	White	:
Translucency	:	Translucent	:	Transparent	:	Transparent	:	Translucent	:
Birefringence	:	First order gray	:	Birefringence = .009	:	Birefringence = .009	:	Not in thin section	:
Indicatrix and optic sign	:	Indeterminate	:	Indeterminate	:	Uniaxial (+)	:	Not in thin section	:
OCCURRENCE	:	Fillings and geopetal fabrics.	:	Parallel linings (.11 mm thick), fillings and geopetal fabrics.	:	Massive fillings and drusey coatings. Individual crystals up to 1 mm long.	:	Single crystals (.03-.04 mm dia) and clusters of crystals.	:

NOTES: (1) Crystal form data is from Frye (1974) and Zoltai and Stout (1984).

(2) Symbols and 3 digit notation is consistent with the usage in Zoltai and Stout (1984).

(3) Florke and others (1976).

identified in diktytaxitic cavities. Single crystals occur on a microscopic scale and are spherical. Aggregates are macro- to cryptocrystalline, and occur as fillings, parallel linings, and drusy coatings.

The identity of silica minerals in macrocrystalline to microcrystalline aggregates has been determined optically through a petrographic microscope. These minerals include chalcedony and quartz. Optic determination of cryptocrystalline silica materials is not possible and XRD analysis is therefore required.

XRD analysis has been performed on randomly oriented powder mounts of cryptocrystalline silica. An indexed diffractogram from one x-ray analysis is shown in Figure 40. The patterns (d-spacings and intensities of peaks) compare well with published x-ray patterns and powder diffraction data for opal-CT, as presented in Jones and Segnit (1971) and Kano and Taguchi (1982).

Opal-CT is low cristobalite that is unidimensionally disordered by interstratified tridymite layers (Jones and Segnit, 1971; Florke and others, 1976). It is intermediate in the transformation of amorphous silica (opal-A, Jones and Segnit, 1971) to quartz during diagenesis and hydrothermal alteration (Kano, 1983). The transformation of opal-CT is marked by the progressive decrease in the d(101) spacing from 4.11 Å to 4.05 Å. This change in d-spacing reflects a decline of interstratified tridymite suggesting the progressive ordering of opal-CT.

The diffractogram in Figure 40 shows that ordering has

OPAL-CT 69b(1) & 69b(2)

CR - Cristobalite
 T - Tridymite
 C - Clinoptilolite
 Q - Quartz

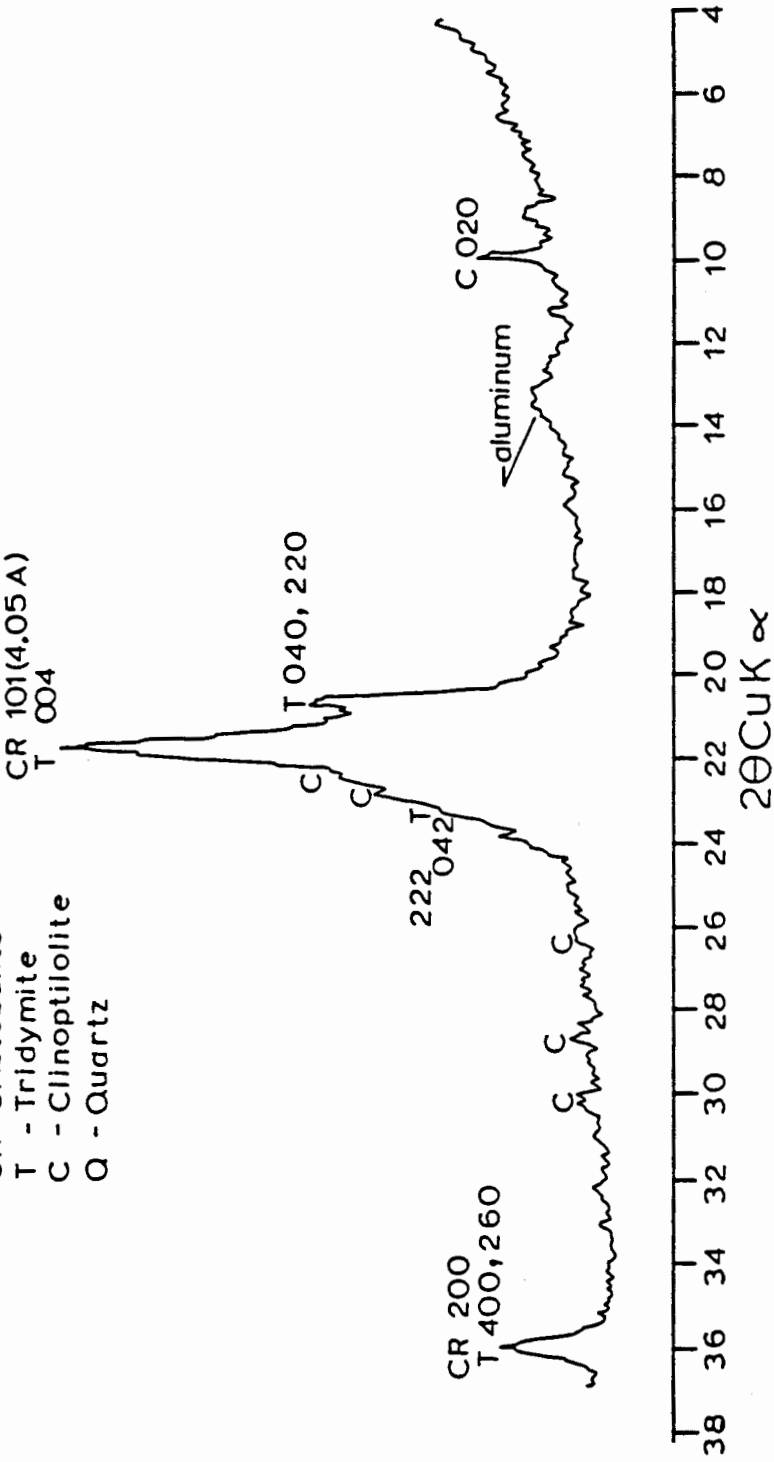


Figure 40. Indexed diffractogram of cryptocrystalline opaline silica. The hkl values shown for opal-CT are from Kano and Taguchi (1982). The hkl values shown for clinoptilolite are from JCPDS 22-1236.

Target- CuK α / Filter- Ni/ Soller slit- MR
 Beam Tunnel- 1 $^\circ$ / Detector slit- .1 $^\circ$ / Rate
 meter- 500 cps/ Time constant- 2.0/ Scan
 speed- 2(2 θ /min)/ Chart speed- 1 in/ min.

progressed to the degree that the $d(101)$ cristobalite peak has decreased to 4.05 Å.

Opal-CT lepispheres

The spherical crystals (.03-.04 millimeter diameter) developed on the substrate of tabular celadonite shown in the S.E.M. photograph in Figure 41 are very similar in appearance and occurrence to SEM photographs of opal-CT lepispheres given in Florke and others (1976). The spherical crystals shown consist of opal-CT blades that are intergrown according to the $(30\bar{3}4)$ and $(10\bar{1}6)$



Figure 41. This S.E.M. photograph shows opal-CT lepispheres, which occur as spheroidal crystals on a celadonite (tabular crystals) substrate. Sample 12e(3), field of view .067 millimeter. The spheroids range from .008-.013 millimeter in diameter.

twinning laws of tridymite (Florke and others, 1976). Energy dispersive analysis of x-rays (EDAX) confirms that these spherical crystals are composed primarily of silica. They occur singly as shown, or in aggregates that appear as white frosted coatings on dark blue-green celadonite vesicle linings in hand sample, and as grape-like clusters as in the S.E.M. photomicrograph in Figure 42. Opal-CT lepispheres are known to occur under conditions of unobstructed growth as in open cavities, and range from partial to complete crystals, to coalescent aggregates (Florke and others, 1976).



Figure 42. Aggregates of opal-CT lepispheres completely cover the celadonite substrate in this S.E.M. photograph. Sample 5b(6), field of view of the enlarged inset is .05 millimeter.

Opal-CT

Opal-CT occurs as cryptocrystalline fillings and geopetal fabrics (Table VIII). The fillings are olive green, and commonly develop on parallel linings of a clay mineral substrate. The geopetal fabric consists of olive green opal-CT, whose upper horizontal surface is laminated with colorless to milky white, massive to granular opal-CT, and intergrown clinoptilolite (Figure 24). The geopetal fabric is similarly developed on a clay mineral substrate.

In thin section, the olive green opal-CT is translucent, pale brown, and very weakly birefringent. The brown coloration may suggest the presence of intergrown clay. Unlike the opal-CT lepispheres, the individual crystal grains are not visible in the olive green opal-CT.

Chalcedony

Chalcedony occurs as colorless parallel linings, fillings, and geopetal fabrics. The linings commonly parallel convoluted filiform celadonite (the most common clay mineral habit associated with chalcedony), as shown in the photomicrograph in Figure 43. The linings occur directly on the filiform clay, or on an intervening zeolite (unidentified zeolite 2). The fillings occur in sharply bounded sections that are developed on the chalcedony linings (Figure 44). The horizontal layering (geopetal fabric) shown in Figure 45, is commonly preserved in chalcedony fillings.

Chalcedony cannot be differentiated from quartz in hand



Figure 43. Chalcedony linings parallel and fill in around the filiform celadonite. The chalcedony has a fibrous extinction pattern. Sample 38d, crossed-polars, field of view 5.2 millimeters.

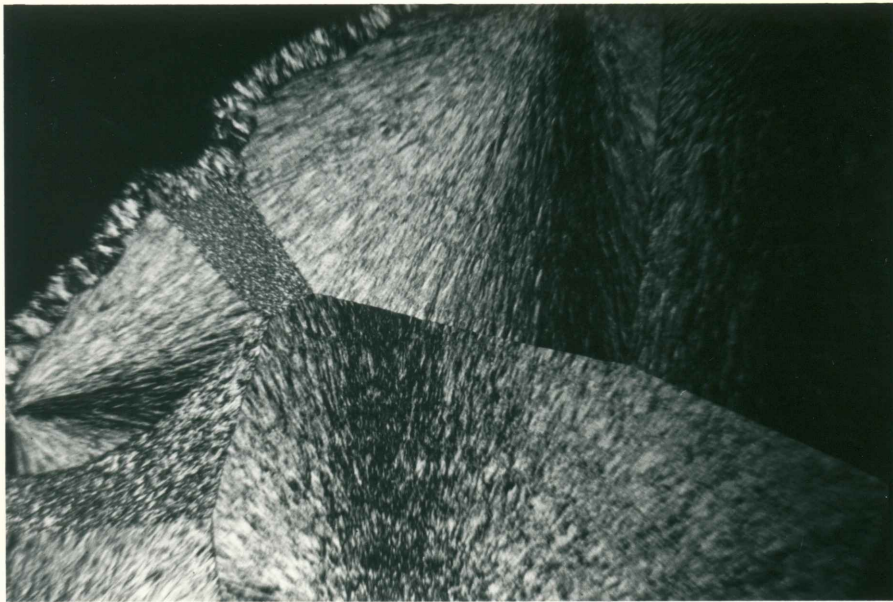


Figure 44. Sharply bounded chalcedony fillings. Sample 21a, crossed-polars, field of view 5.2 millimeters.

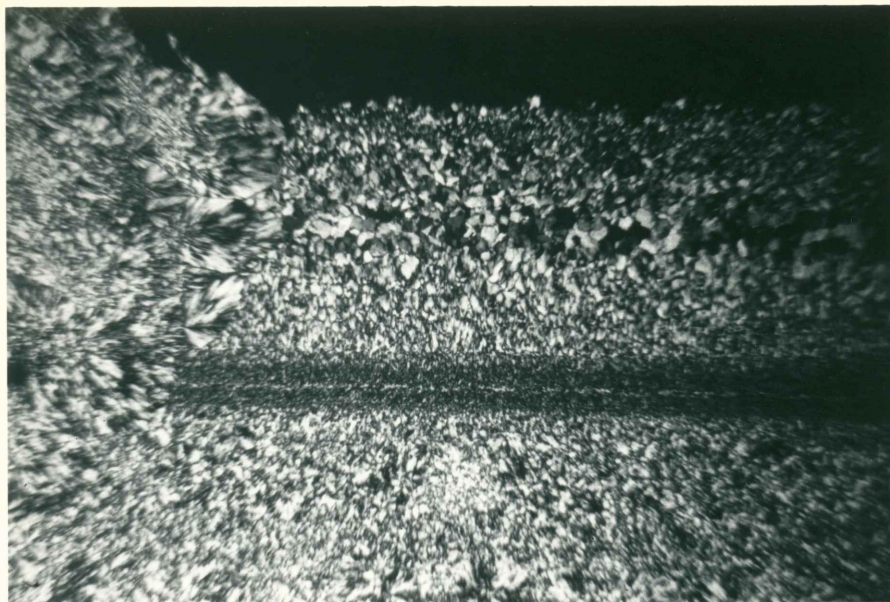


Figure 45. Geopetal fabric developed in chalcedony. The photomicrograph is oriented in the up position, toward the center of the vesicle. Sample 11a, crossed-polars, field of view 5.2 millimeters.

sample, though the two are quite distinct in thin section.

Chalcedony is fibrous microcrystalline quartz with submicroscopic pores (Deer and others, 1963). Consequently it shows a fibrous, fanned extinction pattern. However, quartz crystals are sub- to euhedral, and unless strained, display straight extinction.

Quartz

Quartz occurs as drusy coatings and fillings. Drusy quartz is shown in the photomicrograph in Figure 46, in which the form of individual crystals (up to .8 millimeter long) is well developed. Fillings of quartz are shown developed on a chalcedony substrate in Figure 47. The quartz crystals are gradational with

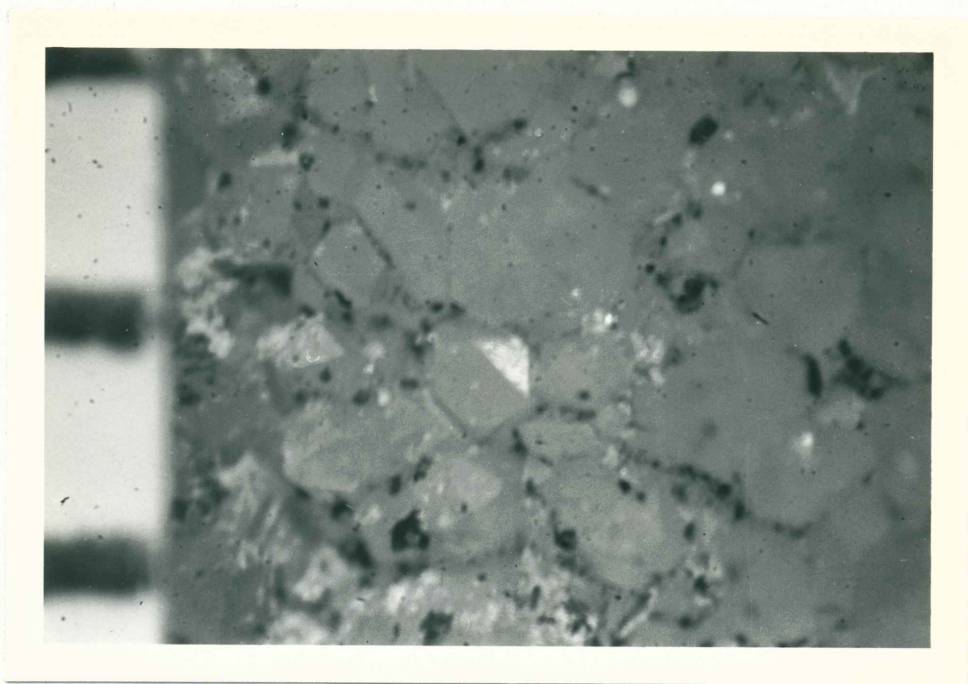


Figure 46. Drusy quartz. Two divisions of a millimeter scale are visible at the left of the photograph. Sample 4b.



Figure 47. Quartz fillings developed in chalcedony. Sample 20e, crossed-polars, field of view 1.3 millimeters.

chalcedony, and the form of individual crystals is not well developed. The optical properties are indicated in Table VIII.

CARBONATE

Carbonate occurs as single crystals and aggregates of crystals. Single crystals are micro- to macroscopic (Table IX). The macroscopic crystals are identified as calcite on the basis of crystal form, and physical properties (hardness and effervescent in acid). However, microcrystalline calcite (up to .05 millimeter in size) is identified on the basis of optical properties including color, high birefringence, and high relative relief. Single macroscopic crystals commonly occur on a substrate of clinoptilolite (Figure 48), and rarely on clay minerals.

Aggregates are composed of macroscopic crystals that line or fill vesicles. Calcite fillings may have developed as the crystals in drusy coatings eventually grew to span the entire length and breadth of the vesicle. Crystals have been found doubly attached on opposite vesicle walls. It is assumed that continued crystal growth would eventually fill the vesicle.

In a rare occurrence, calcite is developed on celadonite vesicle linings and is associated with microcrystalline quartz. The calcite coarsens toward the center of the vesicle, and the microcrystalline quartz appears to be intergrown with calcite.

TABLE IX
SUMMARY OF THE CARBONATE

TYPE	:	Calcite	:
COLOR	:	Colorless, smoky brown or gray.	:
CRYSTAL HABIT	:	Massive, prismatic	:
CRYSTAL FORM (1)			
System	:	Trigonal	:
Space group	:	$R\bar{3}2/c$:
Point group	:	$\bar{3}2/m$:
Cleavage	:	Perfect {104}	:
Twinning	:	(001) {104} {018}	:
Miller indicies:	:	{214} (2)	:
Form	:	Scaleno-hedron	:
OPTICAL PROPERTIES			
Color	:	Colorless	:
Transparency	:	Trans. to transl.	:
Birefringence	:	Birefringence = .172	:
Indicatrix and optic sign	:	Uniaxial (-)	:
Relief	:	High relative to other adjacent minerals.	:
OCCURRENCE	:	Fillings, single crystals (.05-10.0+ mm).	:

NOTES: (1) Crystal form data is from Frye (1974) and Zoltai and Stout (1984).

(2) Symbols and 3 digit notation consistent with usage in Zoltai and Stout (1984).

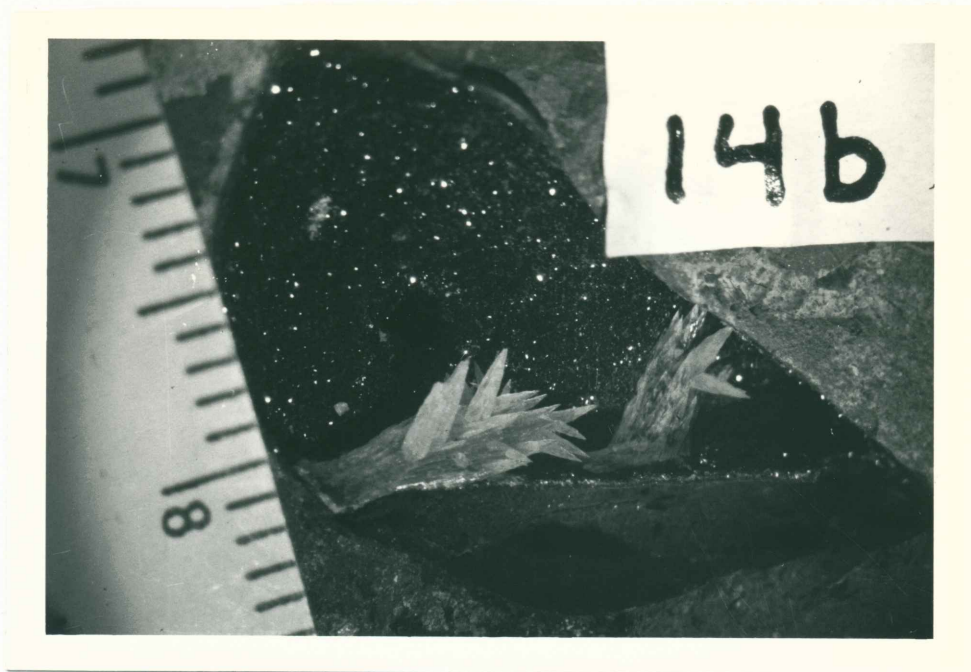


Figure 48. Calcite scalenohedrons developed on clinoptilolite vesicle linings. The calcite is developed on a geopetal surface over a void that was once filled with olive green clay. Millimeter scale.

CHAPTER IV

SECONDARY MINERAL PARAGENESIS

The number of mineral groups in the paragenetic sequence is greatest in the flow-top breccia zone and the brecciated portions of the interflow contact zone. In these settings the overall paragenetic sequence in vesicles and diktytaxitic cavities is clay minerals --> silica minerals --> zeolites --> calcite --> silica minerals --> clay minerals. The paragenetic sequence is abbreviated in the other flow zones. The individual mineral species that compose the mineral groups in the paragenesis differ among the flow zones. The secondary mineral parageneses in context of flow zones is indicated in Table X. In this table secondary mineral species are listed under mineral group headings for each of the flow zones.

Smectite is the first mineral in the paragenesis of the flow-top breccia zone, whereas celadonite is commonly the first mineral in the paragenesis of the interflow contact zone, in the absence of smectite. Where celadonite and smectite are both present, smectite precedes celadonite in the paragenesis. Smectite is also the first mineral in the parageneses in the transition zone of the analog flow and the flow interior zones of both flows. Celadonite may also be present in the flow-top breccia zone and the flow interior zone of the analog flow, though

TABLE X
SECONDARY MINERAL PARAGENESES OF THE OUTCROP IN CONTEXT OF FLOW ZONES

FLOW ZONE :	CLAY MINERALS -->	SILICA MINERALS :	ZBOILITES -->	CARBONATE -->	SILICA MINERALS -->	CLAY MINERALS :
Flow :	smectite	:	:	:	:	:
Interior :	:	:	:	:	:	:
---SUPERJACENT-FLOW---						
Interflow :	+smectite -->	+opal-CT -->	+chalcedony :	+calcite	+opal-CT lepispheres	+celadonite
Contact :	---	--->	--->	---	+chalcedony -->	+smectite
---ANALOG-FLOW---						
Flow-top :	smectite -->	+celadonite :	+opal-CT -->	+chalcedony:	+phillipsite:	+smectite
Breccia :	---	---	---	---	+chalcedony -->	+celadonite
Transition: Smectite						
Flow :	---	---	---	---	---	---
Interior :	smectite -->	+celadonite :	---	---	---	---

Note: Bold faced minerals are those minerals that are most common in occurrence in their respective setting.

it is less common than in the interflow contact zone.

Silica minerals follow clay minerals in the parageneses of the interflow contact and flow-top breccia zones, and are absent in the parageneses of the transition and flow interior zones of either flow. Silica minerals are commonly coprecipitated with clay minerals. In the flow-top breccia zone opal-CT is the most common silica mineral in occurrence, and is coprecipitated with smectite, or less commonly, celadonite. Chalcedony is rare to absent in zones other than the interflow contact zone.

In the interflow contact zone chalcedony is the most common silica mineral in occurrence and precedes quartz in the paragenesis. Chalcedony that is not colorless, but rather brown or yellow in plane polarized light, displays a higher index of refraction than colorless chalcedony, and may be an indication of its coprecipitation with clay minerals. Opal-CT occurs less commonly than chalcedony in the interflow contact zone, though in one occurrence, is coprecipitated with celadonite. Opal-CT precedes chalcedony in the paragenesis of the interflow contact zone.

Clinoptilolite is the major zeolite species in the paragenesis of the flow-top breccia zone, whereas an unidentified zeolite (unidentified zeolite 2) occurs in the interflow contact zone (Table X). Clinoptilolite is also widespread through the transition zone, and possibly the flow interior zone of the analog flow (unidentified zeolite 1), though is not found in the interflow contact zone or flow interior zone of the superjacent

flow. In the flow-top breccia zone phillipsite and chabazite are less common in occurrence than clinoptilolite. Chabazite and clinoptilolite are apparently contemporaneous, though phillipsite follows clinoptilolite in the paragenesis of the flow-top breccia zone (Table X).

The fourth mineral group in the parageneses is represented by calcite. Calcite is presumably widespread over all of the flow zones excepting the flow interior zone of the superjacent flow and the non-brecciated portion of the interflow contact zone.

In the flow-top breccia and interflow contact zones calcite precedes the second occurrence of silica minerals, which are the fifth mineral group in the parageneses. In one vesicle filling, calcite has developed on a substrate of celadonite. The calcite becomes coarser-grained toward the center of the filling, though a portion of the center volume is occupied by microcrystalline quartz. In the cross-sectional view offered by the thin section, the microcrystalline quartz is entirely enclosed by the calcite. The interpretation of this pattern is equivocal, and could be explained by the

- 1) replacement of silica by carbonate,
- 2) infilling of pore space within porous calcite, and
- 3) coprecipitation of calcite and microcrystalline quartz.

Opal-CT lepispheres occur where chalcedony and quartz are absent, and have been observed crystallized upon calcite scalenohedrons.

The early silica minerals have been observed in relation to

the later silica minerals in the parageneses. In one occurrence, opal-CT precedes clinoptilolite, which in turn precedes laminated chalcedony (and quartz). In another occurrence, laminated chalcedony has developed upon a thin clinoptilolite lining. The clinoptilolite lining and the laminated chalcedony are intervened by calcite as evidenced by effervescence in the presence of dilute HCl.

Clay minerals are the sixth mineral group in the flow-top breccia and interflow contact zones parageneses. Celadonite and smectite are apparently contemporaneous and occur in both zones, though celadonite is more common in the interflow contact zone, and smectite in the flow-top breccia zone (Table X). In one occurrence in the interflow contact zone, celadonite occurs upon a calcite scalenohedron, placing calcite earlier in the paragenesis than celadonite.

CHAPTER V

DISCUSSION

Alteration mineral assemblages occur as replacement of the primary mineral assemblage and as precipitated phases in open spaces whether of primary or secondary origin. Replacement phases record the exchange of elements between the rock and the altering solution as the replacement process operates. Precipitated phases record the composition of the solution from which they precipitated. Since the solution is often no longer present, the precipitated phases are an important means to decipher the solution's compositional history. In this study, the focus is on the degree to which the solution composition was uniform during alteration and the factors that influenced solution composition.

Since the examination of the solution composition must be inferred from the precipitated secondary minerals, it is necessary to carefully select those portions of the system most likely to yield answers, and to make certain simplifying assumptions. Of the system, the precipitated phases in vesicles and diktytaxitic cavities have been selected because 1) the diversity of minerals is greater in vesicles and diktytaxitic cavities than in the interclast voids and fractures, 2) vesicles and diktytaxitic cavities allow examination of the influence of variable porosity on mineral precipitates, and 3) the secondary phases are typically

sequentially precipitated rather than coprecipitated, and are thus easier to examine in light of changing solution composition.

To further simplify the system the following assumptions have been developed and are summarized in Table XI:

- 1) In the brecciated portions of flow zones the solution that was within the interclast voids is viewed as a reservoir that interacted with solutions in the vesicles and diktytaxitic cavities in clasts partly as a function of their interconnected porosity. The solution is viewed as an aqueous solution that was ubiquitous in the system. Evidence that a vapor-rich system was present during alteration has not been recognized.
- 2) The influence of the textural diversity in the basalt, the variable reactivity of glass, microlites, etc. to heated solutions, and the extent of reaction of the primary materials with the solutions is not considered. The basalt is viewed as uniform in composition and its incongruent dissolution behavior is ignored. Changes in the extent of reaction of the basalt as conditions change, particularly temperature, are not evaluated in this study. The basalt is viewed as chemically inert but displaying different porosity in the various flow zones. The role of the basalt on solution composition is under investigation as replacement phases are determined and the composition of the basalt and replacement and precipitated phases are determined.

TABLE XI

ASSUMPTIONS

SCALE	SECONDARY MINERAL FEATURE	NUCLEATION	POROSITY
Vesicle to: flow zones and parageneses.	Differences in secondary mineral layers, assemblages, to temperature, surface energy of nucleus, and sites for nucleation.	Kinetics related to temperature, diktytaxitic cavities. May be interconnected.	Provided by vesicles and diktytaxitic cavities. May be interconnected.

SOLUTION	TEMPERATURE	PRESSURE	BULK ROCK
Variable. Aqueous solution not a vapor-rich solution.	Variable. Geothermal or heat applied from the superjacent flow.	Constant.	Uniform on a macro-scale. Water/rock ratio constant.

- 3) Pressure is believed to be constant over the thickness of the analog and superjacent flows. The pressure is related to the thickness of the overlying stratigraphic column at the time of alteration.

This discussion will consider:

- 1) The distribution and type of primary porosity within the flow zones,
- 2) the secondary mineral layers, assemblages and parageneses in relation to temperature and solution composition, and
- 3) the approximate magnitude of the intensive variables during alteration.

The discussion of the implications of the indicated secondary mineral layers, assemblages, and parageneses about the temperature and solution composition during alteration will be prefaced by a short discussion of the relations between secondary minerals and interconnected porosity, and considered at differing scales of observation;

- 1) a vesicle,
- 2) neighboring vesicles,
- 3) hand samples, and
- 4) flow zones.

The secondary mineral features, variables, and constants to be discussed at the scales of observation listed above are summarized respectively in Tables XII, XIII, XIV, and XV.

PRIMARY POROSITY

Primary porosity varies greatly as to type, size of pores, extent of interconnection, and abundance among the flow zones. Interconnected porosity strongly influences accessibility of solutions to rocks. Vertical joint-related fractures are presently an important aspect of the porosity of the flows; however, the lack of secondary alteration phases on these surfaces suggests that these fractures were not present or important at the time of alteration. The platy joints in the base of the superjacent flow are lined by secondary minerals and apparently were present at the time of alteration. The pore space that is important to the alteration history includes vesicles, diktytaxitic cavities, interclast voids, and, to a lesser extent, tree molds and at least some platy joint-related fractures.

Within the flow interior zones the porosity is provided by isolated vesicles and diktytaxitic cavities. The abundance of pore space is estimated from point counts of thin sections to be less than 10% of the rock (Table III).

Thin section examination indicates that deep within the transition zone the pores are largely diktytaxitic cavities and small isolated vesicles. Upward in the zone cavities increase in abundance around developing breccia clasts, and the porosity becomes dominated by interstitial spaces between developed breccia fragments. The abundance, size, and extent of interconnection of these interstitial spaces increases outward through the various layers of breccia that mantle the basalt spines. However, within

the individual breccia clasts the porosity is usually low.

Within the solid parts of the interflow contact zone where rocks generally have low abundance of vesicles and diktytaxitic cavities, porosity is related to microfractures and other major fluid pathways such as tree molds and pipe vesicles.

The zone with the greatest porosity is the flow-top breccia zone where pore spaces include large vesicles, abundant diktytaxitic cavities, and large interclast voids. Microfractures in clasts and vesiculated bands containing large stretched vesicles characterized by thin intervening walls provide open spaces that penetrate deeply into some clasts. The interclast voids are the largest pore spaces and form an interconnected porosity throughout the breccia. This void space is connected to those vesicles and diktytaxitic cavities exposed on the broken surfaces of breccia clasts. Within the flow-top breccia zone and the brecciated parts of the interflow contact zone the porosity within clasts varies greatly (Figure 4 and Table III). Otherwise the interconnection of pores within the clasts is variable, and is directly a function of vesicle and diktytaxitic cavity size, abundance, and nearness to clast boundaries. Though a clast may be highly vesicular, the interconnection between vesicles on the interior of clasts does not appear to be great. The greatest porosity is developed in clasts not only with abundant large vesicles, but with extensive networks of diktytaxitic cavities incorporated into the walls of vesicles and in the groundmass between vesicles.

SECONDARY MINERALS IN RELATION TO TEMPERATURE
AND SOLUTION COMPOSITION

The precipitated secondary minerals imply the presence of an aqueous solution during alteration. In all flow zones excepting the flow interior zone of the superjacent flow, the ubiquitous precipitated secondary minerals imply aqueous solutions occupied pore spaces (interclast voids, vesicles, and diktytaxitic cavities). Diktytaxitic cavities are commonly occupied by parallel linings or fillings. Parallel linings, geopetal fabrics, and/or fillings are the observed patterns of precipitation in vesicles. In breccia clasts, thin, parallel linings are the sole occupants of the innermost vesicles; thick, parallel linings, geopetal fabrics, and fillings become prevalent in the outer vesicles. Consequently, a lower percentage of the volume of the inner vesicles is occupied by secondary minerals than of the outer vesicles.

A given volume of aqueous solution within a vesicle, cannot possibly yield an equivalent volume of secondary minerals, no matter how concentrated the solution may be. Therefore, if a vesicle is filled with precipitated materials, it must be open to a larger reservoir of solution, such as that occupying the interclast voids in the flow-top breccia. The transfer of a solution into a vesicle is influenced by the interconnected porosity provided by vesicles and diktytaxitic cavities. The more interconnected the porosity around a vesicle the greater the percent volume of that vesicle that should be filled by secondary minerals. Thus the variations in

percent volume of individual vesicles occupied by precipitated phases is an indication of the interconnected porosity of the rock around that vesicle. Furthermore, solutions in comparably-sized vesicles surrounded by rock of similar interconnected porosity should precipitate similar volumes of secondary minerals. Therefore, the greater percentage volume filled by precipitated secondary minerals in comparably-sized outer versus inner vesicles within a clast suggests that the interconnected porosity within the clast decreases from the outer surface inward.

Although it is recognized that other factors, including the composition and percentage of the glass in the basalt and water/rock ratios, will influence the percent volume filled in a vesicle, the simplified point of view that interconnected porosity is the main factor is consistent with the assumptions of this argument (Table XI). As a generalization for other portions of the outcrop, the patterns and abundances of precipitated minerals in vesicles, can be used to indicate the relative interconnected porosity.

At The Scale Of A Vesicle

At the scale of a single vesicle (Table XII) the roles of nucleation abundance and rate, interconnected porosity, and the number of solid phases in contact with the solution on the solution composition may be analyzed if temperature is assumed to be constant. If temperature should change, whatever thermal gradients might develop in the vesicle would be short-lived.

TABLE XII
AT THE SCALE OF A VESICLE

SCALE :	SECONDARY MINERAL FEATURE :	NUCLEATION :	POROSITY :	SOLUTION :	TEMPERATURE :
Vesicle :	1) Texturally homogeneous monomineralic filling.	Uniform nucleation rates.	Relatively high.	Uniform, externally controlled by composition of the reservoir.	Constant at any given point in time.
	2) Sequential layers of individual mineral species or coprecipitation of mineral species.	Nonuniform to rates. Variations in # nuclei formed.	Relatively high - Relatively low -	Nonuniform. External control by the precipitation of solid mineral phases.	Variable. May outweigh the influence of interconnected porosity on solution composition.

Nucleation of a secondary phase within a vesicle is an important part of the precipitation process. The kinetics of nucleation are closely related to temperature, surface energy of the nucleus, and the availability of sites suitable for nucleation (Williams and others, 1982). However, a solution saturated with respect to a mineral phase that is the thermodynamically stable phase for the extant conditions, may not nucleate because of kinetic effects. A thorough development of nucleation kinetics is beyond the scope of this study; however the concept is important when considering the evolution of solution compositions.

Where secondary minerals occur within a vesicle, solutions have migrated into that vesicle since vesicles closed to solution would lack significant precipitated secondary minerals. Assuming a vesicle is open, the supply of solution is of constant composition and is constantly being replenished as crystallization proceeds, and the rate of nucleation remains constant, a texturally homogeneous, monomineralic filling should result. Texturally homogeneous, monomineralic fillings have rarely been observed in the analog study outcrop, and then only in the outer vesicles of clasts in the flow-top breccia. The most common pattern however, is sequential layers of different minerals and of differing textures, that occur commonly as parallel linings, and less commonly as horizontal layers in fillings. These patterns indicate that the composition of the solution and possibly nucleation process changed with time.

A change in solution composition may be accomplished in one

of two ways.

- 1) The transfer of solution between a vesicle and the reservoir solution may be extremely limited; compositional shifts in the solution are internally controlled as the first lining nucleates and precipitation proceeds. The compositional shift is produced by depletion in the solution of those elements incorporated into the mineral, and a relative enrichment of others in the solution as precipitation takes place.
- 2) The interconnected porosity and transfer of components between the vesicle and the reservoir solution may be high, thus solution composition is externally controlled. Consequently a composition shift in the reservoir is reflected in the solution composition within the vesicle.

Thin sequential layers of different minerals and differing textures are common in vesicles where solution composition is largely internally controlled. The solution is initially in contact with the first phase precipitated in the sequence, in most cases a clay mineral. As the second phase begins to nucleate, either as another clay or a species of another mineral group, the solution composition changes. Once the second phase completely covers the first phase, isolating it from the solution, the solution is in contact with only the second phase.

Clinoptilolite linings on a clay mineral substrate are a common example of this process. The substrate consists of thin, sequential clay mineral linings, and the clinoptilolite consists

of complete parallel linings, or isolated aggregates of crystals (Table VII). Each subsequent clay mineral lining represents a shift in the solution composition. Once the compositional stability field of clinoptilolite is reached, clinoptilolite begins to nucleate, first as single crystal nuclei. The solution would maintain contact with the surface clay and clinoptilolite until the clinoptilolite completely covers the clay. In some vesicles, those with sheaved clinoptilolite aggregates (Table VII), the pattern may indicate that the nuclei of clinoptilolite may be sparse and the growth of the crystals does not cover the clay substrate. In this setting, clinoptilolite and clay are the last solid phases in contact with the solution.

In vesicles opened by micro-fractures to major fluid pathways solution composition is externally controlled, linings are thick, and coprecipitated phases, although sparse, are more common. Coprecipitated phases such as clinoptilolite + opal-CT increases the number of solid phases in contact with the solution at the beginning of precipitation. Since coprecipitated phases are sparse in vesicles and diktytaxitic cavities, the implications of coprecipitated phases will not be considered further in this study.

The processes by which compositional changes take place in the solution within vesicles are closely related to the interconnected porosity around the vesicle. In the inner vesicles within clasts the process of change may approximate internal control of solution composition, whereas in the outer vesicles the process

may approximate external control of composition and reflects reservoir composition.

The above argument assumes that the solution composition at constant temperature changes as a function of precipitation of secondary minerals or changes in the composition of the reservoir solution. However, it is possible that changes in the solution composition are the result of changing temperature producing chemical reactions between the rock and the fluid phase. In this case the composition of the fluid can change within the reservoir as well as individual vesicles and is less dependent upon the accessibility of solutions to vesicles. The precipitation of a new phase within the vesicle may reflect the shift in solution composition into the chemical stability field of that mineral as a function of changing temperature.

At The Scale Of Neighboring Vesicles

In neighboring vesicles (Table XIII), separated by as little as .1 mm,

- 1) the patterns and relative proportion of phases,
- 2) the percentage volume of vesicles occupied by secondary phases,
- 3) the phases that are missing within the paragenetic sequence, and
- 4) the last phase assemblage that would have been in contact with the solution are often found to be different. Assuming the rock does not enter into reaction with the fluid phase, these

TABLE XIII
AT THE SCALE OF NEIGHBORING VESICLES

SCALE :	SECONDARY MINERAL FEATURE :	NUCLEATION :	POROSITY :	SOLUTION :	TEMPERATURE :
Neighbor- ing vesicles.	Differences in: a) patterns and relative proportions of phases. b) percentage volume of vesicles occupied by secondary minerals. c) phases missing in the paragenetic sequence. d) last phase assemblage in contact with the solution.	May be variable between vesicles. Differences in the number of nuclei. Failure of a phase to nucleate.	Interconnected porosity may be different in neighboring vesicles.	May be originally different in neighboring vesicles. External verses internal control.	Constant at any given point in time.

differences appear to be the result of contrasting solution compositions produced by phase nucleation and the interconnected porosity of the rock around the vesicle.

At the scale of two neighboring vesicles, the temperature is assumed to be constant at any given point in time, thus differences among secondary minerals is due primarily to different solution compositions. The differences in the solution chemistry between such closely spaced neighboring vesicles may be explained by one or more of the following factors:

- 1) The solutions in the neighboring vesicles were originally different.
- 2) The interconnected porosity around one vesicle is different than the other allowing external versus internal control of the solution composition.
- 3) A phase may fail to nucleate in one of the vesicles or there may be differences in the nucleation density within the two vesicles.

At the time of alteration, the original composition of the solutions within neighboring vesicles may have been different. The differences may have resulted from the degassing of the flow at the time of crystallization or interaction of groundwater or surface water with the flow after the flow cooled. In a real sense, these differences are produced by differing accessibility of magmatic gases and meteoric water to the vesicles. However, patterns in the secondary minerals have not been recognized to support this idea.

During alteration the composition of the solution may change because of differing interconnected porosity around the vesicles. As discussed above, the composition of the solution may be controlled internally by the precipitation of solid phases or externally by the composition of the reservoir solution.

If the composition of the solution in neighboring vesicles and the interconnected porosity of the surrounding rock is the same, the solutions may compositionally evolve differently due to the failure of a phase to nucleate or differences in nucleation density within neighboring vesicles. Even if a solution is saturated with respect to a particular phase, and conditions are within the stability range of that phase, kinetic factors may preclude nucleation of the phase. This is particularly true in lower temperature alteration systems. The kinetics of reactions and nucleation at low temperatures is a particularly vexing problem. The precipitation of metastable phases or the failure of phases to nucleate are common problems encountered in experimental studies at all temperatures; particularly at low temperatures. For example, in reactions of Umtanum basalt with synthetic groundwater in Dickson-type rocking autoclaves, solutions calculated to be approximately saturated with respect to calcite at the termination of 300° C reactions failed to precipitate calcite (Moore and others, 1985). The absence of calcite in these experiments suggests insufficient time to attain equilibrium, or unfavorable reaction kinetics. Kinetic barriers to nucleation are overcome and reaction times decreased experimentally through

elevated temperatures.

At The Scale Of A Hand Sample

Hand sample-sized (Table XIV) clasts from the flow-top breccia zone commonly show a zoned distribution of the precipitated phases that is parallel to the clast boundary. From the inner to outer vesicles the percent volume occupied by precipitated phases also increases. The parallel linings increase in thickness, and the surface clay linings range in color from brown to orange to yellow to green to blue, from the inner to outer vesicles. The inner vesicles contain sparse isolated crystals and aggregates of zeolites (clinoptilolite, phillipsite, chabazite) that have nucleated on a brown clay substrate (Figures 27, 34, 35, Table VII). In addition to clay mineral linings, the outer vesicles commonly contain calcite or clay mineral fillings, and partly filled geopetal fabrics with the upper portion of the vesicle lined by clinoptilolite. Clinoptilolite linings in the outer vesicles are complete, in contrast to the isolated aggregates within the inner vesicles.

At this scale of observation, the temperature is assumed to be constant. A thermal gradient could be produced, though not maintained for a significant length of time in a hand sample-sized piece of rock lacking an insulating glassy selvage. Therefore, assuming constant temperature at any given point in time, the differences in the precipitated phases among vesicles is a function of solution composition.

TABLE XIV
AT THE SCALE OF A HAND SAMPLE

SCALE :	SECONDARY MINERAL FEATURE :	NUCLEATION :	POROSITY :	SOLUTION :	TEMPERATURE :
Hand sample.	Zoned distribution of precipitated phases parallel to clast boundaries. From clast interior outward: a) Percent volume occupied by precipitated phases increases. b) Brown-orange-yellow-green-blue clay linings. c) Inner vesicles- isolated crystals or aggregates of zeolites. Outer vesicles- zeolite linings, geopetal fabrics or fillings.	As discussed.	The interconnected porosity of the clast decreases from the outer surface inward.	Nonuniform. Inner vesicles- internal control. Outer vesicles- external control. Chemical gradient parallels clast boundary.	Constant at any given point in time. Variable over time.

The zoned pattern in secondary phases, the change in mineral assemblage, and the increase in the percentage volume filled by secondary phases from the inner to the outer vesicles argues that the main controlling factor on solution composition at the hand sample scale is interconnected porosity within the rock. In such a clast having variable porosity, chemical gradients in the secondary precipitated phases would develop in the clast paralleling the clast boundary and other permeable pathways.

If the composition of the reservoir solution is variable with time, the precipitation products in vesicles would reflect these variations. A chemical perturbation of the reservoir solution would eventually perturb the solution composition within vesicles, and perhaps result in the nucleation and precipitation of a different phase (or phases). The inner vesicles would be less subject to variations in the reservoir solution composition. The composition of the reservoir solution is not directly measurable since it is no longer present, and can only be evaluated indirectly, perhaps through direct measurements in similar systems that are currently active, or through laboratory experimentation.

At the hand sample scale the observed patterns are due primarily to the interconnected porosity within the rock and potential variability in the reservoir solution composition.

At The Scale Of The Flow Zone

The character of porosity among the flow zones (Table XV)

TABLE XV
AT THE SCALE OF THE FLOW ZONE

SCALE :	SECONDARY MINERAL FEATURE :	NUCLEATION :	POROSITY :	SOLUTION :	TEMPERATURE :
Flow zone. Flow					
interiors.:	Parageneses are different	: As discussed.	: Assumed to be similar in both flows.	: Different in the two zones. Solution may have been absent in the flow interior of the superjacent flow.	: A possible variable.
Solid part:	Fillings predominate, and linings are rare. Marked differences in parageneses.	: As discussed.	: Assumed to be similar in the two zones.	: Different in the two zones.	: Different in the two zones.
Flow-top breccia zone.	Gross paragenetic sequence is similar. Differences in the mineral species of the mineral groups that comprise the sequence. High to low in the zone: a) Silica minerals decrease. b) Clay minerals increase. High in the zone: c) Abundant celadonite, sparse smectite. d) Arborescent celadonite. e) Olive green clays. f) Clinoptilolite. Low in the zone: g) Abundant smectite, sparse celadonite. h) Arborescent smectite. i) Brown clays. j) Phillipsite, chabazite.	: As discussed.	: High, largely due to intercast voids. Constant throughout the zone.	: Nonuniform due to thermal gradient across the zone, or the solution composition was inhomogeneous within the zone.	: Thermal gradient across the zone. Ambient geothermal gradient (22 m/°C) 5°C difference across the two flows, <1°C difference across the zone. Heat applied from the superjacent flow. Opal-CT relations (50-60°C) Stability relations among silica minerals: chalcedony quartz saturation (150-170°C).

varies substantially (Table III, Figure 4), and is related to the cooling history of the analog and superjacent flows. Flow zones of similar porosity should have similar secondary mineral patterns and parageneses providing the solution composition is not different. However, the secondary mineral patterns and parageneses are different among flow zones of similar porosity suggesting solution composition differences. These differences in solution composition are reasonably explained if a thermal gradient is present in the system during alteration.

The analog and superjacent flow interior zones have similar types and amounts of porosity (Table III). Thus it is assumed that their interconnected porosities are similar. The textural differences noted between the two flows in this zone is the percentage of glass; the analog flow interior zone is holocrystalline whereas the superjacent flow interior is hypocrySTALLINE (25% glass). It is expected that for a solution in contact with hypocrySTALLINE verses holocrystalline rock, the alteration effect, assuming all else is equal, should be greater for the former than the latter. However, the reverse is true; the variety and abundance of precipitated secondary minerals is greater in the holocrystalline analog flow interior zone, than the superjacent flow interior zone. The difference in behavior in the two zones either reflects solutions of differing composition or a lack of solutions in the vesicles of the superjacent flow during alteration.

The percentage of cavities and the percentage of glass is

similar in the solid parts of the transition and interflow contact zones (Table III). The character of the porosity is such that large voids are surrounded by dense basalt that contains little porosity. In the interflow contact zone the porosity is provided by pipe vesicles and tree molds; in the transition zone it is developed between breccia fragments. In both zones the pore space is filled by secondary phases; linings are rare. There are marked differences, however, in the paragenesis and the mineral assemblage found in these two zones. In the interflow contact zone the paragenetic sequence is celadonite --> unidentified zeolite 2 --> chalcedony --> quartz; in the transition zone it is smectite --> clinoptilolite (Table X).

In comparing these two zones that have similar porosity patterns, it is apparent that the solution composition was different as indicated by the mineral assemblage and paragenetic differences. The differences in solution composition suggest that the temperature was different in the two zones during alteration.

In the flow-top breccia zone the porosity is defined by the interclast voids, and vesicles and diktytaxitic cavities within clasts. The porosity is largely due to the interclast voids and thus is essentially constant through the flow zone. Since the flow zone is highly porous, it is not likely that chemical gradients would be developed or be maintained in solution occupying the interclast voids, if held at constant temperature.

Analysis of the distribution of secondary minerals in the inner and outer vesicles in breccia clasts indicates that

systematic differences occur in the relative proportion of phases in phase assemblages and, although the gross paragenetic sequences are similar through the zone, there are differences in the mineral species of the mineral groups that comprise the paragenetic sequence. The following patterns are discernable within the zone. The silica minerals, opal-CT primarily, decrease in abundance and disappear downward in the zone, whereas clay minerals increase in abundance downward in the zone. Clay minerals change from smectite and abundant celadonite high in the zone to sparse celadonite and abundant smectite low in the zone. Arborescent celadonite occurs high in the zone whereas arborescent smectite occurs low. High in the flow zone olive green clays are the dominant clay mineral, whereas low in the flow zone brown clays are dominant. In the medial portions of the zone there is a transition from olive green to brown clays. The olive green and brown clays appear to be contemporaneous in their development. In the inner vesicles of clasts, clinoptilolite covers a substrate of clay minerals high in the zone, at lower levels phillipsite or chabazite may occur directly upon a clay substrate or upon a substrate of clinoptilolite.

The indicated differences suggest that the fluid composition was not uniform within the zone during alteration. The solution composition may vary within the zone because of

- 1) a thermal gradient or
- 2) inhomogenous solution composition within the zone at the beginning of alteration.

One means of developing the observed patterns would be by imposing a thermal gradient across the zone. This would lead to development of different solution composition by reactions between the basalt and the groundwater within the interclast voids and outer vesicles and a somewhat independent shift in composition in solutions within the inner vesicles of clasts. The contrasting temperatures would promote the stabilities of differing phases and a systematic change in mineralogy where settings of similar interconnected porosity are compared.

If the composition of the solution within the zone varied throughout the zone, perhaps as an artifact of original groundwaters in the flow top, then the precipitated phases would be different, providing the chemical gradients were maintained during alteration. This seems unlikely however, since the possibility of mixing within the solution would be great within the highly porous interclast void space, and the flow top would have been thoroughly turbated and the groundwater mixed during the emplacement of the superjacent flow.

SUMMARY

From the preceding discussion the variations in the secondary mineral assemblages within the vesicles and diktytaxitic cavities are the result of differing solution composition. Given the assumptions of this study the main variables considered have been interconnected porosity, nucleation, and temperature. A consideration of the interaction of the basalt, particularly

interstitial glass, with the solution at constant temperature has not been evaluated in this study. The differences in the percentage of glass in different flow zones indicated in Table III probably plays an important role in the alteration process. This role is being carefully investigated as part of the analog study in which the secondary phases in all settings including precipitated as well as replacement phases will be integrated with basalt textures and composition to arrive at the conditions and variables that are important in this system.

Indications of the differences in solution composition occur at all scales of observation; however, the factors that may influence solution composition may differ at the differing levels of observation.

At the scale of a vesicle, whether the solution composition is internally controlled by the precipitating phases or externally controlled by the composition of the reservoir solution is a function of the interconnected porosity of the rock surrounding the vesicle. Internal or external control are reflected in patterns observed in the secondary phases and the secondary mineral suite within vesicles.

At the scale of two neighboring vesicles different mineral suites may be produced by differing interconnected porosity around the vesicles but can also be produced by differing patterns of nucleation within the adjacent vesicles. This would be particularly true for those vesicles where solution composition is internally controlled.

At the scale of a hand sample the main differences appear to be closely related to the interconnected porosity within the rock. In breccia clasts the differences are particularly noticed in inner verses outer vesicles.

At the scale of different flow zones the differences appear to be more readily ascribed to differences in temperature across the flows at the time of alteration. Where differences in variables such as interconnected porosity can be eliminated, the solution in the rocks still shows compositional differences. Under the assumptions of the discussion, these differences are most readily explained by the imposition of a thermal gradient during alteration.

TEMPERATURE

The secondary mineralogical evidence suggests a thermal gradient in the outcrop at the time of alteration. The presence of a thermal gradient raises the questions 1) how the thermal gradient was generated and 2) the magnitude of the thermal gradient.

The thermal gradient may have resulted from 1) the ambient geothermal gradient or 2) heat generated from the superjacent flow during its cooling.

The temperature at the depth of the outcrop can be inferred from the maximum depth of burial assuming an overburden of 600+ m (2000 ft) and the geothermal gradient. The depth of overburden is determined from the difference in elevation between the top of the

uppermost stratigraphic unit exposed north of the study area and the analog study outcrop. If the regional gradient (approximately 22 m/° C) in the Pasco Basin is assumed for the Troy area (based on ambient temperatures of 60° C at 1000 m, and a mean annual temperature of 15° C), the maximum temperature at the depth of the analog and superjacent flow horizon would have been near 30° C. Using this same regional gradient, the temperature difference between the top of the superjacent flow and the lowermost exposure of the analog flow would have been less than 5° C. The temperature difference between the top and bottom of the flow-top breccia would be insignificant (<1° C) under this thermal gradient.

The local geothermal gradient may have been elevated since basalt feeder dikes are known in the area (Ross, 1978; Stoffel, 1984). If the gradient were elevated due to the presence of cooling feeder dikes in the area, and assuming the lower value of the range in gradients (11 m/° C - 99 m/° C) measured in holes drilled in the United States (Friedman and Sanders, 1978), the temperature at the analog/ superjacent flow horizon would have been 55° C. The temperature difference between the top of the superjacent flow and the exposed portion of the analog flow would have been <10° C, and the difference between the top and bottom boundaries of the flow-top breccia zone would again be insignificant (<1° C). Even an extreme geothermal gradient does not produce a thermal contrast that can account for differences in secondary mineralogy within the analog and superjacent flows.

Thermal gradients may have developed in flow zones of the

analog flow at the time of emplacement of the superjacent flow. The temperatures would have been highest in the interflow contact zone, and lowest in the flow interior zone of the analog flow. The isotherms would have been parallel to the interflow contact, suggesting that secondary minerals should be vertically zoned relative to the interflow contact. The secondary mineral patterns have been discussed in relation to the different flow zones and are found to be distributed relative to the location of the interflow contact. The changing patterns occur over thicknesses that range from abrupt changes noted over a matter of a few centimeters at the contact between the superjacent flow and the underlying flow-top breccia to a matter of a few meters within the flow-top breccia zone.

The statistical treatment of homogenization temperature data obtained through fluid inclusion analysis, is the most direct method of evaluating the temperature of secondary mineral formation, providing the fluid inclusions in a secondary mineral are of workable size. The secondary minerals examined in the suite from analog study outcrop did not yield workable inclusions, so an indirect means of estimating the magnitude of the gradient must be employed. The magnitude of the temperature at the analog and superjacent flow horizon can be estimated using temperature and age relations governing the stability of the silica minerals. This estimation is fraught with problems because of the number of assumptions that must be made. The argument is offered herein to provide an estimate of the temperature

conditions within the flow zones.

The magnitude of the thermal gradient can be estimated using temperature-age relations that govern the ordering of Opal-CT during hydrothermal alteration or diagenesis. Opal-CT, as indicated, occurs in the flow-top breccia zone up to 2 meters below the interflow contact, and does not occur in the interflow contact zone. The d(101) spacing of this opal-CT is 4.05 Å as indicated. Kano (1983) presents a figure (6) showing the relationship between d(101) spacing and temperature for opal-CT in 5-15 million year old sediments. The temperature range for a particular d(101) spacing is within a narrow band (the vertical difference between the line A-A' and line B-B' in Figure 6) and is $\pm 5-8^{\circ}$ C.

If the opal-CT in vesicles of Grande Ronde basalt is a product of the transformation of opal-A during diagenesis, the degree of ordering, as indicated by the d-spacing, should be consistent with the age of the basalt (Middle Miocene) and the temperature (30° C) inferred from the thickness of overburden (600+ m) and the present assumed geothermal gradient in the area (22 m/ $^{\circ}$ C). The temperature estimated from Figure 6 in Kano (1983) for a d(101) spacing of 4.05 Å, is approximately 55° C $\pm 5-8^{\circ}$ C, in contrast to the inferred temperature of burial of 30° C. If the geothermal gradients were elevated above the present-day gradient in the area due to the nearness of basalt feeder vents, a gradient double that above (11 m/ $^{\circ}$ C) would be required to produce a temperature of burial of 55° C.

The stability relations among the silica minerals have been presented by Fournier (1985). The precipitation of the various silica minerals requires supersaturation of the solution relative to quartz. If we assume that opal-CT was precipitated directly from solution, the d(101) spacing indicates a temperature of 50 to 60° C. At these temperatures the solution would contain from 100 to 200 ppm SiO₂. If it is further assumed that such a concentration was in the solutions within the vesicles at the base of the superjacent flow, the chalcedony-quartz saturation limit suggests a temperature of 170° C within these vesicles. If on the other hand amorphous silica were precipitated in the interflow contact zone, then the solution would have contained approximately 100 ppm SiO₂. Again if it is assumed that a solution of similar concentration were within the vesicles at the base of the superjacent flow, the chalcedony-quartz saturation line is approximately 150° C. Data to support these assumptions are sparse, however, what appeared to be a fluid inclusion within calcite was heated to a temperature of 125° C before it decrepetated along the cleavage.

REEVALUATION OF ASSUMPTIONS

The assumptions upon which the preceding discussion has been based must be reevaluated to assess their validity.

The assumption of constant pressure during alteration appears to be reasonable.

The altering solutions have been viewed as aqueous.

However, a vapor phase may have been important at the time of emplacement of the superjacent flow. The evidence determined from secondary minerals and textures does not preclude such an early vapor phase; however, no direct evidence of its existence has been identified.

The sequentially precipitated secondary minerals in vesicles infer chemically differing solutions through time. It is reasonable that the composition of the solution in vesicles is influenced by the solution in the reservoir within the interclast voids. This influence is a function of the extent to which the solution within the vesicle interacts with the reservoir solution through the interconnected porosity in the surrounding basalt. Those assumptions that treat the surrounding basalt as though chemically inert to solutions during alteration are not reasonable. Interactions between the basalt and solution may outweigh the influence of the interconnected porosity, kinetics, and temperature on the solution composition. The data in Table III indicate that each flow zone contains differing proportions of glass and crystalline phases. Petrographic analyses not reported in this study indicate that these differences in association with differing patterns of porosity have influenced the extent of alteration of the basalt. In vesicles within the interiors of breccia clasts the alteration of the surrounding basalt may be the controlling factor on solution composition in internally controlled settings. However, the influence of the surrounding basalt may not be as great in those vesicles where solution

composition is controlled externally, those vesicles closely connected to the reservoir solution within interclast voids. The interactions with the basalt may also be viewed in terms of water/rock ratios. The ratios would be higher for those settings where solution composition is externally controlled. These relations are the subject of continuing investigation.

CHAPTER VI

CONCLUSIONS

- 1) The analog flow and the superjacent flow have been divided into flow zones including the flow interior, transition, flow-top breccia, and interflow contact zones, that are defined on the basis of textures observed in thin section and intraflow structures observed in the field. The transition zone and the interflow contact zone are atypical of Grande Ronde Basalt, the former having textures transitional between the flow interior zone and the flow-top breccia zone, and the latter having interflow structures that reflect the dynamic emplacement of the superjacent flow.
- 2) The characteristics of the porosity and the extent of interconnection are distinct in the various flow zones. The major interconnected porosity of the flow interior zones is platy and vertical joint-related fractures; vesicles and diktytaxitic cavities are minor in comparison. Within the transition zone, the predominant interconnected porosity is the interclast voids within the loosely fused in situ breccias that mantle the dense spines. The flow-top breccia zone and the brecciated portions of the interflow contact zone are the most

- porous of the flow zones due to the large interclast voids. The interconnected porosity in the solid portion of the interflow contact zone is provided by platy jointing, and to a lesser extent, pipe vesicles and tree molds.
- 3) The precipitated secondary mineral suite in vesicles and diktytaxitic cavities has been characterized and includes clay minerals, zeolites, silica minerals, and a carbonate. Clay minerals include smectite and celadonite; zeolites include clinoptilolite, phillipsite, chabazite, and two unidentified zeolites; silica minerals include quartz, chalcedony, opal-CT lepispheres, and opal-CT; and carbonates include calcite. The variety of secondary minerals is greatest in the interflow contact zone, and flow-top breccia zone of the analog flow.
 - 4) The paragenetic sequence of the interflow contact and flow-top breccia zones is clay minerals --> silica minerals --> zeolites --> carbonate --> silica minerals --> clay minerals. The paragenetic sequences of the flow interior and transition zones are abbreviated, though appear to agree with the sequence above. The individual mineral species differ among the flow zones. In the flow-top breccia zone smectite, clinoptilolite, and opal-CT are the major occurring secondary minerals. In the interflow contact zone, celadonite, chalcedony, and quartz are the major occurring minerals.

- 5) The sequentially precipitated secondary mineral layers within vesicles and diktytaxitic cavities are the result of differing solution composition. Assuming the basalt is chemically inert to altering solutions, i. e. the solution composition is not influenced by the relative proportions of glass and crystalline phases in the basalt or water/rock ratios, the immediate controls on solution composition are interconnected porosity, kinetics, and/or temperature depending on the scale of observation. Petrographic data not reported in this study suggest that these assumptions require modification, particularly for vesicles within the interiors of clasts in those settings where the solution composition is controlled internally. The influence on solution composition of the basalt may potentially outweigh the influence of the interconnected porosity, kinetics, and temperature.
- 6) Heat from the cooling of the superjacent flow imposed a thermal gradient on the outcrop at the time of alteration. The magnitude of the thermal gradient can only be inferred from indirect mineralogic evidence, since workable fluid inclusions are not available in this outcrop.

REFERENCES

- Allen, C. C., and Strope, M. B., 1983, Microcharacterization of basalt--considerations for a nuclear waste repository, in Gooley, R., ed., Microbeam Analysis-1983: San Francisco Press, Inc., San Francisco, Ca, p. 51-53.
- Ames, L. L., 1980, Hanford basalt flow mineralogy: Richland, Washington, Pacific Northwest Laboratory Report PNL-2847, 447 p.
- Benson, L. V., 1978, Secondary minerals, oxidation potentials, pressure and temperature gradients in the Pasco Basin of Washington State: Richland Washington, Rockwell Hanford Operations RHO-BWI-C-34, 21 p.
- Benson, L. V., Teague, L. S., Mouton, C. A., Frisch, C. J., Stolzman, R. A., and Corrigan, D. J., 1979a, A study of rock-water-nuclear waste interactions in the Pasco Basin, Washington, Part I: Distribution and composition of secondary and primary mineral phases in basalts of the Pasco Basin, Washington: University of California, Lawrence Berkeley Laboratory LBL-9677, 24 p.
- Benson, L. V., Carnahan, C. L., and Che, M., 1979b, A study of rock-water-nuclear waste interactions in the Pasco Basin, Washington, Part II: Equilibrium-step simulations of basalt-water-nuclear waste interactions: University of California, Lawrence Berkeley Laboratory LBL-9677, 24 p.
- Benson, L. V., and Teague, L. S., 1982, Diagenesis of basalts from the Pasco Basin, Washington- 1. Distribution and composition of secondary mineral phases: *Journal of Sedimentary Petrology*, v. 52, p. 595-613.
- Boles, J. R., 1972, Composition, optical properties, cell dimensions, and thermal stability of some heulandite group zeolites: *American Mineralogist*, v. 57, p. 1463-1493.
- Carnahan, C. L., 1978, Simulation of geochemical reactions by equilibrium step codes, topical report number 2: Richland Washington, Rockwell Hanford Operations, RHO-BWI-C-37, 17 p.
- Deer, W. A., Howie, R. A., and Zussman, J., 1963, Rock-forming minerals, vol. 4, Framework Silicates: Longmans: London, 528 p.

- Florke, O. W., Hollmann, R., Von Rad, U., and Rosch, H., 1976, Intergrowth and twinning in opal-CT lepispheres: Contributions to Mineralogy and Petrology, v. 58, p. 235-242.
- Fournier, R. O., 1985, Silica minerals as indicators of conditions during gold deposition, in Tooker, E. W., ed., Geologic characteristics of sediment- and volcanic-hosted disseminated gold deposits; Search for an occurrence model: U. S. Geological Survey Bulletin 1646, p. 15-26.
- Friedman, G. M., and Sanders, J. E., 1978, Principles of sedimentology: John Wiley & Sons: New York, 792 p.
- Frye, K., 1974, Modern Mineralogy: Prentice-Hall, Inc., Englewood, Cliffs: New Jersey, 325 p.,
- Gephart, R. E., Price, S. M., Jackson, R. L., and Myers, C. W., 1984, Geohydrologic factors and current concepts relevant to characterization of a potential nuclear waste repository site in Columbia River Basalt, Hanford Site, Washington, in McVay, G. L., ed., Scientific Basis For Nuclear Waste Management VII, Materials Research Society symposia proceedings: Elsevier Science Publishing Co., Inc., v. 26, p. 85-94.
- Gottardi, G., and Galli, E., 1985, Natural Zeolites: Springer Verlag, New York, 409 p.
- Horton, D. G., 1985, Status report on secondary minerals in Rocky Coulee and Cohasset flow tops: Richland Washington, Rockwell Hanford Operations, SD-BWI-TI-302, 107 p.
- Joint Committee on Powder Diffraction Standards (JCPDS), 1974, Selected powder diffraction data for minerals, v. 1, 2.
- Jones, J. B., and Segnit, E. R., 1971, The nature of opal. I. Nomenclature and constituent phases: Journal of the Geological Society of Australia, v. 18, p. 57-68.
- Kano, K., 1983, Ordering of opal-CT in diagenesis: Geochemical Journal, v. 17, p. 87-93.
- Kano, K., and Taguchi, K, 1982, Experimental study on the ordering of opal-CT: Geochemical Journal, v. 16, p. 33-41.
- Lane, D. L., Allen, C. C., and Adee, R. R., 1985, Progress report on the hydrothermal interaction of defense waste glasses with basalt and groundwater at 150°C: Richland Washington, Rockwell Hanford Operations, SD-BWI-TI-312, 98 pp.

- Long, P. E., 1984, Repository Horizon Identification Report: Richland Washington, Rockwell Hanford Operations, SD-BWI-TY-001, 567 p.
- Long, P. E., and Strobe, M. B., 1983, Composition of augite and pigeonite in basalt flows that are candidates for a nuclear waste repository: Richland Washington, Rockwell Hanford Operations, RHO-BW-SA-295P, 8 p.
- Long, P. E., and Wood, B. J., 1986, Structures, textures, and cooling histories of Columbia River basalt flows: Bulletin Geological Society of America, v. 97, p. 1144-1155.
- McCall, T. B., and Krogness, J. C., 1986, The reference waste package design for a nuclear waste repository in basalt, in Burkholder, H. C., ed., Nuclear Waste Disposal: Battelle Press, Columbus - Richland, p. 525-531.
- Moore, E. L., Ulmer, G. C., and Grandstaff, D. E., 1985, Hydrothermal interaction of Columbia plateau basalt from the Umtanum Flow (Washington, U.S.A.) with its coexisting groundwater: Chemical Geology, v. 49, p. 53-71.
- Noonan, A. F., Fredricksson, K., and Nelen, J., 1981, Phase chemistry of the Umtanum basalt, a preferred repository host in the Columbia Plateau, in Moore, J. G., ed., Scientific basis for nuclear waste management: New York, Plenum Press, v. 3, p. 51-58.
- Orzol, L. L., and Cummings, M. L., 1986, Phreatic structures in flows of the Grande Ronde basalt, Columbia River Basalt Group, near Troy, Oregon [abs]: Abstracts with Programs Geological Society of America, v. 18, no. 2, p.167-168.
- Passaglia, E., 1970, The crystal chemistry of chabazites: American Mineralogist, v. 55, p. 1278-1301.
- Price, S. M., 1977, An evaluation of dike-flow correlation indicated by geochemistry, Chief Joseph dike swarm, Columbia River basalt: unpublished Ph.D. dissertation, Moscow, Idaho, University of Idaho, 320 p.
- Rawson, S. A., 1986, X-ray diffraction study of selected Cohasset and Rocky Coulee Flowtops: Richland Washington, Rockwell Hanford Operations, SD-BWI-TI-269, 287 p.
- Reidel, S. P., 1983, Stratigraphy and petrogenesis of the Grande Ronde Basalt from the deep canyon country of Washington, Oregon, and Idaho: Bulletin Geological Society of America, v. 94, p. 519-542.

- Ross, M. E., 1978, Stratigraphy, structure, and petrology of Columbia River Basalt in a portion of the Grande Ronde River-Blue Mountains area of Oregon and Washington: Ph.D. Dissertation, Moscow, Idaho: University of Idaho, 407 p.
- Ross, M. E., 1980, Tectonic controls of topographic development within Columbia River basalts in a portion of the Grande Ronde River-Blue Mountains Region, Oregon and Washington: Oregon Geology, v. 42, no. 10, p. 167-171, 174.
- Ross, M. E., 1983, Chemical and mineralogic variations within four dikes of the Columbia River Basalt Group, southeastern Columbia Plateau: Bulletin Geological Society of America, v. 94, p. 1117-1126.
- Scheetz, B. E., Smith, D. K., Barnes, M. W., Komarneni, S., Stull, L. M., and Smith, C. A., 1978, Simulated high-level water-basalt interaction experiments: Richland Washington, Rockwell Hanford Operations, RHO-BWI-C-33, 40 p.
- Schiffman, P., and Lofgren, G. E., 1982, Dynamic crystallization studies on the Grande Ronde pillow basalts, Central Washington: Journal of Geology, v. 90, p. 49-78.
- Sheppard, R. A. and Gude, A. J., 1973, Zeolites and associated authigenic silicate minerals in tuffaceous rocks of the Big Sandy Formation, Mohave County, Arizona: U. S. Geological Survey Professional Paper 830, 36 p.
- Stoffel, K. L., 1984, Geology of the Grande Ronde lignite field, Asotin County, Washington: Washington Department of Natural Resources Division of Geology and Earth Resources Report of Investigations 27, 79 p.
- Swanson, D. A., and Wright, T. L., 1976, Magnetostratigraphic units in the Yakima Basalt, southeast Washington [abs]: Geological Society of America Abstracts with Programs, v. 8, p. 413-414.
- Taubeneck, W. H., 1970, Dikes of Columbia River basalt in northeastern Oregon, western Idaho, and southeastern Washington, in Gilmour, E. H., and Stradling, D., eds., Proceedings of the Second Columbia River Basalt Symposium, Cheney, Washington, March 1969, Cheney, Washington, Eastern Washington State College Press, p. 73-96.
- Teague, L. S., 1980, Secondary minerals found in cores DC2 A1 and DC2 A2 taken from the Grande Ronde Basalt formation, Pasco Basin, Washington: University of California, Lawrence Berkeley Laboratory LBL-10387, 29 p.

- White, A. F., Yee, A., and Flexser, S., 1985, Surface oxidation-reduction kinetics associated with experimental basalt-water reaction at 25° C: *Chemical Geology*, v. 49, p. 73-86.
- Williams, H., Turner, F. J., Gilbert, C. M., 1982, *Petrography: An introduction to the study of rocks in thin sections*: San Francisco, W. H. Freeman Company, 626 p.
- Wright, T. L., Grolier, M. J., and Swanson, D. A., 1973, Chemical variation related to the stratigraphy of the Columbia River Basalt: *Bulletin Geological Society of America*, v. 84, p. 371-386.
- Yung, S. C., Toyooka, R. T., and McCall, T. B., 1986, Thermal analysis for BWIP waste package advanced conceptual design, in Post, R., ed., *Waste Management 86*, University of Arizona/American Nuclear Society.
- Zoltai, T., and Stout, J. H., 1984, *Mineralogy concepts and principles*: Burgess Publishing Company: Minneapolis, 505 p.

APPENDIX A

TABLE XVI

PETROGRAPHIC SUMMARY OF INDIVIDUAL SAMPLES
FLOW INTERIOR ZONE/ ANALOG FLOW

SAMPLE: 84a

PRIMARY TEXTURES:

	Modal Analysis (%)	:	Size (mm)
Microphenocrysts	5.9		
Plagioclase	4.0		1.3
Pyroxene	1.9		1.1
Groundmass	89.6		
Plagioclase (1)	43.9		0.30
Pyroxene (1)	30.0		0.30
Opagues	11.9		0.15
Glass (2)	3.8		
Cavities (3)	4.6		0.4

Textural patterns:

Vert. position (4)	-21.0:	Pyroxene buds (5)	No
Inter- pyroxene (6)		: Crystallites	No
Preferred Orient (7)	No	: Polyhedral	Yes
Microlites (8)	No	: Disseminated	No
Cavities (3)	No	: Dendritic	No

Textural relations: Sample 84a is holocrystalline (incipient alteration of groundmass phases point-counted as glass) intergranular as defined by anhedral pyroxene microlites and polyhedral opaques which occupy interstices between plagioclase microlites and microphenocrysts. The size contrast between microphenocrysts and microlites is small. Only isolated diffuse masses of diktytaxitic cavities and no vesicles are present.

Notes: (1) Microlites.

(2) Original or altered glass.

(3) Vesicles + diktytaxitic cavities.

(4) Vertical position above (+) or below (-) the interflow contact.

(5) Pyroxene buds on opposing sides of plagioclase lath.

(6) Interpenetrating pyroxene/plagioclase microphenocrysts.

(7) Preferred orientation.

(8) Plagioclase microlites.

SAMPLE: 83a

PRIMARY TEXTURES:	Modal Analysis (%)	:	Size (mm)
Microphenocrysts	3.4		
Plagioclase	1.7		1.5
Pyroxene	1.7		0.6
Groundmass	90.5		
Plagioclase (1)	39.0		0.15
Pyroxene (1)	33.5		0.07
Opakes	10.0		0.05
Glass (2)	8.0		
Cavities (3)	6.0		1.3

Textural patterns:

Vert. position (4)	-12.0:	Pyroxene buds (5)	Yes
Inter- pyroxene (6)	Yes :	Crystallites	No
Preferred Orient (7)	:	Polyhedral	Yes
Microlites (8)	Yes :	Disseminated	Yes
Cavities (3)	No :	Dendritic	No

Textural relations: Sample 83a is holocrystalline intergranular as 84a, though the size contrast between microphenocrysts and microlites is greater. Dark streaks of disseminated opakes occur in a dominant light colored groundmass with polyhedral opakes. Only diktytaxitic cavities are present.

SAMPLE: 83b

PRIMARY TEXTURES:	Modal Analysis (%)	:	Size (mm)
Microphenocrysts	3.5		
Plagioclase	2.0		1.4
Pyroxene	1.5		0.7
Groundmass	94.0		
Plagioclase (1)	43.0		0.10
Pyroxene (1)	39.0		0.07
Opakes	7.0		0.03
Glass (2)	5.0		
Cavities (3)	2.5		1.3

Textural patterns:

Vert. position (4)	-11.5:	Pyroxene buds (5)	No
Inter- pyroxene (6)	No :	Crystallites	No
Preferred Orient (7)	:	Polyhedral	Yes
Microlites (8)	Yes :	Disseminated	Yes
Cavities (3)	No :	Dendritic	No

Textural relations: Sample 83b is holocrystalline intergranular with size contrast between microphenocrysts and microlites as in 83a. However, streaks of finely disseminated opakes become more prominent, extensive, and have sharper boundaries against the lighter colored groundmass, and the development of diktytaxitic cavities is more pronounced than in 83a.

TABLE XVII

PETROGRAPHIC SUMMARY OF INDIVIDUAL SAMPLES
TRANSITION ZONE/ ANALOG FLOW

SAMPLE 8b:

PRIMARY TEXTURES:	Modal Analysis (%)	:	Size (mm)
Microphenocrysts	3.0		
Plagioclase	1.8		1.0
Pyroxene	1.2		0.7
Groundmass	81.6		
Plagioclase (1)	30.1		0.08
Pyroxene (1)	17.9		0.06
Opagues	7.6		0.08
Glass (2)	26.0		
Cavities (3)	15.4		4.0

Textural patterns:

Vert. position (4)	- 2.0: Pyroxene buds (5)	Yes
Inter- pyroxene (6)	No : Crystallites	No
Preferred Orient (7)	: Polyhedral	Yes
Microlites (8)	Yes : Disseminated	Yes
Cavities (3)	No : Dendritic	No

Textural relations: Sample 8b is matrix-supported breccia in which the matrix is hypocrySTALLINE with intersertal glass (5-7% diktytaxitic cavities) and a rounded vesicular (28-30%) clast is darker colored than the matrix due to finely disseminated opaques. The matrix has less disseminated opaques and opaque polyhedra. The boundary between clast and matrix is gradational over 3-5 mm.

SAMPLE: 28a

PRIMARY TEXTURES:

	Modal Analysis (%)	:	Size (mm)
Microphenocrysts	4.0		
Plagioclase	2.6		1.1
Pyroxene	1.4		0.6
Groundmass	91.7		
Plagioclase (1)	42.1		0.11
Pyroxene (1)	21.1		0.05
Opakes	28.5		0.08
Glass (2)	0.0		
Cavities (3)	4.3		2.7

Textural patterns:

Vert. position (4)	- 3.5: Pyroxene buds (5)	No
Inter- pyroxene (6)	No : Crystallites	No
Preferred Orient (7)	: Polyhedral	Yes
Microlites (8)	Yes : Disseminated	No
Cavities (3)	Yes : Dendritic	No

Textural relations: Sample 28a is holocrystalline intergranular in which sub- to anhedral pyroxene microlites and opaque polyhedra occur interstitial to plagioclase laths. Size contrast between microphenocrysts and microlites is noticeable. Small (8mm) rounded clasts with 15-20% vesicles occur in a groundmass with no vesicles and 8-13% diktytaxitic cavities.

SAMPLE: 28c(a)

	Modal Analysis (%)	:	Size (mm)
Microphenocrysts	3.6		
Plagioclase	2.3		0.9
Pyroxene	1.3		0.5
Groundmass	85.6		
Plagioclase (1)	40.2		0.16
Pyroxene (1)	30.2		0.09
Opakes	9.6		0.08
Glass (2)	5.6		
Cavities (3)	10.8		3.8

Textural patterns:

Vert. position (4)	- 3.5: Pyroxene buds (5)	No
Inter- pyroxene (6)	No : Crystallites	No
Preferred Orient (7)	: Polyhedral	Yes
Microlites (8)	Yes : Disseminated	Yes
Cavities (3)	Yes : Dendritic	No

Textural relations: Sample 28c(a) is holo- to hypocrytalline. Holocrystalline parts are intergranular with finely disseminated opakes. Hypocrytalline parts have lighter colored groundmass polyhedral opakes, and intersertal glass. An incipient vesiculated clast (10 mm dia) has disseminated opakes. Elongate cavities surround clast and patches of disseminated opakes.

SAMPLE: 28c(b)

PRIMARY TEXTURES:	Modal Analysis (%)	:	Size (mm)
Microphenocrysts	3.0		
Plagioclase	1.9		1.2
Pyroxene	1.1		0.8
Groundmass	92.2		
Plagioclase (1)	43.8		0.09
Pyroxene (1)	25.7		0.06
Opagues	10.3		0.17
Glass (2)	12.4		
Cavities (3)	4.8		1.0

Textural patterns:

Vert. position (4)	- 3.5: Pyroxene buds (5)	No
Inter- pyroxene (6)	No : Crystallites	No
Preferred Orient (7)	: Polyhedral	Yes
Microlites (8)	Yes : Disseminated	Yes
Cavities (3)	Yes : Dendritic	No

Textural relations: Sample 28c(b) is hypocrySTALLINE with intersertal glass, and has dark streaks or angular forms of finely disseminated opaques in a dominant light colored groundmass with opaque polyhedra. The dark streaked domains have sharp boundaries marked by oriented plagioclase laths and elongate diktytaxitic cavities. No clast fragments are present.

SAMPLE: 69d

PRIMARY TEXTURES:	Modal Analysis (%)	:	Size (mm)
Microphenocrysts	3.7		
Plagioclase	2.6		1.3
Pyroxene	1.1		0.9
Groundmass	74.7		
Plagioclase (1)	30.0		0.08
Pyroxene (1)	21.9		0.05
Opagues	2.1		0.07
Glass (2)	20.7		
Cavities (3)	21.6		6.0

Textural patterns:

Vert. position (4)	- 6.0: Pyroxene buds (5)	No
Inter- pyroxene (6)	No : Crystallites	No
Preferred Orient (7)	: Polyhedral	Yes
Microlites (8)	Yes : Disseminated	Yes
Cavities (3)	Yes : Dendritic	No

Textural relations: Sample 69d is matrix-supported breccia with light colored hypocrySTALLINE matrix (15-20% diktytaxitic cavities) and dark angular breccia fragments (30% vesicles). Breccia fragments are mostly fused to the matrix, though are partly surrounded by cavities or intersticies. The clasts are up to 1.8 cm in diameter. Dark patches or streaks or patches of disseminated opaques are also present.

SAMPLE: 83c

PRIMARY TEXTURES:	Modal Analysis (%)	:	Size (mm)
Microphenocrysts	4.5		
Plagioclase	2.8		1.1
Pyroxene	1.7		1.2
Groundmass	92.2		
Plagioclase (1)	29.7		0.15
Pyroxene (1)	19.9		0.06
Opagues	5.4		0.05
Glass (2)	37.2		
Cavities (3)	3.3		1.8

Textural patterns:

Vert. position (4)	-10.0: Pyroxene buds (5)	No
Inter- pyroxene (6)	Yes : Crystallites	No
Preferred Orient (7)	: Polyhedral	Yes
Microlites (8)	Yes : Disseminated	Yes
Cavities (3)	No : Dendritic	No

Textural relations: Sample 83c is hypocrystalline with abundant disseminated opaques in the groundmass. One small (2 cm dia) vesiculated (10-12%) clast is present that is darker in color than the surrounding basalt groundmass. The rounded clast boundary is gradational and is not surrounded by cavities.

Notes: (1) Microlites.

(2) Original or altered glass.

(3) Vesicles + diktytaxitic cavities.

(4) Vertical position above (+) or below (-) the interflow contact.

(5) Pyroxene buds on opposing sides of plagioclase lath.

(6) Interpenetrating pyroxene/plagioclase microphenocrysts.

(7) Preferred orientation.

(8) Plagioclase microlites.

TABLE XVIII

PETROGRAPHIC SUMMARY OF INDIVIDUAL SAMPLES
FLOW-TOP BRECCIA ZONE/ ANALOG FLOW

SAMPLE 271:

PRIMARY TEXTURES:

	Modal Analysis (%)	:	Size (mm)
Microphenocrysts	3.1		
Plagioclase	2.3		1.2
Pyroxene	0.8		0.7
Groundmass	76.9		
Plagioclase (1)	31.2		0.10
Pyroxene (1)	16.5		0.04
Opagues	1.1		0.34
Glass (2)	28.1		
Cavities (3)	20.0		9.0

Textural patterns:

Vert. position (4)	- 2.5: Pyroxene buds (5)	Yes
Inter- pyroxene (6)	Yes : Crystallites	Rare
Preferred Orient (7)	: Polyhedral	Yes
Microlites (8)	No : Disseminated	Rare
Cavities (3)	No : Dendritic	Yes

Textural relations: Sample 271 is hypocrystalline with intersertal glass between microlites. Dendritic opaques occur near vesicle walls within the groundmass. Disseminated opaques and crystallites are rare only occurring within 2 angular domains 0.5 x 3 mm. These domains are partly surrounded by diktytaxitic cavities.

Notes: (1) Microlites.

(2) Original or altered glass.

(3) Vesicles + diktytaxitic cavities.

(4) Vertical position above (+) or below (-) the interflow contact.

(5) Pyroxene buds on opposing sides of plagioclase lath.

(6) Interpenetrating pyroxene/plagioclase microphenocrysts.

(7) Preferred orientation.

(8) Plagioclase microlites.

TABLE XIX

PETROGRAPHIC SUMMARY OF INDIVIDUAL SAMPLES
INTERFLOW CONTACT ZONE/ ANALOG AND SUPERJACENT FLOWS

SAMPLE 36e:

PRIMARY TEXTURES:

	Modal Analysis (%)	:	Size (mm)
Microphenocrysts	4.0		
Plagioclase	2.5		0.8
Pyroxene	1.5		0.6
Groundmass	67.3		
Plagioclase (1)	28.1		0.20
Pyroxene (1)	5.0		0.15
Opagues	2.8		0.08
Glass (2)	31.4		
Cavities (3)	28.6		7.0

Textural patterns:

Vert. position (4)	- 1.5: Pyroxene buds (5)	No
Inter- pyroxene (6)	No : Crystallites	Yes
Preferred Orient (7)	: Polyhedral	Yes
Microlites (8)	No : Disseminated	No
Cavities (3)	No : Dendritic	No

Textural relations: Sample 36e is hypocrystalline with intersertal glass between microlites and rod- to hair-like crystallites within the glass. The crystallites appear to be gradational with microlites, particularly plagioclase. The crystallites are up to 0.6 mm long, 0.002 mm in diameter, colorless in plane light, and weakly birefringent to isotropic in cross polarized light.

Notes: (1) Microlites.

(2) Original or altered glass.

(3) Vesicles + diktytaxitic cavities.

(4) Vertical position above (+) or below (-) the interflow contact.

(5) Pyroxene buds on opposing sides of plagioclase lath.

(6) Interpenetrating pyroxene/plagioclase microphenocrysts.

(7) Preferred orientation.

(8) Plagioclase microlites.

TABLE XX

PETROGRAPHIC SUMMARY OF INDIVIDUAL SAMPLES
FLOW INTERIOR ZONE/ SUPERJACENT FLOW

SAMPLE 51:

PRIMARY TEXTURES:

	Modal Analysis (%)	:	Size (mm)
Microphenocrysts	3.5		
Plagioclase	2.7		0.9
Pyroxene	0.8		0.9
Groundmass	88.3		
Plagioclase (1)	32.9		0.30
Pyroxene (1)	25.2		0.30
Opagues	14.1		0.13
Glass (2)	16.1		
Cavities (3)	8.3		1.9

Textural patterns:

Vert. position (4)	+ 0.5: Pyroxene buds (5)	No
Inter- pyroxene (6)	Yes : Crystallites	Yes
Preferred Orient (7)	: Polyhedral	Yes
Microlites (8)	Yes : Disseminated	No
Cavities (3)	No : Dendritic	No

Textural relations: Sample 51 is hypocrySTALLINE with intersertal glass between microlites. The original basaltic glass is red-brown in plane light, and isotropic in cross polarized light. Size contrast between microphenocrysts and microlites is low. Only rounded diffuse patches of diktytaxitic cavities and no vesicles are present.

SAMPLE: 22h

PRIMARY TEXTURES:	Modal Analysis (%)	:	Size (mm)
Microphenocrysts	2.0		
Plagioclase	1.5		2.4
Pyroxene	0.5		0.2
Groundmass	93.0		
Plagioclase (1)	39.0		0.18
Pyroxene (1)	21.5		0.13
Opauques	6.5		0.07
Glass (2)	26.0		
Cavities (3)	5.0		0.6

Textural patterns:

Vert. position (4)	+ 1.0:	Pyroxene buds (5)	No
Inter- pyroxene (6)	No	: Crystallites	No
Preferred Orient (7)	:	Polyhedral	Yes
Microlites (8)	No	: Disseminated	No
Cavities (3)	No	: Dendritic	No

Textural relations: Sample 22h is hypocrystalline with intersertal glass between microlites. This sample has darker colored groundmass than sample 51 possibly due to the alteration of glass and/or finely disseminated opaques. Diktytaxitic cavities are sparse, small, and occur in rounded diffuse patches. Rare small (.60 mm dia) vesicles are present.

Notes: (1) Microlites.

(2) Original or altered glass.

(3) Vesicles + diktytaxitic cavities.

(4) Vertical position above (+) or below (-) the interflow contact.

(5) Pyroxene buds on opposing sides of plagioclase lath.

(6) Interpenetrating pyroxene/plagioclase microphenocrysts.

(7) Preferred orientation.

(8) Plagioclase microlites.

APPENDIX B

PRIMARY TEXTURES

The primary igneous textures vary among the flow zones comprising the analog and superjacent flows. The variations are developed in response to varying conditions within the flows at the time of crystallization. Since the textural patterns influence how rocks respond to hydrothermal alteration, it is of value to identify the relations that occur within the flow zones. As might be expected, overlapping and/or gradational textural variations may define several relations within the same flow zone. The textural relations are characterized by the relative abundance, patterns, and distribution among crystalline phases and glass, vesicles and diktytaxitic cavities, and breccias. These textural features and their relations are readily observed in thin section though not in the field. The general textural relations, their characteristics and distinguishing features are summarized in Table III.

Standard thin and/or polished sections were prepared from representative samples from the analog and superjacent flows of the study outcrop, and these samples were examined with a Zeiss Universal petrographic microscope using transmitted polychromatic light. The textural relations summarized in Table III are based on the standard petrographic analysis of 46 samples. Petrographic

summaries of selected individual samples from the various flow zones are included in Tables XVI through XX (See Appendix A). Modal abundances were determined by 1000 point point-counts for 35 of the 46 samples analyzed. Visual estimates of modal abundances have been used as supplemental data for the 11 samples not point-counted. Visual estimates of grain and cavity size are included in Tables XVI through XX (Appendix A).

ANALOG FLOW

The primary textural relations within the flow interior, transition, and flow-top breccia zones are described below.

Flow Interior Zone

The textural relations within the flow interior flow zone are characterized by the proportions of crystalline phases versus glass, and the abundance and character of vesicles and diktytaxitic cavities. Samples 84a, 83a, 83b, and 83c are representative of the characteristic textural features and relations within the flow interior zone. Petrographic descriptions and locations within the flow zone are given in Table XVI for each sample (See Appendix A). Table III contains a summary of petrographic data for all samples analyzed from this zone.

The flow interior zone of the analog flow ranges from holocrystalline intergranular to hypocrySTALLINE intersertal. Crystals of plagioclase and pyroxene are large with respect to

groundmass crystals of plagioclase, pyroxene, and opaques. Since most of the larger crystals of plagioclase and pyroxene can only be detected with a microscope, they will be termed microphenocrysts, and the texture they define microporphyritic, after the convention of Williams and others (1982). Plagioclase and pyroxene in the groundmass will be termed microlites.

Microphenocrysts are more prominent high in the flow interior zone than deeper where the groundmass is coarser grained. Plagioclase microphenocrysts are 1.0 to 1.5 millimeters long, sub to euhedral, stubby to elongate, and have sharp to gradational grain boundaries against the groundmass. The sharpness of the grain boundary is a function of grain size; the smaller the microphenocryst the more gradational the boundary is with microlites in the groundmass.

Pyroxene microphenocrysts are 0.6 to 1.2 millimeters long, sub- to anhedral, equant to stubby, and have sharp to slightly gradational boundaries against the groundmass. Pyroxene and plagioclase commonly occur as single grains or are in accidental contact with each other. However, several relations between the two minerals are distinctive.

Figure 49 is a photomicrograph of lath-shaped plagioclase microphenocrysts intergrown with augite in the form of opposing bud-shaped crystals. The pyroxene buds are disposed symmetrically to the plagioclase lath and are believed to surround the plagioclase grain in three dimensions. The plagioclase lath is constricted at the point where the pyroxene is attached to the grain and widens away from the point of attachment. The pyroxene

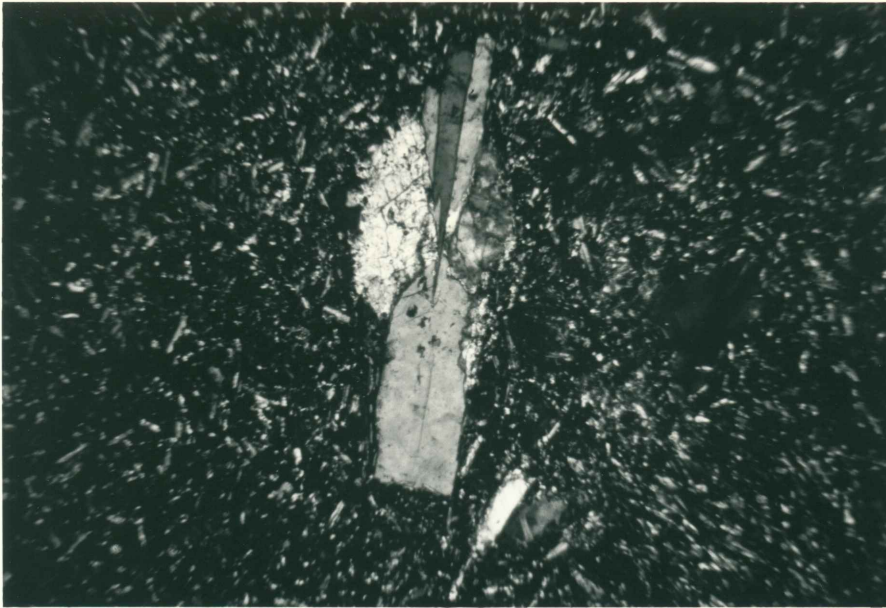


Figure 49. Plagioclase lath intergrown with augite in the form of opposing, optically discontinuous bud-shaped crystals. Sample 83a, crossed-polarized light, field of view 1.3 millimeters.

crystals are optically discontinuous and within the buds display fan-shaped radiating extinction positions outward from the point of attachment. The average frequency of occurrence is such that at least one out of three thin sections contains samples of this texture (See Table III). The texture is more common in samples from high in the flow interior than those from deeper in the zone.

Another texture is illustrated in Figure 50. Optically continuous subhedral pyroxene microphenocrysts are intergrown with lath-shaped plagioclase. The angle between the crystals commonly approximates 60° and ranges toward 90° . The interpenetrating phenocrysts are also found high in the flow interior zone where at least one thin section out of three contains one or more



Figure 50. Optically continuous pyroxene microphenocryst (horizontally disposed near the center of photograph) intergrown with plagioclase. Sample 83a, plane-polarized light, field of view 1.3 millimeters.

occurrences of the given texture. The frequency of occurrence of these interpenetrating phenocrysts is indicated in Table III.

Pyroxene, particularly augite, occurs as inclusions within plagioclase microphenocrysts and also forms coronas around plagioclase and orthopyroxene. Orthopyroxene is rare and where present is typically rimmed by augite (Figure 51).

Cumuloporphyritic masses similar to those described by Horton (1985) of pyroxene and plagioclase are common in most samples (Figure 52). These clusters contain up to six crystals and are up to 0.6 millimeters in diameter.

The plagioclase and pyroxene microphenocrysts are commonly fractured; however, displacement is not common across the

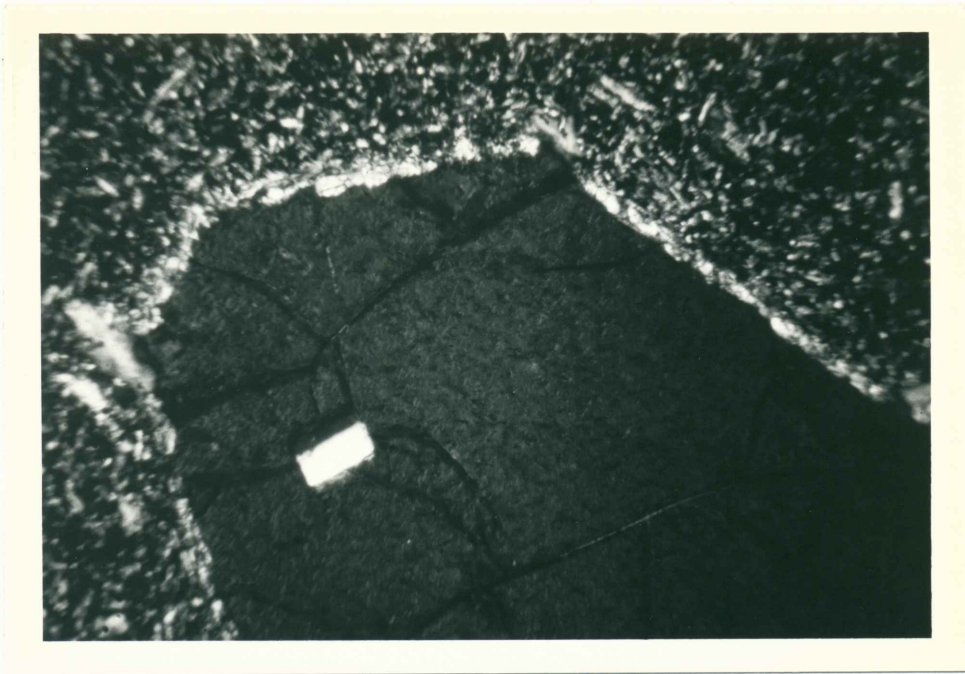


Figure 51. Orthopyroxene at partial extinction (dark gray in photomicrograph) is rimmed by augite (light-colored birefringent corona). Sample 83a, cross-polarized light, field of view 1.3 millimeters.



Figure 52. Cumuloporphyritic mass of pyroxene and plagioclase microphenocrysts. Sample 27g, cross-polarized light, field of view 1.3 millimeters.

fractures. Where displacement is noted, the fracture extends into the surrounding groundmass. Where displacement is not noted, many of the fractures extend into the groundmass, though they may be restricted to the microphenocryst. Microphenocrysts may also be bent along their \underline{c} crystallographic axis as indicated by distortions of crystal shape and optical patterns within the crystals. Fracturing and bending of microphenocrysts is more common high in the flow interior zone and becomes common in the overlying transition zone.

The groundmass is composed of microlites, opaques, and cavities. Microlites are tabular to prismatic and birefringent, whereas crystallites are rod-like and hair-like isotropic forms (Williams and others, 1982). Microlites are abundant in the flow interior zone, though crystallites are not. Opaques occur as polyhedral grains, and anhedral disseminated grains. Cavities include diktytaxitic cavities and vesicles. Vesicles are characterized by rounded walls against the groundmass reflecting development while the flow was still molten. The diktytaxitic cavities are developed interstitially to microlites and have their shapes controlled by the shape of crystals in the groundmass. A continuum exists between the two cavity types.

Microlites range from .10 to .30 millimeter in long dimension for plagioclase and .06 to .30 millimeter across for pyroxene. In the flow interior zone microlites define an intergranular texture (Figure 53). Plagioclase microlites are lath-shaped and a weakly developed preferred orientation is noted



Figure 53. Intergranular holocrystalline texture. Sample 84a, plane-polarized light, field of view 1.3 millimeters.

in samples high in the flow interior zone. Pyroxene microlites are sub- to anhedral, and equant to stubby and near colorless in plane polarized light. The grain boundaries of pyroxene and plagioclase microlites are sharp against the surrounding materials. Microlites produce the main textural elements of the groundmass.

Opaque grains are important constituents of the groundmass. Opaques occur as equant polyhedra up to 0.15 millimeter in diameter and as anhedral disseminated grains less than .03 millimeter in diameter. The modal percentage and other data are included in Table III.

Equant polyhedra are the most common morphological habit for the opaques and is the main occurrence found within the deeper

portions of the flow interior zone. Opaques are also closely associated with pyroxene and may occur as inclusions within microphenocrysts or in contact with microlites. Higher within this zone disseminated opaques occur with opaque polyhedra. Disseminated opaques produce a dark-colored groundmass in thin section, whereas the groundmass is lighter colored where the opaque polyhedra are dominant. High in the flow interior zone the occurrence of disseminated opaques is patchy within a light-colored groundmass where opaque polyhedra dominate.

As indicated, the patterns of opaque distribution change upwards through the flow interior zone. The transition from one pattern to another is illustrated by samples 83b (Table XVI) and 83c (Table XVII). In sample 83b disseminated opaques occur in dark streaks or patches that are volumetrically less than the lighter colored portions of the groundmass containing opaque polyhedra. In sample 83c, one half meter higher in the flow interior, disseminated opaques dominate over the opaque polyhedra. Sample 83c has been assigned to the transition flow zone based on the dominant occurrence of disseminated over polyhedral opaques, and the presence of a small breccia clast two centimeters in diameter.

The abundance, type, and shape of cavities varies through the flow interior zone. Deep within the flow interior zone the cavities are rounded and less than 0.4 millimeter in diameter. Vesicles occur singly and are round to oval. Diktytaxitic cavities occur in diffuse rounded patches of cavities. Elongate

cavities are not present in the flow interior zone. The overall percentage of cavities ranges from 2.5 to 6.0 percent (Table III).

Transition Zone

The transition zone is the texturally most complicated zone because its textures are transitional from the underlying flow interior zone to the overlying flow-top breccia zone. The transition zone contains non-brecciated and brecciated rocks. Textures in the non-brecciated portions, although similar to those in the flow interior zone, contain interstitial to intersertal glass. The brecciated rocks, however, are markedly different from those in the flow-top breccia zone. Breccia clasts within the transition zone are fused together, whereas this is not the case in the flow-top breccia zone.

Much of the complexity of the transition zone arises from the various types of breccias that are developed in the zone and their spatial and textural relationships to each other and the non-brecciated portions of the zone. Transition zone breccias are subdivided into five groups that are totally transitional. These include

- 1) incipient breccias,
- 2) breccias in which clasts are surrounded by small cavities,
- 3) breccias in which clasts have been partly resorbed by the matrix,
- 4) breccias in which clasts are strongly fused, and

5) breccias in which clasts are loosely fused.

The first three types are matrix-supported breccias and the last two types are clast-supported.

The initiation of the brecciation process appears to be related to the development of differing textural domains through a physical mixing of solidified rock and unsolidified melt during the extrusion and cooling of the analog flow. These textural domains are best indicated by the distribution of opaques. Domains of varying size, some containing polyhedral opaques in a light-colored groundmass and others disseminated opaques in a dark-colored groundmass, alternate within the zone. The domains of disseminated opaques may occur as angular forms or streaks. The size of these domains is such that several forms may occur in the same thin section or the domain may encompass the entire thin section. Boundaries between domains are often sharp as illustrated in Figure 54, a photomicrograph of one such boundary. Microlites are commonly aligned parallel to the domain boundaries. The boundaries between domains are important because they are the sites along which cavities develop and ultimately breakage occurs to form breccia fragments. The localization of cavities along the domain boundaries is illustrated in Figure 55. The cavities may be round or, more commonly, are strongly elongate parallel to the boundary.

The transition in textures from non-brecciated to incipient brecciated to brecciated rock is illustrated respectively by samples 28c(a), 28c(b), and 69d (Table XVII, See Appendix A).

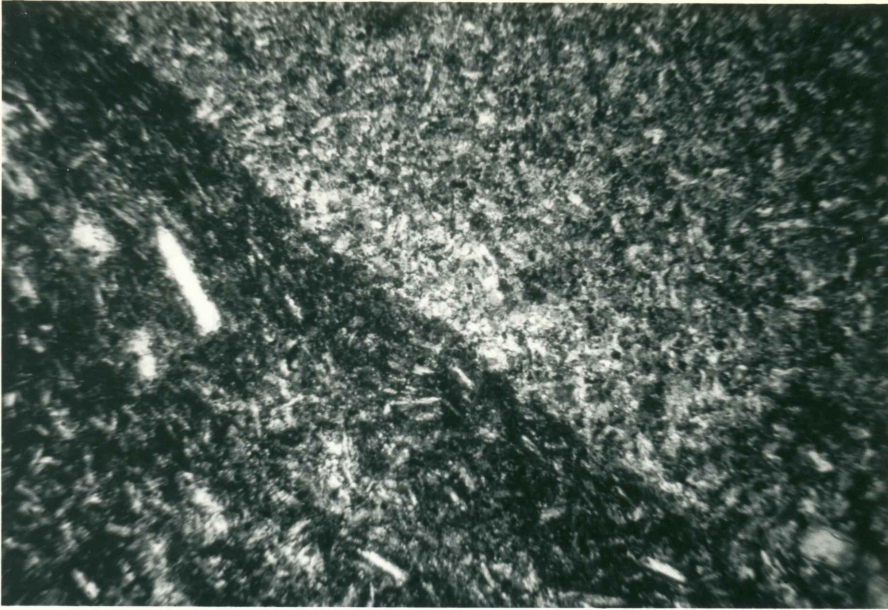


Figure 54. Sharp boundary between light-colored groundmass having opaque polyhedra, and a dark-colored disseminated opaque domain. Sample 83c, plane-polarized light, field of view 1.3 millimeters.



Figure 55. Mixed disseminated and polyhedral opaque domains, showing the alignment of plagioclase microlites and the development of cavities along sharp domain boundaries. Sample 28c(b), plane-polarized light, field of view 5.2 millimeters.

Sample 28c(b) contains no breccia fragments, though has mixed disseminated and polyhedral opaque domains with sharp boundaries that are partly surrounded by cavities as shown in the photomicrograph in Figure 55. Located immediately above 28c(b), sample 28c(a) contains an incipient clast in addition to mixed textural domains (Figure 56). Sample 69d contains angular dark colored breccia fragments in a lighter colored groundmass. The incipient clast and angular breccia fragments in the latter two samples are dark-colored due to finely disseminated opaques in the groundmass, which are similar in texture to the disseminated opaque domains in the nonbrecciated sample. The angular breccia fragments have fewer tack points between cavities than the incipient clast. Breakage occurs along the trains of cavities that surround the incipient clast to form fragments. The breakage process is progressive and the individual clasts may not be separated from the mass of the rock but still tightly fused to the rock mass as illustrated in Figure 57. The degree of fusing is also gradational with fewer and fewer tack points identified until the clasts become separated from each other and form a clast-supported breccia.

A second type of pattern occurs in which the distinction between the clast and the surrounding material is noted as one of differing degree of vesiculation. This is illustrated in sample 28a (Table XVII, Appendix A). Here the rounded clasts have a dark gray groundmass, from 15 to 20 percent vesicles, and occur within a basalt with equant polyhedral opaques, no vesicles, and 8 to 13

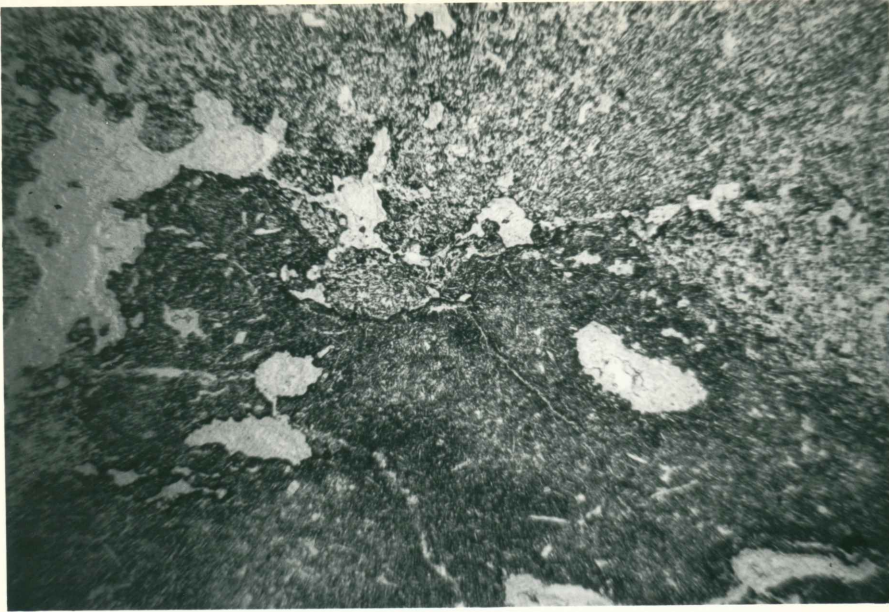


Figure 56. Incipient dark-colored clast (lower 2/3 of photomicrograph) showing sharp to gradational boundaries, and differing cavity patterns between the incipient clast and light-colored matrix. Sample 28c(a), plane-polarized light, field of view 5.2 millimeters.

percent diktytaxitic cavities. The grain size of the groundmass in the clast is coarser than that of the surrounding basalt. The boundary between the clast and surrounding material is gradational and not marked by diktytaxitic cavities. Another example is 8b in which the clasts and surrounding basalt both have finely disseminated opaques in a dark gray groundmass. The clast has rounded vesicles (28 to 30 percent), and the surrounding basalt contains diktytaxitic cavities (5 to 7 percent). The boundary between the clast and surrounding basalt is similarly gradational over 5 millimeters, and not marked by diktytaxitic cavities. These textures suggest that the rounded vesicular clasts found in these samples were formed elsewhere and were later incorporated

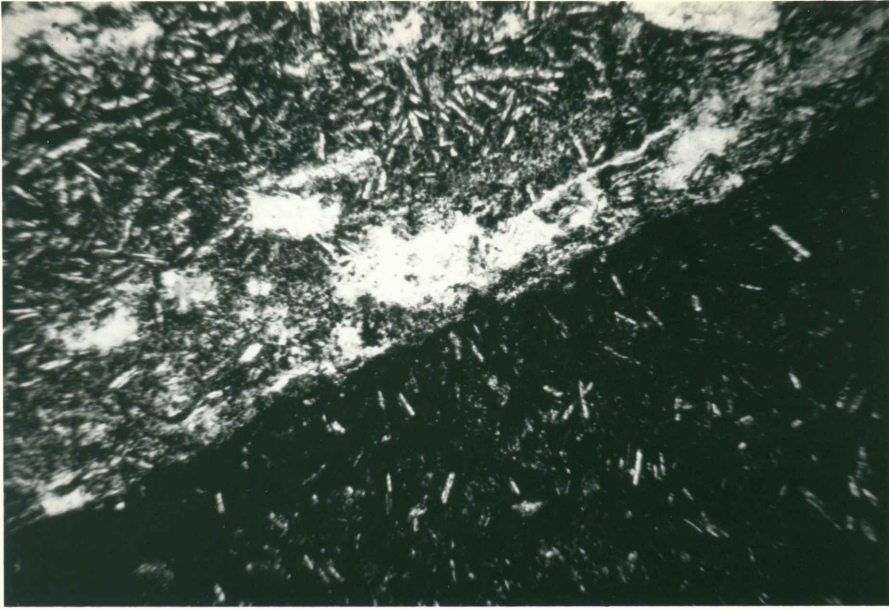
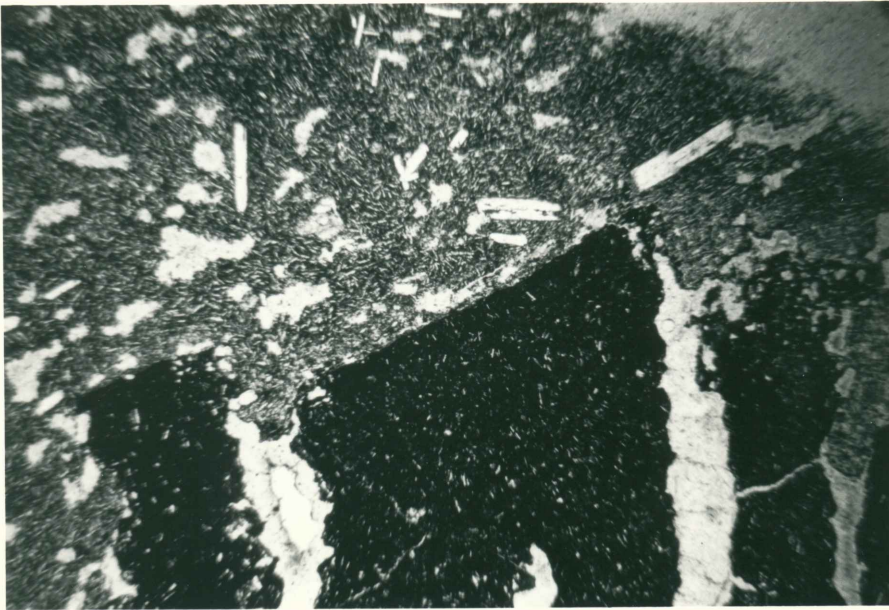


Figure 57. The photomicrograph shown above is a close-up (1.3 millimeter field of view) of a portion of a boundary of a dark-colored clast shown in the photomicrograph below (5.2 millimeter field of view). The cavities along the clast boundary show signs of deformation. Sample 69d, plane-polarized light.



and partially resorbed into the crystallizing basalt that surrounds the clasts.

The distribution of breccia types is relative to the basalt spines that protrude upward into the flow-top breccia zone. The cores of such spines are composed of basalt containing holocrystalline intergranular textures, with (8b, 83c) or without (28a) disseminated opaques (Table XVII, Appendix A). The textures are similar to those found in the upper portions of the flow interior zone. One to three meters outward from the spine center non-brecciated hypocrySTALLINE rocks (28c(b)) with mixed textural domains of disseminated and polyhedral opaques become prominent. Next in occurrence are dark-colored incipient breccia clasts and fragments surrounded by hypocrySTALLINE basalt (28c(a), 69d) similar to the non-brecciated hypocrySTALLINE rocks that mantle the spine (Table XVII, Appendix A). The hypocrySTALLINE basalt surrounding the clasts decreases outward from the spine until the breccias are clast-supported and from strongly to loosely fused. The transition from non-brecciated mixed textural domains to the weakly fused breccia occurs over a distance from 1 to 3 meters. The various breccia types successively mantle the basalt spines as shown in the sketch in Figure 5.

The textures and modal percentages of microphenocrysts within the various breccia types and the basalt spines are similar to those encountered in the flow interior zone. The modal range of microlites, however, is less whereas the abundance of glass is greater in the outer portions of the breccias. The various data

relative to the textures in this zone are recorded in Table III.

Plagioclase microlites are commonly oriented within this zone. The alignment of microlites is parallel to dark streaks in the mixed textural domains, in flow patterns around incipient breccia fragments, and may be aligned within some breccia fragments.

Flow-top Breccia Zone

The flow-top breccia zone extends from the top of the transition zone upward to the base of the interflow contact zone. Textural relations in the flow-top breccia zone are characterized by microphenocrysts, groundmass crystallinity, opaque habit, and vesicle and diktytaxitic cavity patterns and abundance. The flow-top breccia is clast-supported and the clasts are non-fused. Textural relations are similar to those found within the flow interior and transition zones. However, these textures are characterized by

- 1) lower percentages of microlites and higher percentages of glass;
- 2) the presence of crystallites;
- 3) the presence of dendritic opaques, and the absence of finely disseminated opaques;
- 4) the greater abundance of cavities, particularly vesicles, that range from 11 to 62 percent of the rock;
- 5) the greater size range of vesicles and diktytaxitic cavities, and the larger size of the smallest cavities of

each type (Table III).

Preferred orientations in plagioclase microlites are not as common as in the upper portion of the flow interior zone and transition zone. However, interpenetrating pyroxene/plagioclase microphenocrysts, and pyroxene buds on plagioclase microphenocrysts are much more common in occurrence in the flow-top breccia zone than the flow interior and transition zones (Table III).

The textural relationship between glass and crystallites in the groundmass is illustrated in Figure 58. The crystallites are colorless, rod- to hair-like, up to .06 millimeter long, .002 millimeter wide, and weakly birefringent in cross-polarized light.



Figure 58. Glass and crystallites. Sample 36e, plane-polarized light, field of view .32 millimeter.

The crystallites form a hair-like mat within the glass. The crystallites appear to be gradational with the microlite grain boundaries.

Dendritic opaque textures are not prominent within clasts in the flow-top breccia zone. However, an example of these textural relations is shown in Figure 59, a photomicrograph of a sample in which the dendrites are more prominent near vesicle walls.



Figure 59. Dendritic opaques. Sample 271, plane-polarized light, field of view .32 millimeter.

Interpenetrating pyroxene/plagioclase microphenocrysts, and pyroxene buds on plagioclase microphenocrysts occur most consistently in breccia clasts or fragments that have crystallite textures in the groundmass, and with second most consistency in clasts with dendritic opaque textures in the groundmass.

Interflow Contact Zone

The interflow contact zone encompasses the interflow contact itself and extends downward into the breccias below the contact where interpenetrative tongues from the superjacent flow have invaded the flow-top breccia and where blocks shed from the superjacent flow occur within the flow-top breccia. Its upper boundary is within the base of the superjacent flow above that portion of the flow base where pipe vesicles and tree casts are no longer recognized.

Textural relations in the interflow contact zone are similar to those encountered in the adjacent flow-top breccia and superjacent flow interior zones in that rocks are all hypocrySTALLINE with intersertal glass textures. However, textures in tongues, lenses, and blocks from the superjacent flow, as well as in walls of tree molds can be distinguished from clasts in the flow-top breccia derived from the analog flow. In tongues, lenses, and blocks from the superjacent flow

- 1) crystallites are more abundant in the altered glassy groundmass,
- 2) dendritic opaque grains are absent,
- 3) skeletal plagioclase microphenocrysts contain intersertal glass,
- 4) bending and offset on fractures is common within microphenocrysts, and
- 5) plagioclase microlites, vesicles, and diktytaxitic

cavities show a common preferred orientation (See Table III).

In the case of the walls of tree molds, disseminated opaques and concentric curvilinear arrangement of cavities parallel to the walls of the mold are also noted. In general the abundance of cavities (6 to 29 percent) is between that of the superjacent flow interior zone (5 to 11 percent), and breccia clasts and fragments of the flow-top breccia zone (11 to 62 percent) (Table III, Figure 4). The more frequent occurrence of pyroxene buds on plagioclase microphenocrysts also characterizes tongues, lenses, and blocks from the superjacent flow.

Thus clasts and blocks from the superjacent flow that have become mixed into the flow-top breccia can be distinguished with some certainty on the basis of the field characteristics already mentioned and textural relations in thin sections as described above. This is important, because blocks of the superjacent flow in the flow-top breccia may not be immediately adjacent to the interflow contact or penetrative tongues and lenses, but may occur a few meters below the contact.

SUPERJACENT FLOW

Petrographic analyses have been performed on samples from the flow interior zone, though not the flow-top breccia zone of this flow.

Flow Interior Zone

Only the lower portion of the superjacent flow interior zone adjacent to the interflow contact zone has been petrographically analyzed. The lower portion of the superjacent flow interior zone is hypocrySTALLINE with intersertal glass textures as shown in Figure 60. The red-brown glass is isotropic in cross-polarized light. The size contrast between microphenocrysts and microlites in the groundmass is less in this zone than in the interflow contact zone (Figure 4), though intersertal glass is absent in the analog flow interior zone (Table III). The superjacent flow interior zone is similar to the analog flow interior zone in that

- 1) pyroxene buds on plagioclase microphenocrysts are sparse,
- 2) interpenetrating pyroxene/plagioclase microphenocrysts are rare,
- 3) preferred orientations in cavities are absent and weakly developed in plagioclase microlites, and
- 4) opaques occur only as polyhedra (Table III).

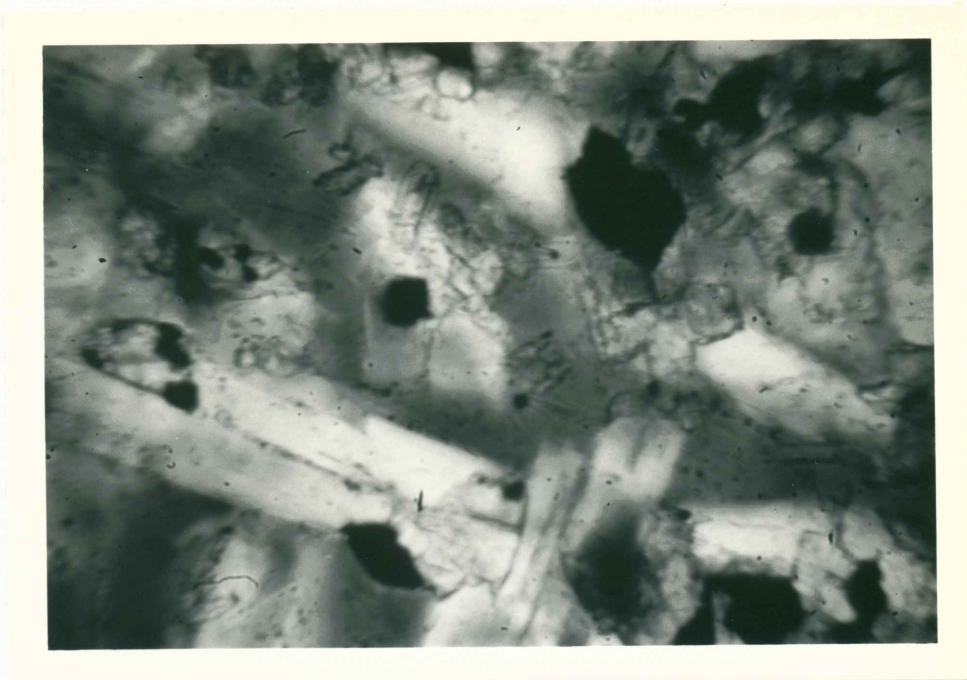


Figure 60. HypocrySTALLINE groundmass showing intersertal glass textures. Sample 51, plane-polarized light, condenser in, field of view .32 millimeter.